Heterogeneous Domain Decomposition Methods for Coupled Flow Problems

Dissertation
zur Erlangung des Doktorgrades
der Mathematisch-Naturwissenschaftlichen Fakultät
der Universität Augsburg

vorgelegt von
Paulo Fidel Porta
aus Augsburg

Augsburg,
im November 2004

Erster Gutachter: Prof. Dr. Ronald H. W. Hoppe, Augsburg
Zweiter Gutachter: Prof. Dr. Kunibert G. Siebert, Augsburg
Dritter Gutachter: Prof. Dr. Josef Kačur, Bratislava
Vierter Gutachter: Prof. Dr. Peter Bastiam, Heidelberg

Tag der mündlichen Prüfung: 4. Februar 2005

Para Santiago y Felipe

que son tan mios
como yo de ustedes

Preface

The study of complex environmental processes as the transport of contaminants in water systems is receiving increasing attention due to higher quality standards. The classical approach is the coupled solution of momentum and transport equations. This involves the solution of the flow dynamics, i.e., the determination of the velocity field, which is used as the convective field in the transport equation. A problem of significant relevance in applications is the coupling of surface and subsurface flows. The need for more accurate models and efficient solvers opens a whole research area were Applied Mathematics plays a key role.

Water flow above a porous medium is an important but still not solved problem. The difficulties stem from several factors:
i) The subsurface flow is not well defined as long as no good interface transmission conditions are specified.
ii) Higher order terms in general Navier/Stokes flows, namely inertial and viscous terms, are not present in the Darcy flow.

This thesis attempts to contribute to some insight in this problem by considering coupled Stokes/Darcy flow. It presents a mathematical model for the coupled flow and a finite element approximation. In particular, emphasis is put on the development, analysis, and implementation of efficient solvers based on a heterogeneous domain decomposition methodology. This is a natural and rather flexible approach for the solution of problems which involve more than one operator on different (disjoint) regions of the domain.

A theoretical and experimental analysis is performed. We investigate the dependence of the different algorithms with respect to model coefficients, domain geometry and boundary conditions, in order to evaluate feasibility and performance of the proposed schemes.

Acknowledgment

The work leading up to this thesis would not have been possible without the advice and assistance of many people. Foremost, I thank my advisor, Prof. Dr. Ronald H. W. Hoppe. He taught me the high standards of academic research and gave me unrelenting support throughout the preparation of the thesis.

I am deeply indebted to Dr. Yuri Vassilevski. I am grateful to him for the many enlightening discussions we had, and the insightful feedback he provided during my work. He has been a resource for many issues and a great support.

This work was conducted while holding a position as a Research Assistant at the Center for Environmental Simulation, University of Augsburg, funded by the State of Bavaria within the High-Tech-Initiative (HTO) Bavaria.

Finally, I am grateful to all my colleagues at the Chair of Applied Analysis/Numerics, Institute of Mathematics, University of Augsburg. They created a pleasant atmosphere highly conducive to concentrated and creative work.

Augsburg, November 2004 *Paulo Porta*

Contents

1 Introduction **1**
- 1.1 Background 1
- 1.2 Organization of the present work 3
- 1.3 Preliminaries 4

2 Formulation of the model **7**
- 2.1 Strong formulation of the coupled problem 7
- 2.2 Transmission conditions 9
- 2.3 Justification of the coupled Stokes/Darcy flow 11
- 2.4 Weak formulation of the coupled problem 12
- 2.5 Associated Poincaré–Steklov operators 19
  - 2.5.1 The operator for the balance of the normal stress . . . 19
  - 2.5.2 The operator for the continuity of the flux 23
- 2.6 Finite element approximation 30

3 An iterative substructuring method **33**
- 3.1 The Neumann–Dirichlet (N-D) iteration 34
- 3.2 Analysis of the N-D iteration 35
- 3.3 Implementation at the finite element level 39
- 3.4 Algebraic form of the iterative procedure 41
- 3.5 Numerical experiments 42
  - 3.5.1 Approximation of an analytical solution 42
  - 3.5.2 Effects of boundary conditions 44
  - 3.5.3 Influence of model coefficients 52

4 An alternative direct method **59**
- 4.1 Direct recovery 59
- 4.2 Approximate recovery 60

4.3 Numerical experiments 61
4.3.1 Interaction of channel and subsurface flows 61
4.3.2 Approximate recovery for channel problem 66

5 Reduction to the interface **73**
5.1 The case of flux continuity across the interface 74
5.2 Normal stress continuity on the interface 76
5.3 Numerical experiments 78
5.3.1 Infiltration from a straight channel 78
5.3.2 Impact of channel configuration 82

Chapter 1

Introduction

1.1 Background

One of major problems of interest in any development and management of water resources system is that of water quality. In fact, with the increasing demand for water in most parts of the world and with the intensification of water utilization, the quality problem becomes a limiting factor. Special attention should be devoted to the pollution of groundwater in aquifers due to the very slow velocity of the water and the enhanced interaction between the pollutant and the solid matrix. The problem of groundwater pollution need not be associated only with water supply for domestic, industrial or agricultural purposes. Serious environmental problems arise when polluted groundwater emerges at ground surface or discharges into rivers and lakes.

It is a well known fact that the underground flow is governed by the piezometric head distribution, the material properties of the soil (e.g., the hydraulic conductivity) and the boundary conditions to be imposed for the piezometric head. The strategy for the simulation of pollutant transport in underground water is to couple this flow with the appropriate transport equation for a scalar quantity (e.g., the concentration of a tracer): the pattern of the tracer is then defined by the flow pattern. In general, charts with the recorded history of the piezometric head are available for large scale fields, allowing thus to define a *mean vector* for the piezometric head gradient (e.g. its mean absolute value and a mean direction). This approach, however, is not suited for the cases in which a small scale analysis is needed.

There are several practical situations in which the criteria of a mean vec-

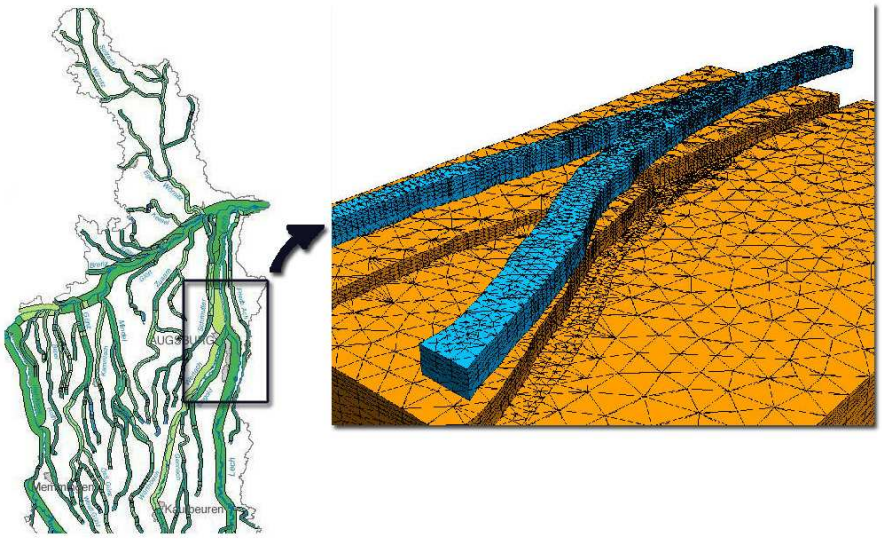

Figure 1.1: River system near Augsburg (Bavaria) and a detail of the three dimensional grid for the confluence of rivers Wertach and Lech

tor do not make sense. A typical situation is when a detailed study of the transport of contaminants close to a system of channels and rivers has to be performed. In a case like the one depicted in Figure 1.1, a mean direction of flow, although being accessible, is useless for any practical computation involving contaminants transport and exchange between the aquifer and the surface water flow because of the impossibility to resolve the details.
Our motivation is oriented by the evaluation of the contaminants distribution and the mass exchange between the aquifer and the surface flow. For this, we need to solve for velocity both in the porous media and in the surface water body accounting for appropriate conditions on the common interface.

The focus of the present work is on the evaluation of the coupled surface and subsurface flow in order to compute the velocity field and the mass exchange across the common interface, to be used in the calculation of contaminants transport.

Our approach is based on a description of the situation, where the whole region under analysis is divided into two parts, namely the surface and the subsurface flow regions. It is obvious that the conditions to be imposed on the common interface play a major role in the construction of a reasonable model. Any proposed solution strategy should be capable of incorporating them either as natural or as essential boundary conditions.

1.2 Organization of the present work

The present work is organized as follows:

- In the next section, we briefly present an abstract description of the problem based on heterogeneous domain decomposition strategy.

- In Chapter 2, we formulate the mathematical model for the Stokes-Darcy system. We pose the differential problem and discuss the transmission conditions for the common interface. Then, we construct the coupled variational problem and its finite element approximation. For this, we discuss some possible weak formulations in order to incorporate different boundary conditions. Finally, we introduce the so-called Poincaré–Steklov problem. In this context, we analyze the associated Poincaré–Steklov operators whose properties are the key to propose appropriate solution concepts.

- In Chapter 3, we study a possible solution approach: after a review of the state-of-the-art in this field, we suggest a Neumann-Dirichlet iteration and develop and analyze a corresponding algorithm. Supported by theoretical findings, the analysis reveals an intrinsic low efficiency of the procedure for some important scenarios and thus, severe limitations in its practical applicability.

- Therefore, in Chapter 4 we present an alternative solution procedure to overcome these difficulties, based on the recovery of the iteration operator. Due to the fact that this is a direct method, with a high computational cost, we explore also, a lower-dimensional approximation and evaluate its performance.

- Finally, in Chapter 5 we investigate another strategy by reducing the problem to one on the interface. In fact, we derive an interface equation

which allows for a direct solution of the decoupled subproblems. There are two possible interface equations: one is based on matching fluxes under the assumption of constant normal stress, whereas the other is based on matching the normal stress under the assumption of a constant flux. The analysis of both strategies indicates that the last formulation is the one with the most promising practical applicability. As an application, we apply this strategy to the scenario illustrated in Figure 1.1.

1.3 Coupling Darcy and Stokes flows: preliminaries

As mentioned before, the modeling of the flows can be done by considering two non overlapping subdomains with a common boundary. In one of these subdomains, the Darcy flow is realized, whereas in the other the flow is governed by the Navier-Stokes equations. Of course, the situation can be extended to more than two non overlapping subdomains with various types of flows. The mathematical theory and the numerical analysis of each subproblem is well developed and reliable codes are available (see, e.g., [Bea79], [Hor92], [Lio96], [GR79], [Pir89], [Tem84]). Nevertheless, the mathematical theory of the coupled problem is not completely understood. We will consider the case where the Navier-Stokes flow is replaced by Stokes flow.

A very natural way to perform the coupling of Stokes' and Darcy's flows is to use a heterogeneous domain decomposition approach. This approach [QV99] directly gives rise to an iterative substructuring method. Typically, a sequence of subproblems in Ω_1 and Ω_2 with appropriate Dirichlet or Neumann data on the internal boundary is considered. The abstract mathematical setting can be described as follows (cf., e.g., Figure 1.2).

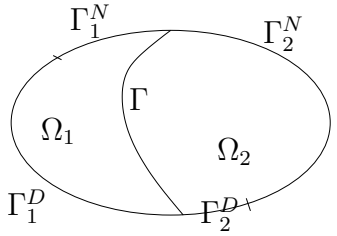

Figure 1.2: Schematic domain partition and notation

We denote by $\mathcal{S}$ and $\mathcal{D}$ the Stokes and the Darcy operators and refer to $\Omega_k, 1 \leq k \leq 2$, as the two subdomains that provide a non overlapping partition of the domain $\Omega \subset \Re^d$ with boundaries $\partial\Omega_k = \Gamma_k^D \cup \Gamma_k^N \cup \Gamma, 1 \leq k \leq 2$, where Γ is the common interface. We consider the following multi-domain problem:

Problem 1 *Find* $\mathbf{U_1} := (\mathbf{u}_1, p) : \Omega_1 \rightarrow \Re^d \times \Re$ *(velocity and pressure) and* $\mathbf{U}_2 := \phi : \Omega_2 \rightarrow \Re$ *(piezometric head) such that*

$$\mathcal{S}\mathbf{U}_1 = \mathbf{f}_1 \text{ in } \Omega_1 \quad , \quad \mathcal{D}\mathbf{U}_2 = \mathbf{f}_2 \text{ in } \Omega_2, \tag{1.1}$$

together with suitable boundary conditions for $\mathbf{U}_i$ *on* $\partial\Omega_i \backslash \Gamma$.

$$\mathbf{B}_{\mathcal{S}}(\mathbf{U}_1) = \mathbf{g}_1 \text{ on } \partial\Omega_1 \backslash \Gamma \quad , \quad \mathbf{B}_{\mathcal{D}}(\mathbf{U}_2) = \mathbf{g}_2 \text{ on } \partial\Omega_2 \backslash \Gamma. \tag{1.2}$$

Moreover, the unknown functions $\mathbf{U}_1$ *and* $\mathbf{U}_2$ *are supposed to satisfy* k *appropriate transmission conditions on* Γ *which can be formulated according to:*

$$\Phi_j(\mathbf{U}_1) = \Phi_j(\mathbf{U}_2) \text{ on } \Gamma \quad , \quad 1 \leq j \leq k \ , \tag{1.3}$$

where the functions Φ_j *as well as* Γ *depend on the nature of the individual problem.* ■

For the solution of Problem 1 it is possible to split it into two subproblems coupled by an interface function λ. Starting from an initial guess λ^0 for each subproblem, two sequences $\{\mathbf{U}_1^k\}$, $\{\mathbf{U}_2^k\}$ can be generated by means of the so-called Neumann-Dirichlet iteration:

Procedure 1 *Neumann–Dirichlet iteration*

1. *Given* λ^0, *for* $k \geq 0$ *solve*

$$\begin{cases} \mathcal{D}\mathbf{U}_2^{k+1} = f_2 & \text{in } \Omega_2 \\ \mathbf{B}_{\mathcal{D}}(\mathbf{U}_2^{k+1}) = g_2 & \text{on } \partial\Omega_2 \backslash \Gamma \\ \frac{\partial \mathbf{U}_2^{k+1}}{\partial \mathbf{n}} = \lambda^k & \text{on } \Gamma \end{cases}$$

2. *Solve*

$$\begin{cases} \mathcal{S}\mathbf{U}_1^{k+1} = f_1 & \text{in } \Omega_1 \\ \mathbf{B}_{\mathcal{S}}(\mathbf{U}_1^{k+1}) = g_1 & \text{on } \partial\Omega_1 \backslash \Gamma \\ \mathbf{U}_1^{k+1} = \mathcal{R}_1(\mathbf{U}_2^{k+1}) & \text{on } \Gamma \end{cases}$$

3. Update

$$\lambda^{k+1} = \theta \mathcal{R}_2(\mathbf{U}_{1|\Gamma}^{k+1}) + (1-\theta)\lambda^k$$

■

As will be shown in Chapter 3, this iteration can be interpreted as a preconditioned Richardson iteration.

Another approach considered in [QV91a], [QV91b] and [QV99] is to reduce the coupled problem to a problem on the interface given in terms of the Poincaré–Steklov operator S (cf., e.g., [Ste03] and the references therein). The transmission conditions are enforced according to

$$S\lambda = \chi \quad \text{on } \Gamma, \tag{1.4}$$

where χ depends on the data of the problem. Once the solution λ has been computed, we obtain $\mathbf{U}_1$ and $\mathbf{U}_2$ via the solution of the subproblems given by (1.1).

The operator S is defined by extension operators $K_{\mathcal{S}}$ and $K_{\mathcal{D}}$ and corresponding Stokes and Darcy extensions $K_{\mathcal{S}}\lambda$ and $K_{\mathcal{D}}\lambda$. The exact form will be presented in Chapter 2. Moreover, it depends on the choice of the interface equation enforced by (1.4). We will show that S can be split into two terms, say $S_{\mathcal{S}}$ and $S_{\mathcal{D}}$ associated with Ω_1 and Ω_2.

From the numerical point of view, any finite dimensional approximation of the Poincaré-Steklov operator yields a Schur complement system where the Schur complement matrix is usually ill-conditioned due to the unboundedness of the continuous operators. Iterative procedures are henceforth in order, and preconditioning techniques have to be adopted.

Chapter 2

Formulation of the mathematical model

2.1 Strong formulation of the coupled problem

As stated in Section 1.3, the coupling of the surface and the subsurface flows corresponds to the situation where an incompressible fluid in a domain $\Omega \subset \Re^d$ can flow both ways across the interface Γ between two non-overlapping subdomains Ω_1 and Ω_2 representing an arbitrary flow and Darcy's flow, respectively. In this chapter, the porous medium occupying Ω_2 is assumed to be saturated with the fluid. No special boundary conditions are expected on $\partial\Omega$ where Dirichlet conditions on $\partial\Omega_D$ and Neumann conditions on $\partial\Omega_N$ are assumed.

Following standard formulations of the individual problems (see [Bea79], [Lio96] and [Tem84]), we state the coupled problem as follows:

Problem 2 *Find* $(\mathbf{u}_1, p) : \Omega_1 \times [0,T] \to \Re^d \times \Re$, *and* $\phi : \Omega_2 \times [0,T] \to \Re$, *representing the velocity, the pressure, and the piezometric head, respectively, such that:*

$$\begin{cases} \dfrac{Du_1}{dt} - div\,\mathbf{T} = \mathbf{f_1} & in\ \Omega_1 \\ div\,\mathbf{u_1} = 0 & in\ \Omega_1 \\ \mathbf{u_1} = \mathbf{u_1}^D & on\ \Gamma_1^D \\ \mathbf{n}_1 \cdot \mathbf{T} \cdot \mathbf{n}_1 = m & on\ \Gamma_1^N \\ transmission\ conditions & on\ \Gamma \end{cases} \tag{2.1}$$

$$\begin{cases} S_0 \dfrac{\partial \phi}{\partial t} + div\, \epsilon \mathbf{u_2} &= f_2 & in\ \Omega_2 \\ \epsilon \mathbf{u_2} &= -\mathbf{K} \cdot grad\, \phi & in\ \Omega_2 \\ \phi &= \phi^D & on\ \Gamma_2^D \\ -\mathbf{n}_2 \cdot \mathbf{K} \cdot grad\, \phi &= \phi^N & on\ \Gamma_2^N \\ transmission\ conditions & & on\ \Gamma \end{cases} \tag{2.2}$$

where $\Gamma_1 = \overline{\Gamma_1^D} \cup \Gamma_1^N = \partial\Omega_1 \backslash \Gamma$, $\Gamma_2 = \overline{\Gamma_2^D} \cup \Gamma_2^N = \partial\Omega_2 \backslash \Gamma$. *The operator* $\frac{D}{Dt} = \frac{\partial}{\partial t} + \mathbf{u} \cdot \nabla$ *represents the substantial or Reynolds derivative.*

The tensor $\mathbf{T}$ in Navier-Stokes equation is the second order symmetric stress tensor, divided by the density, which can be linked to the symmetric second order rate of strain $\mathbf{D}(\mathbf{u}_1) := \frac{1}{2}[\mathrm{grad}\mathbf{u}_1 + (\mathrm{grad}\mathbf{u}_1)^T]$ via Newton's constitutive law:

$$\mathbf{T} = -p\mathbf{I} + 2\nu\mathbf{D}(\mathbf{u}_1). \tag{2.3}$$

Here, p represents the isotropic pressure divided by the density, and ν stands for the kinematic viscosity. In Darcy's model, ϵ refers to the porosity, $\mathbf{K}$ is the conductivity tensor, and the source term f_2 is assumed to satisfy the compatibility condition

$$\int_{\Omega_2} f_2 \, dx = 0 \ ,$$

if a no-flow condition is imposed on Γ_2, or if the boundary condition is of pure Neumann type.

Three remarks are in order with respect to the coupled system:

1. A simple inspection of the coupled problem reveals that the orders of the corresponding differential operators are different for the velocity. Consequently, it is not clear what kind of conditions should be imposed at the common interface.

2. Singularities may occur in a vicinity of the manifolds $\Gamma \cap \partial\Omega$ due to incompatibilities between the imposed boundary conditions and the transmission conditions.

3. The piezometric head, and hence the Darcy velocity are obtained by averaging values over representative elementary volumes -REVs- (see [BV87], [BB90] and [Hor92]). Therefore, one can not directly apply first principles to obtain the transmission laws at the interface.

The specification of appropriate transmission conditions will be addressed in the following section.

2.2 Transmission conditions

As discussed before, appropriate transmission conditions have to be provided on the interface Γ. The first transmission condition is an expression for the dynamic equilibrium in the form of a balance of the normal forces across Γ: The traction exerted on the fluid is given by:

$$\mathbf{t} = \mathbf{n}_1 \cdot \rho\mathbf{T} \ . \tag{2.4}$$

Here, $\mathbf{T}$ is the stress tensor, divided by the density, and $\mathbf{n}_1$ stands for the outward unit normal on $\partial\Omega_1$ (see Figure 2.1). The traction exerted by the

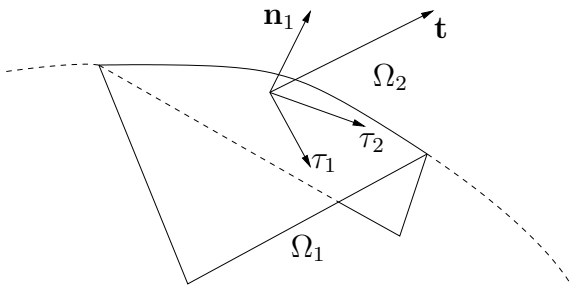

Figure 2.1: The traction vector on Γ and the local coordinate system

fluid on the interface is $-\mathbf{t}$. Since the only force in Ω_2 is given by the piezometric head ϕ (or more precisely, the Darcy pressure $\rho g\phi$), the continuity of the normal component of the forces implies:

$$-\mathbf{t} \cdot \mathbf{n}_1 = -\mathbf{n}_1 \cdot \rho\mathbf{T} \cdot \mathbf{n}_1 = \rho g\phi \qquad \text{on } \Gamma. \tag{2.5}$$

Replacing $\mathbf{T}$ by Newton's constitutive law (2.3), we obtain

$$-\mathbf{n}_1 \cdot (-p\mathbf{I} + 2\nu\mathbf{D}(\mathbf{u}_1)) \cdot \mathbf{n}_1 = p - 2\nu\mathbf{n}_1 \cdot \mathbf{D}(\mathbf{u}_1) \cdot \mathbf{n}_1 = g\phi \quad \text{on } \Gamma. \tag{2.6}$$

The second condition on the interface states the continuity of the normal component of velocity across Γ:

$$\mathbf{u}_1 \cdot \mathbf{n}_1 + \mathbf{u}_2 \cdot \mathbf{n}_2 = 0 \qquad \text{on } \Gamma. \tag{2.7}$$

This relation is not sufficient to specify appropriate Dirichlet boundary conditions on Γ. The flows in the surface water body and in the porous medium require the specification of the whole velocity vector. Therefore, we have to specify the tangential component of the velocity field on the interface. The usual non-slip condition, assuming a vanishing tangential component of the velocity, is not in accordance with experiments. An experimentally verified condition is due to Beavers, Joseph and Saffman (cf., e.g., [PS98, JM00]).

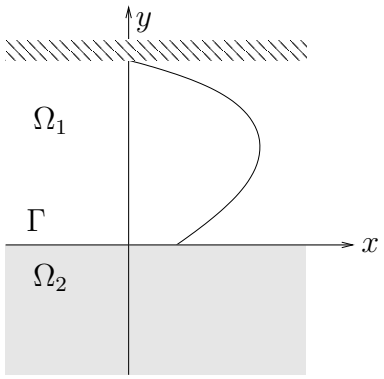

Figure 2.2: Velocity profile for bounded, unidirectional flow next to the interface with a saturated porous medium

In [BJ67], the shear flow at the interface between the porous and the open medium is investigated in a simple geometry shown in Figure 2.2. Here, the flow is parallel to the $x-$ direction, so that $\mathbf{u}_j = (u_j, 0, 0), 1 \leq j \leq 2$. The result states that the difference between the slip velocity of the free fluid and the tangential component of the seepage velocity $(u_1 - u_2)$ is proportional to the shear rate of the free fluid, i.e.,

$$\frac{\partial u_1}{\partial y} = \frac{\alpha}{\sqrt{\kappa}}(u_1 - u_2) \ , \tag{2.8}$$

where α is a non-dimensional parameter called the slip coefficient. It is independent of the fluid viscosity, but depends on the structure of the permeable material at the interface ([BSM74]). It is understood that in (2.8) u_1 and $\frac{\partial u_1}{\partial y}$ are evaluated at $y = 0^+$, whereas u_2 is evaluated at $y = 0^-$.

For the general flow next to the interface, (2.8) gives rise to the following condition expressing the relation between the difference of the slip velocity of the free fluid and the tangent component of the traction (see [Jon73]):

$$(\mathbf{u}_1 - \mathbf{u}_2) \cdot \tau_j = \frac{\sqrt{\tau_j \cdot \kappa \cdot \tau_j}}{\mu\alpha}(-\mathbf{n}_1 \cdot \rho\mathbf{T}) \cdot \tau_j \ . \tag{2.9}$$

Here, $\tau_j, 1 \leq j \leq d-1$, is the set of orthonormal tangent vectors on Γ, and κ is the second order symmetric permeability tensor which is related to the conductivity $\mathbf{K}$ according to

$$\mathbf{K} = \frac{g\ \kappa}{\nu}$$

with g denoting the gravity acceleration modulus.

Despite a good agreement with experiments, it has been observed ([Saf71], [NB92]) that the term $\mathbf{u}_2 \cdot \tau_j$ is much smaller than the others. As explained in [Saf71] by statistical arguments, the Beaver-Joseph relation should be written as

$$u_1 = \frac{\alpha}{\sqrt{\kappa}} \frac{\partial u_1}{\partial y} + \mathcal{O}(\kappa). \tag{2.10}$$

Having this in mind and introducing Newton's constitutive law, the corresponding extension to the general case reads as follows:

$$\mathbf{u}_1 \cdot \tau_j = -2\frac{\sqrt{\tau_j \cdot \kappa \cdot \tau_j}}{\alpha}\mathbf{n}_1 \cdot \mathbf{D}(\mathbf{u}_1) \cdot \tau_j, \quad 1 \leq j \leq d-1 \ \text{ on } \Gamma \ . \tag{2.11}$$

This expression, the so-called Beavers/Joseph/Saffman condition, is supported by other independent work (cf., e.g., [Dag79, Tay71, SK92]). In particular, the derivation in [SK92] is based on the so-called Brinkman extension. The Brinkman equation is a viscous extension of Darcy's equation, originally proposed by Brinkman ([Bri47]) and further developed by other authors (cf., e.g., [GO76, Whi99]). This model also includes an empirical coefficient: the apparent viscosity μ^* which is usually different from μ and reflects the additional resistance of the porous structure.

2.3 Justification of the coupled Stokes/Darcy flow

In the sequel, we discuss the coupled Stokes/Darcy flow:

Problem 3 *Find* $(\mathbf{u}_1, p) : \Omega_1 \to \Re^d \times \Re$, *and* $\phi : \Omega_2 \to \Re$, *representing the velocity, the pressure, and the piezometric head, respectively, such that:*

$$\begin{cases} -grad\ p + 2\nu\, div\, \mathbf{D}(\mathbf{u_1}) &= \mathbf{f_1} & in\ \Omega_1 \\ div\, \mathbf{u}_1 &= 0 & in\ \Omega_1 \\ \mathbf{u_1} &= \mathbf{u_1}^D & on\ \Gamma_1^D \\ \mathbf{n}_1 \cdot \mathbf{T} \cdot \mathbf{n}_1 &= m & on\ \Gamma_1^N \\ transmission\ conditions & & on\ \Gamma \end{cases} \tag{2.12}$$

$$\begin{cases} -div\,(\mathbf{K} \cdot grad\,\phi) &= f_2 & in\ \Omega_2 \\ \phi &= \phi^D & on\ \Gamma_2^D \\ -\mathbf{n}_2 \cdot \mathbf{K} \cdot grad\,\phi &= \phi^N & on\ \Gamma_2^N \\ transmission\ conditions & & on\ \Gamma \end{cases} \tag{2.13}$$

where $\Gamma_1 = \overline{\Gamma_1^D} \cup \Gamma_1^N = \partial\Omega_1 \backslash \Gamma$, $\Gamma_2 = \overline{\Gamma_2^D} \cup \Gamma_2^N = \partial\Omega_2 \backslash \Gamma$.

This simplification is justified by the following two remarks:

1. The first equation in Problem 2 is the unsteady Navier-Stokes equation. As noted, for instance in [Pir89], the steady Stokes problem is the basic constitutive part of any approximation of the full time-dependent Navier-Stokes equations. Indeed, if we perform a time discretization of Navier-Stokes equation, we obtain

   $$\frac{1}{\Delta t}\mathbf{u}^{n+1} - \mathrm{grad}p^{n+1} + 2\nu \mathrm{div}\mathbf{D}(\mathbf{u}^{n+1}) = \tilde{\mathbf{f}}\ ,$$

   where $\mathbf{u}^{n+1}$ is the approximation of the velocity and $\tilde{\mathbf{f}}$ is some approximation of the convective term at $t = t_{n+1}$.

2. The time scale for fluctuations in the porous medium flow is much bigger than that for the surface flow. This fact is in total agreement with experimental evidence (cf., e.g., [ESP75]). Since the hypothesis of steady surface flow implies an arbitrary large time scale for surface flow fluctuations, we may consider the steady state as a good working approximation of the subsurface part of the flow.

2.4 Weak formulation of the coupled problem

Since finite element approximations are based on the weak formulation, we will derive a weak formulation for Problem 3. For this purpose, we introduce

the spaces

$$\begin{aligned} H_{\Gamma_1} &:= \{v \in H^1(\Omega_1) : v = 0 \text{ on } \Gamma_1^D\}, \\ H_1 &:= \{H_{\Gamma_1}\}^d, \\ Q &:= L^2(\Omega_1), \\ H_2 &:= \{\psi \in H^1(\Omega_2) : \psi = 0 \text{ on } \Gamma_2^D\} \ . \end{aligned}$$

We further introduce the functions $\phi_e \in H^1(\Omega_2)$, $\phi_e = \phi^D$ on Γ_2^D, and $\mathbf{u}_e \in \{H^1(\Omega_1)\}^d, \mathbf{u}_e = \mathbf{u}_1^D$ on Γ_1^D, so that the solution can be split according to

$$\mathbf{u} = \mathbf{u}_1^0 + \mathbf{u}_e,\ \mathbf{u}_1^0 \in H_1 \quad , \quad \phi = \phi_0 + \phi_e,\ \phi_0 \in H_2 \ .$$

We first consider the equation governing the porous medium flow in Problem 3. Multiplying the equation by a test function $\psi \in H_2$ and applying Green's formula, we obtain:

$$\begin{aligned} &\int_{\Omega_2} \text{grad}\psi \cdot \mathbf{K} \cdot \text{grad}\phi_0 - \int_{\partial\Omega} \psi \mathbf{n}_2 \cdot \mathbf{K} \cdot \text{grad}\phi = \\ &= \int_{\Omega_2} f_2 \psi - \int_{\Omega_2} \text{grad}\psi \cdot \mathbf{K} \cdot \text{grad}\phi_e \quad \forall \psi \in H_2 \ . \end{aligned} \tag{2.14}$$

The surface integral can be partitioned into a part over Γ_2^D, a part over Γ_2^N, and a part over Γ. The first vanishes, since $\psi \in H_2$. The second occurs as a natural boundary condition, so that only the third one remains. The reduced equation shows that in view of the transmission condition with respect to the continuity of the normal velocities continuity (cf. (2.7)), we can replace $\mathbf{n}_2 \cdot \mathbf{K}$ gradϕ by the coupling term $\epsilon \mathbf{u}_1 \cdot \mathbf{n}_1$ on the interface Γ.

For the Stokes problem, we proceed in a similar way. Choosing a test function $\mathbf{w} \in H_1$, we get

$$\int_{\Omega_1} \text{grad}\, p \cdot \mathbf{w} - \int_{\Omega_1} 2\nu\, \text{div}\mathbf{D}(\mathbf{u}_1^0) \cdot \mathbf{w} = \\ = \int_{\Omega_1} \mathbf{f} \cdot \mathbf{w} + \int_{\Omega_1} 2\nu\, \text{div}\mathbf{D}(\mathbf{u}_e) \cdot \mathbf{w}, \quad \forall\, \mathbf{w} \in H_1. \tag{2.15}$$

Using Green's formula and using the notation $A : B = \sum_{ij}^{d} A_{ij} B_{ij}$:

$$-\int_{\Omega_1} p\, \text{div}\, \mathbf{w} + \int_{\Omega_1} \text{div}\, (p\mathbf{w}) + \int_{\Omega_1} 2\nu\, \mathbf{D}(\mathbf{u}_1^0) : \text{grad}\mathbf{w} + \\ - \int_{\Omega_1} 2\nu \text{div}(\mathbf{D}(\mathbf{u}_1^0) \cdot \mathbf{w}) = \int_{\Omega_1} \mathbf{f} \cdot \mathbf{w} + \int_{\Omega_1} 2\nu \text{div}\mathbf{D}(\mathbf{u}_e) \cdot \mathbf{w}, \;\; \forall\, \mathbf{w} \in H_1.$$

Due to the symmetry of $\mathbf{D}(\cdot)$, we have $\mathbf{D}(\mathbf{u}_1^0) : \text{grad}\, \mathbf{w} = \mathbf{D}(\mathbf{u}_1^0) : \mathbf{D}(\mathbf{w})$ (cf., e.g., [Pir89, GR79]). Consequently, we obtain

$$-\int_{\Omega_1} p\text{div}\mathbf{w} + \int_{\Omega_1} 2\nu \mathbf{D}(\mathbf{u}_1^0) : \mathbf{D}(\mathbf{w}) + \int_{\Omega_1} [\text{div}(p\mathbf{w}) - 2\nu \text{div}\, (\mathbf{D}(\mathbf{u}_1) \cdot \mathbf{w})] = \\ = \int_{\Omega_1} (\mathbf{f} + 2\nu \text{div}\mathbf{D}(\mathbf{u}_e)) \cdot \mathbf{w}, \quad \forall \mathbf{w} \in H_1\ . \tag{2.16}$$

The third integral on the left-hand side of (2.16) can be rewritten by means of Gauss' theorem

$$\int_{\Omega_1} \text{div}\, [(pI - 2\nu \mathbf{D}(\mathbf{u}_1)) \cdot \mathbf{w}] \;\; = \tag{2.17}$$
$$= \int_{\partial\Omega_1 \backslash \Gamma} [p\mathbf{n}_1 - 2\nu \mathbf{n}_1 \cdot \mathbf{D}(\mathbf{u}_1)] \cdot \mathbf{w} \;\; + \;\; \int_{\Gamma} [p\mathbf{n}_1 - 2\nu \mathbf{n}_1 \cdot \mathbf{D}(\mathbf{u}_1)] \cdot \mathbf{w}\ .$$

This equation can be further simplified. A similar argument as in case of the Darcy problem can be applied to the integral over $\partial\Omega_1 \backslash \Gamma$. Using the boundary partition given by $\partial\Omega_1 \backslash \Gamma = \Gamma_1^D \cup \Gamma_1^N$, the integral splits into a part associated with the Dirichlet boundary condition and a part associated with the Neumann boundary condition. The integral involving Γ in (2.17) is related to the transmission conditions (2.6) and (2.11). In fact, following [LSY03], we note that the vector integral over Γ can be written as the

sum of d integrals by expressing the integrand as the sum of d vector components, one normal to Γ and $d-1$ tangential ones with regard to the local $\{\mathbf{n}_1, \tau_1, \cdots, \tau_{d-1}\}$ coordinate system:

$$\int_\Gamma [p\mathbf{n}_1 - 2\nu\mathbf{n}_1 \cdot \mathbf{D}(\mathbf{u}_1)] \cdot \mathbf{w} = \int_\Gamma [p - 2\nu\mathbf{n}_1 \cdot \mathbf{D}(\mathbf{u}_1) \cdot \mathbf{n}_1]\mathbf{n}_1 \cdot \mathbf{w} + \\ + \sum_{i=1}^{d-1} \int_\Gamma [-2\nu\mathbf{n}_1 \cdot \mathbf{D}(\mathbf{u}_1) \cdot \tau_i]\tau_i \cdot \mathbf{w} \ .$$

The expression $p - 2\nu\mathbf{n}_1 \cdot \mathbf{D}(\mathbf{u}_1) \cdot \mathbf{n}_1$ in the integrand of the normal component integral can be used to ensure the transmission condition given by (2.6). The tangential components can be linked to the Beavers/Joseph/Saffman condition (2.11). In particular, in view of (2.11) the expression $-2\nu\mathbf{n}_1 \cdot \mathbf{D}(\mathbf{u}_1) \cdot \tau_i$ can be rewritten according to

$$-2\nu\mathbf{n}_1 \cdot \mathbf{D}(\mathbf{u}_1) \cdot \tau_j = \frac{\alpha\nu}{\sqrt{\tau_j \cdot \kappa \cdot \tau_j}} \mathbf{u}_1 \cdot \tau_j \ .$$

We have thus incorporated the three transmission conditions into a weak formulation of the problem. The transmission conditions (2.7) and (2.6) provide the coupling of the two subproblems, whereas (2.11) is included in the boundary integral.

Introducing the bilinear forms

$$a_{\mathcal{D}}(\lambda, \mu) := \int_{\Omega_2} \text{grad}\, \mu \cdot \mathbf{K} \cdot \text{grad}\, \lambda \ , \tag{2.18}$$

$$a_{\mathcal{S}}(\mathbf{v}_1, \mathbf{v}_2) := \int_{\Omega_1} 2\nu\mathbf{D}(\mathbf{v}_1) : \mathbf{D}(\mathbf{v}_2) + \\ + \sum_{i=1}^{d-1} \int_\Gamma \left[\frac{\alpha\nu}{\sqrt{\tau_j \cdot \kappa \cdot \tau_j}} \mathbf{v}_1 \cdot \tau_j \right] \mathbf{v}_2 \cdot \tau_j, \tag{2.19}$$

the weak formulation of Problem 3 reads as follows:

Problem 4 *Find* $\mathbf{u}_1^0 \in H_1$, $\phi_0 \in H_2$ *and* $p \in Q$ *such that:*

$$\begin{aligned} a_{\mathcal{D}}(\phi_0, \psi) - \int_\Gamma \epsilon\psi(\mathbf{u}_1^0 + \mathbf{u}_e)\cdot\mathbf{n}_1 = \\ = \int_{\Omega_2} f_2\ \psi - a_{\mathcal{D}}(\phi_e, \psi) - \int_{\Gamma_2^N} \phi^N\psi, \quad \forall\psi \in H_2 \\ a_{\mathcal{S}}(\mathbf{u}_1^0, \mathbf{w}) - \int_{\Omega_1} p\ div\,\mathbf{w} + \int_\Gamma g(\phi_0+\phi_e)\mathbf{n}_1\cdot\mathbf{w} = \\ = \int_{\Gamma_1^N} m\mathbf{n}_1\cdot\mathbf{w} + \int_{\Omega_1} [\mathbf{f}_1\ + 2\nu div\,\mathbf{D}(\mathbf{u}_e)]\cdot\mathbf{w}, \quad \forall\mathbf{w}\in H_1 \\ \int_{\Omega_1} q\,div\,\mathbf{u}_1^0 = -\int_{\Omega_1} q\,div\,\mathbf{u}_e, \qquad \forall q \in Q \end{aligned}$$

were the third equation reflects the incompressibility condition. ■

In order to prove existence and uniqueness of a solution of the coupled problem, we state some auxiliary results. Consider the Hilbert space $\mathcal{W} := H_1 \times H_2$ with the norm

$$\|W\|_{\mathcal{W}} := (\|\mathbf{w}\|^2_{H^1(\Omega_1)} + \|\psi\|^2_{H^1(\Omega_2)})^{\frac{1}{2}} \qquad \forall W = (\mathbf{w}, \psi) \in \mathcal{W}\ ,$$

and define the bilinear forms

- for all $V = (\mathbf{v}, \varphi) \in \mathcal{W}$ and all $W = (\mathbf{w}, \psi) \in \mathcal{W}$,

$$\mathcal{A}(V, W) := a_{\mathcal{S}}(\mathbf{v}, \mathbf{w}) + a_{\mathcal{D}}(\varphi, \psi) - \int_\Gamma \epsilon\psi(\mathbf{v}\cdot\mathbf{n}_1) + \int_\Gamma g\varphi(\mathbf{n}_1\cdot\mathbf{w})$$

- for all $W = (\mathbf{w}, \psi) \in \mathcal{W}$ and all $q \in Q$,

$$\mathcal{B}(W, q) := -\int_{\Omega_1} q\mathrm{div}\mathbf{w}$$

as well as the linear functional

- for all $W = (\mathbf{w}, \psi) \in \mathcal{W}$

$$\begin{aligned} \langle\mathcal{F}, W\rangle := \int_{\Omega_1} \mathbf{f}_1\cdot\mathbf{w} + \int_{\Omega_2} f_2\psi - a_{\mathcal{D}}(\phi_e, \psi) + \\ + \int_{\Omega_1} 2\nu\mathrm{div}[\mathbf{D}(\mathbf{u}_e)]\cdot\mathbf{w} + \int_{\Gamma_1^N} m\mathbf{n}_1\cdot\mathbf{w} - \int_{\Gamma_2^N}\psi\phi^N\ . \end{aligned}$$

Then, Problem 4 can be formulated as:

Problem 5 *Find $U = (\mathbf{u}_1^0, \phi_0) \in \mathcal{W}$ and $p \in Q$ such that*

$$\begin{aligned} \mathcal{A}(U, W) + \mathcal{B}(W, p) &= \langle \mathcal{F}, W \rangle \quad \forall W = (\mathbf{w}, \psi) \in \mathcal{W} \\ \mathcal{B}(U, q) &= 0 \qquad\qquad \forall q \in Q \end{aligned}$$

■

Lemma 1 *[DQ03]*

1. *$\mathcal{A}(\cdot, \cdot)$ is continuous and coercive on $\mathcal{W}$ and, in particular, coercive on the space*
$$Z^0 =:= \{V \in \mathcal{W} | \mathcal{B}(V, q) = 0, \quad \forall q \in Q\} \ .$$

2. *$\mathcal{B}(\cdot, \cdot)$ is continuous on $\mathcal{W} \times Q$ and satisfies the following Brezzi–Babuska condition: There is a positive constant $C_{\mathcal{B}} > 0$ such that $\forall q \in Q$ there exists $W \in \mathcal{W}$ such that*
$$\mathcal{B}(W, q) \geq C_{\mathcal{B}} \|W\|_{\mathcal{W}} \|q\|_{L^2(\Omega_1)} \ .$$

3. *$\mathcal{F}$ is a continuous linear functional on $\mathcal{W}$*

Proof:

1. The trace inequalities (cf., e.g., [LM68])
   - $\|\mathbf{v}_{|\Gamma}\|_{\Lambda} \leq C_1 \|\mathbf{v}\|_{H^1(\Omega_1)}, \quad \forall \mathbf{v} \in H_1$
   - $\|\psi_{|\Gamma}\|_{\Lambda} \leq C_2 \|\psi\|_{H^1(\Omega_2)}, \quad \forall \psi \in H_2$

   and the Cauchy–Schwarz inequality imply the continuity of $\mathcal{A}(\cdot, \cdot)$:
   $$\mathcal{A}(V, W) \leq \gamma \|V\|_{\mathcal{W}} \|W\|_{\mathcal{W}}, \qquad \forall V, W \in \mathcal{W},$$
   where $\gamma := 2 \max\{2\nu, g M_{\mathbf{K}}, C_1 C_2 g\}$, and $M_{\mathbf{K}} = \sup_{\|\alpha\|=1} \frac{\alpha \cdot \mathbf{K} \cdot \alpha}{\epsilon}$.
   The coercivity is a consequence of Korn's inequality (cf., e.g., [QV99])
   $$\int_{\Omega_1} \mathbf{D}(\mathbf{v}) : \mathbf{D}(\mathbf{v}) \geq \frac{\kappa_1}{4} \|\mathbf{v}\|^2_{H^1(\Omega_1)} \quad , \quad \mathbf{v} \in H_1 \ ,$$

and the Poincaré inequality (cf., e.g., [QV94])

$$\|\psi\|^2_{L^2(\Omega_2)} \leq C_P \| \, |\mathrm{grad}\psi| \, \|^2_{L^2(\Omega_2)} \quad \forall \, \psi \in H_2 \ ,$$

which give

$$\mathcal{A}(V,V) \geq C_{\mathcal{A}} \|V\|^2_{\mathcal{W}}$$

with $C_{\mathcal{A}} = \frac{1}{2}\min\{\nu\kappa_1, m_{\mathbf{K}} \min(1, C_P^{-1})\}$, and $m_{\mathbf{K}} = \inf_{\|\alpha\|=1} \frac{\alpha\cdot\mathbf{K}\cdot\alpha}{\epsilon}$.

2. As far as the continuity is concerned, the Cauchy–Schwarz inequality yields

$$|\mathcal{B}(W,q)| \leq \|q\|_{L^2(\Omega_1)} \|W\|_{\mathcal{W}}, \qquad \forall \, W \in \mathcal{W}, \ q \in Q \ .$$

Moreover, it can be shown (cf., e.g., [QV99]) that there exists a constant $C_{\mathcal{B}} > 0$ such that for all $q \in Q$ there exists $\mathbf{w} \in H_1$, $\mathbf{w} \neq 0$, satisfying

$$-\int_{\Omega_1} q \mathrm{div}\ \mathbf{w} \geq C_{\mathcal{B}} \|\mathbf{w}\|_{H^1(\Omega_1)} \|q\|_{L^2(\Omega_2)} \ ,$$

which allows to conclude by choosing $W = (\mathbf{w}, 0) \in \mathcal{W}$.

3. Finally, the Cauchy–Schwarz inequality and the trace inequalities give

$$|\langle \mathcal{F}, W \rangle| \leq \sqrt{2} C_{\mathcal{F}} \|W\|_{\mathcal{W}},$$

where $C_{\mathcal{F}} = \max\{\|\mathbf{f}_1\|_{L^2(\Omega_1)} + 2\nu\|\mathbf{u}_e\|_{H^1(\Omega_1)} + \|m\|_{H^{1/2}(\Gamma_1^N)}, \|\mathbf{f}_2\|_{L^2(\Omega_1)} + M_{\mathbf{K}}\|\phi_e\|_{H^1(\Omega_2)} + \|\phi^N\|_{H^{1/2}(\Gamma_2^N)}\}$. ■

We can state the following theorem:

Theorem 1 *Problem 5, or equivalently Problem 3, admits a unique solution* $(\mathbf{u}_1^0, p, \phi_0) \in H_1 \times Q \times H_2$, *satisfying the following a priori estimates:*

$$\|(\mathbf{u}_1^0, \phi_0)\|_{\mathcal{W}} \leq \frac{\sqrt{2} C_{\mathcal{F}}}{C_{\mathcal{A}}},$$

$$\|p\|_{L^2(\Omega_1)} \leq \frac{\sqrt{2} C_{\mathcal{F}}}{C_{\mathcal{B}}} (1 + \frac{\gamma}{C_{\mathcal{A}}})$$

where the constants are defined as in Lemma 1.

Proof:
The proof is a straightforward consequence of the existence and uniqueness theorem of Brezzi (cf., e.g., [Bre74, GR79, BF91]). ■

2.5 Associated Poincaré–Steklov operators

As indicated in Section 1.3, a possible approach to the solution of the coupled Stokes-Darcy flow is to reduce it to the interface by a Poincaré–Steklov problem in terms of appropriate Poincaré–Steklov operators. As pointed out in [QV99], these operators are useful tools for the analysis of iterative substructuring methods, like the one that will be presented in the Chapter 3.

In this section, we address the construction of the Poincaré–Steklov operators for Problem 3 with the transmission conditions given by (2.6), (2.7), and (2.11).

As seen in Section 2.4, the transmission condition (2.11) is a restriction on the velocity field for the Stokes region entering the formulation as a natural boundary condition. It does not provide a coupling with the velocity field in the Darcy region. This coupling is in fact represented either by the balance of the normal stress on the interface (see (2.6)) or by the continuity of the flux across the interface (see (2.7)). Any of these equations can be used as the interface equation.

2.5.1 The operator for the balance of the normal stress

The transmission condition (2.6) states the continuity of the normal stress across the interface Γ, i.e., the dynamical balance on the interface. As noted before, this condition extends the hydrostatic model which requires a continuous pressure across the interface, allowing thus for a discontinuous pressure across Γ and incorporating the deviatoric stress effect due to the surface flow. We write

$$\lambda := \frac{p}{g} - \frac{2\nu}{g}\mathbf{n}_1 \cdot \mathbf{D}(\mathbf{u}_1) \cdot \mathbf{n}_1 = \phi \ . \tag{2.20}$$

We intend to reduce the coupled problem to the interface and use λ for that purpose. The idea is to solve a problem on the interface first, and then to extend the solution to the whole domain by solving two decoupled problems. To do so, we proceed as follows: Referring to the notation introduced in Section 1.3, we use the spaces H_1, H_2, and Q as well as $\Lambda = H^{\frac{1}{2}}(\Gamma)$, and consider the following problems:

On Ω_1 , with $K_{\mathcal{S}} = (K_{\mathcal{S}}^{\mathbf{u}}, K_{\mathcal{S}}^{p})$, such that $K_{\mathcal{S}}^{\mathbf{u}} : \Lambda \to H_1$ and $K_{\mathcal{S}}^{p} : \Lambda \to Q$, and $(\mathbf{u}_1^*, p^*) \in H_1 \times Q$, solve

$$\left\{\begin{array}{l} \mathcal{S}(K^{\mathbf{u}}_{\mathcal{S}}\lambda, K^{p}_{\mathcal{S}}\lambda) = 0 \text{ in } \Omega_1 \\ \mathbf{B}_{\mathcal{S}}(K^{\mathbf{u}}_{\mathcal{S}}\lambda) = 0 \text{ on } \partial\Omega_1\backslash\Gamma \\ \dfrac{1}{g}(K^{p}_{\mathcal{S}}\lambda) - \dfrac{2\nu}{g}\mathbf{n}_1\cdot\mathbf{D}(K^{\mathbf{u}}_{\mathcal{S}}\lambda)\cdot\mathbf{n}_1 = \lambda \\ \qquad\qquad\qquad\qquad\qquad\qquad \text{on } \Gamma \\ -\dfrac{2\nu}{g}\mathbf{n}_1\cdot\mathbf{D}(K^{\mathbf{u}}_{\mathcal{S}}\lambda)\cdot\tau_j = -\dfrac{\alpha\nu}{\tau_j\cdot\kappa\cdot\tau_j}K^{\mathbf{u}}_{\mathcal{S}}\lambda\cdot\tau_j \\ \qquad\qquad\qquad\qquad\qquad\qquad j=1,2 \text{ on } \Gamma \end{array}\right. \qquad \left\{\begin{array}{l} \mathcal{S}(\mathbf{u}^*_1, p^*) = \mathbf{f}_1 \text{ in } \Omega_1 \\ \mathbf{B}_{\mathcal{S}}(\mathbf{u}^*_1) = \mathbf{g}_1 \text{ on } \partial\Omega_1\backslash\Gamma \\ \dfrac{1}{g}p^* - \dfrac{2\nu}{g}\mathbf{n}_1\cdot\mathbf{D}(\mathbf{u}^*_1)\cdot\mathbf{n}_1 = 0 \\ \qquad\qquad\qquad\qquad\qquad\qquad \text{on } \Gamma \\ -\dfrac{2\nu}{g}\mathbf{n}_1\cdot\mathbf{D}(\mathbf{u}^*_1)\cdot\tau_j = 0 \\ \qquad\qquad\qquad\qquad\qquad\qquad j=1,2 \text{ on } \Gamma \end{array}\right. \tag{2.21}$$

On Ω_2 , with $K_{\mathcal{D}} : \Lambda \to H_2$, and $\phi^* \in H_2$, solve

$$\left\{\begin{array}{l} \mathcal{D}(K_{\mathcal{D}}\lambda) = 0 \text{ in } \Omega_2 \\ \mathbf{B}_{\mathcal{D}}(K_{\mathcal{D}}\lambda) = 0 \text{ on } \partial\Omega_2\backslash\Gamma \\ K_{\mathcal{D}}\lambda = \lambda \text{ on } \Gamma \end{array}\right. \qquad \left\{\begin{array}{l} \mathcal{D}(\phi^*) = \mathbf{f}_2 \text{ in } \Omega_2 \\ \mathbf{B}_{\mathcal{D}}(\phi^*) = \mathbf{g}_2 \text{ on } \partial\Omega_2\backslash\Gamma \\ \phi^* = 0 \text{ on } \Gamma \end{array}\right. \tag{2.22}$$

Lemma 2 *Let λ be the solution of the Poincaré–Steklov problem*

$$\mathbf{n}_1\cdot\left[K^{\mathbf{u}}_{\mathcal{S}}\lambda + \frac{1}{\epsilon}\mathbf{K}\cdot \mathit{grad}(K_{\mathcal{D}}\lambda)\right] = -\mathbf{n}_1\cdot\left[\mathbf{u}^*_1 + \frac{1}{\epsilon}\mathbf{K}\cdot \mathit{grad}(\phi^*)\right] \quad \textit{on } \Gamma. \tag{2.23}$$

Then, the solution of Problem 3 is given as follows

$$\left[\begin{array}{c} \mathbf{u}_1 \\ p \end{array}\right] = \left[\begin{array}{c} K^{\mathbf{u}}_{\mathcal{S}}\lambda + \mathbf{u}^*_1 \\ K^{p}_{\mathcal{S}}\lambda + p^* \end{array}\right] \quad , \quad \phi = K_{\mathcal{D}}\lambda + \phi^* \ .$$

Remark
The Poincaré–Steklov problem is nothing but an expression of the continuity of the normal component of the velocity across the interface. In fact,

$$\mathbf{n}_1\cdot[K^{\mathbf{u}}_{\mathcal{S}}\lambda + \mathbf{u}^*_1] = -\mathbf{n}_1\cdot\left[\frac{1}{\epsilon}\mathbf{K}\cdot\mathrm{grad}(K_{\mathcal{D}}\lambda + \phi^*)\right] \quad \text{on } \Gamma \ ,$$

$$\mathbf{n}_1\cdot\mathbf{u}_1 = -\mathbf{n}_1\cdot\frac{1}{\epsilon}\mathbf{K}\cdot\mathrm{grad}(\phi) = \mathbf{n}_1\cdot\mathbf{u}_2 = -\mathbf{n}_2\cdot\mathbf{u}_2 \quad \text{on } \Gamma \ .$$

Proof:
By direct inspection, it can be seen that the functions $(\mathbf{u}_1, p) = (K^{\mathbf{u}}_{\mathcal{S}}\lambda + \mathbf{u}^*_1, K^{p}_{\mathcal{S}}\lambda + p^*)$ and $\phi = K_{\mathcal{D}}\lambda + \phi^*$ satisfy $\mathcal{S}(K^{\mathbf{u}}_{\mathcal{S}}\lambda + \mathbf{u}^*_1, K^{p}_{\mathcal{S}}\lambda + p^*) = \mathbf{f}_1$ and $\mathcal{D}(K_{\mathcal{D}}\lambda + \phi^*) = f_2$, i.e., (2.12.a), (2.12.b) , and (2.13.a) , (2.13.b). Moreover, they satisfy the boundary conditions $\mathbf{B}_{\mathcal{S}}$ on $\partial\Omega_1\backslash\Gamma$ –Equations 2.12.c and 2.12.d– and $\mathbf{B}_{\mathcal{D}}$ on $\partial\Omega_2\backslash\Gamma$, i.e., (2.13.c) and (2.13.d). With regard to the

transmission conditions, these functions satisfy the Beavers/Joseph/Saffman condition (2.11) as well as the continuity of the normal stress (2.6). The continuity of the normal velocity is guaranteed, since λ is the solution of the Poincaré–Steklov problem (2.23). ■

Lemma 3 *Properties of the Poincaré–Steklov operator*

1. *The Poincaré–Steklov operator can be split according to* $S = S_{\mathcal{S}} + S_{\mathcal{D}}$.
2. $S_{\mathcal{S}}$ *is continuous.*
3. $S_{\mathcal{D}}$ *is symmetric, continuous, and coercive.*

Proof:

1. In view of (2.23), for $\eta, \mu \in \Lambda$ we have

$$\langle S_{\mathcal{S}}\eta, \mu\rangle := \int_\Gamma \mu(\mathbf{n}_1 \cdot K^{\mathbf{u}}_{\mathcal{S}}\eta)_{|\Gamma} \ ,$$

   and

$$\langle S_{\mathcal{D}}\eta, \mu\rangle := \int_\Gamma \frac{\mu}{\epsilon}\mathbf{n}_2 \cdot [\mathbf{K} \cdot \mathrm{grad}(K_{\mathcal{D}}\eta)]_\Gamma \ ,$$

   where $< \cdot, \cdot >$ refers to the dual pairing between Λ and Λ'.

2. Consider an arbitrary extension operator $H : \Lambda \to H_1$ vanishing on $\partial\Omega_1\backslash\Gamma$ and satisfying $H\mu \cdot \mathbf{n}_1 = \mu$ on Γ. We obtain

$$\int_{\partial\Omega_1\backslash\Gamma} \mathbf{n}_1 \cdot K^{\mathbf{u}}_{\mathcal{S}}\eta(H\mu \cdot \mathbf{n}_1) = 0 \ .$$

   With this and together with the above expression for $\langle S_{\mathcal{S}}\eta, \mu\rangle$, we write

$$\begin{aligned}
\langle S_{\mathcal{S}}\eta, \mu\rangle &= \int_\Gamma \mathbf{n}_1 \cdot K^{\mathbf{u}}_{\mathcal{S}}\eta(H\mu \cdot \mathbf{n}_1) + \int_{\partial\Omega_1\backslash\Gamma} \mathbf{n}_1 \cdot K^{\mathbf{u}}_{\mathcal{S}}\eta(H\mu \cdot \mathbf{n}_1) \\
&= \int_{\partial\Omega_1} \mathbf{n}_1 \cdot K^{\mathbf{u}}_{\mathcal{S}}\eta(H\mu \cdot \mathbf{n}_1) = \int_{\Omega_1} \mathrm{div}\,(K^{\mathbf{u}}_{\mathcal{S}}\eta(H\mu \cdot \mathbf{n}_1)) = \\
&= \int_{\Omega_1} (K^{\mathbf{u}}_{\mathcal{S}}\eta \cdot \mathrm{grad}(H\mu \cdot \mathbf{n}_1)) + \int_{\Omega_1} (H\mu \cdot \mathbf{n}_1)\mathrm{div}\,(K^{\mathbf{u}}_{\mathcal{S}}\eta) \ .
\end{aligned}$$

The second integral vanishes because $\operatorname{div}(K^{\mathbf{u}}_{\mathcal{S}}\eta) = 0$ in Ω_1, and hence,

$$\langle S_{\mathcal{S}}\eta, \mu\rangle = \int_{\Omega_1} (K^{\mathbf{u}}_{\mathcal{S}}\eta \cdot \operatorname{grad}(H\mu \cdot \mathbf{n}_1)) \ . \tag{2.24}$$

Choosing H as a harmonic extension, and in view of (2.24), we get

$$\begin{aligned}
\left| \int_{\Omega_1} ([K_{\mathcal{S}}\eta]_{\mathbf{u}} \cdot \operatorname{grad}(H\mu \cdot \mathbf{n}_1)) \right| &= |\, ([K_{\mathcal{S}}\eta]_{\mathbf{u}}, (H\mu \cdot \mathbf{n}_1)')_{L^2} \,| \\
&\leq \|[K_{\mathcal{S}}\eta]_{\mathbf{u}}\|_{L^2} \, \|(H\mu \cdot \mathbf{n}_1)'\|_{L^2} \\
&\leq \|[K_{\mathcal{S}}\eta]_{\mathbf{u}}\|_{1,\Omega_1} \, \|(H\mu \cdot \mathbf{n}_1)\|_{1,\Omega_1} \\
&\leq \hat{C}_K \|[K_{\mathcal{S}}\eta]_{\mathbf{u}}\|_{\Lambda} \, \hat{C}_H \|(\mu)\|_{\Lambda} \\
&\leq \hat{C}_1 \|[K_{\mathcal{S}}\eta]_{\mathbf{u}}\|_{\Lambda} \, \|(\mu)\|_{\Lambda} \ ,
\end{aligned}$$

which proves continuity.

3. For $\eta, \mu \in \Lambda$, we consider

$$\langle S_{\mathcal{D}}\eta, \mu\rangle = \int_{\Gamma} \frac{\mu}{\epsilon} \mathbf{n}_2 \cdot \mathbf{K} \cdot \operatorname{grad}(K_{\mathcal{D}}\eta) \ .$$

Due to the fact that $\int_{\partial\Omega_2 \setminus \Gamma} \frac{K_{\mathcal{D}}\mu}{\epsilon} \mathbf{n}_2 \cdot \mathbf{K} \cdot \operatorname{grad}(K_{\mathcal{D}}\eta) = 0$, we can write

$$\begin{aligned}
\langle S_{\mathcal{D}}\eta, \mu\rangle &= \int_{\partial\Omega_2} \frac{K_{\mathcal{D}}\mu}{\epsilon} \mathbf{n}_2 \cdot \mathbf{K} \cdot \operatorname{grad}(K_{\mathcal{D}}\eta) = \\
&= \int_{\Omega_2} \operatorname{div}\left[\frac{K_{\mathcal{D}}\mu}{\epsilon} \mathbf{K} \cdot \operatorname{grad}(K_{\mathcal{D}}\eta) \right] = \\
&= \int_{\Omega_2} \left[\operatorname{grad} K_{\mathcal{D}}\mu \cdot \frac{\mathbf{K}}{\epsilon} \cdot \operatorname{grad}(K_{\mathcal{D}}\eta) \right] + \\
&\qquad + \int_{\Omega_2} \frac{K_{\mathcal{D}}\mu}{\epsilon} \operatorname{div}\left[\mathbf{K} \cdot \operatorname{grad}(K_{\mathcal{D}}\eta) \right] \ .
\end{aligned}$$

The second integral vanishes, since $\mathcal{D}(K_{\mathcal{D}}\eta) = 0$ in Ω_2, whence

$$\langle S_{\mathcal{D}}\eta, \mu\rangle = \int_{\Omega_2} \left[\operatorname{grad}(K_{\mathcal{D}}\mu) \cdot \frac{\mathbf{K}}{\epsilon} \cdot \operatorname{grad}(K_{\mathcal{D}}\eta) \right] \tag{2.25}$$

which readily shows symmetry.

Moreover, with $M_{\mathbf{K}} > 0$, $M_{\mathbf{K}} = \sup_{\|\alpha\|=1} \frac{\alpha \cdot \mathbf{K} \cdot \alpha}{\epsilon}$, it follows that

$$\begin{aligned} |\langle S_{\mathcal{D}}\eta, \mu\rangle| &\leq M_{\mathbf{K}} \, |((K_{\mathcal{D}}\eta)', (K_{\mathcal{D}}\mu)')_{L^2}| \\ &\leq M_{\mathbf{K}} \|(K_{\mathcal{D}}\eta)'\|_{L^2} \, \|(K_{\mathcal{D}}\mu)'\|_{L^2} \\ &\leq M_{\mathbf{K}} \|K_{\mathcal{D}}\mu\|_{1,\Omega_2} \|K_{\mathcal{D}}\eta\|_{1,\Omega_2} \ . \end{aligned}$$

Using $\|K_{\mathcal{D}}\mu\| \leq_{1,\Omega_2} \hat{C}\|\mu\|_{\Lambda}$, $\forall \mu \in \Lambda$, we get

$$|\langle S_{\mathcal{D}}\eta, \mu\rangle| \leq M_{\mathbf{K}} \hat{C}_2^2 \|K_{\mathcal{D}}\mu\|_{\Lambda} \|K_{\mathcal{D}}\eta\|_{\Lambda} \ ,$$

which proves continuity.
Now, setting $m_{\mathbf{K}} > 0$, $m_{\mathbf{K}} = \inf_{\|\alpha\|=1} \frac{\alpha \cdot \mathbf{K} \cdot \alpha}{\epsilon}$, we have

$$\langle S_{\mathcal{D}}\eta, \eta\rangle \geq m_{\mathbf{K}} |K_{\mathcal{D}}\eta|^2_{1,\Omega 2} \ .$$

By Poincaré's inequality

$$\langle S_{\mathcal{D}}\eta, \eta\rangle \geq \frac{m_{\mathbf{K}}}{C_P} \|K_{\mathcal{D}}\eta\|^2_{1,\Omega 2} \ ,$$

and recalling that $\|K_{\mathcal{D}}\eta\|_{1,\Omega_2} \geq \check{C}\|\eta\|_{\Lambda}$, $\forall \eta \in \Lambda$, we conclude

$$\langle S_{\mathcal{D}}\eta, \eta\rangle \geq \frac{m_{\mathbf{K}} \check{C}^2}{C_P} \|\eta\|^2_{\Lambda} \ ,$$

which proves coercivity.

■

2.5.2 The operator for the continuity of the flux

The transmission condition (2.7) states the continuity of flux across Γ as well as the non-existence of sources. With the help of Darcy's law (2.13.b), we define λ according to

$$\lambda := \mathbf{u}_1 \cdot \mathbf{n}_1 = -\mathbf{u}_2 \cdot \mathbf{n}_2 = \frac{1}{\epsilon} \mathbf{n}_2 \cdot \mathbf{K} \cdot \text{grad } \phi. \text{ on } \Gamma \ . \tag{2.26}$$

As before, using the spaces H_1, H_2, Q and $\Lambda = H^{\frac{1}{2}}(\Gamma)$, we consider the problem:

On Ω_1 , with $K_{\mathcal{S}} = (K^{\mathbf{u}}_{\mathcal{S}}, K^{p}_{\mathcal{S}})$, such that $K^{\mathbf{u}}_{\mathcal{S}} : \Lambda \to H_1$ and $K^{p}_{\mathcal{S}} : \Lambda \to Q$

$$\left\{\begin{array}{l} \mathcal{S}(\mathbf{v}, K^p_{\mathcal{S}} p) = 0 \text{ in } \Omega_1 \\ \mathbf{B}_{\mathcal{S}}(\mathbf{v}) = 0 \text{ on } \partial\Omega_1 \backslash \Gamma \\ K^{\mathbf{u}}_{\mathcal{S}} \lambda = \lambda \text{ on } \Gamma \\ -2\nu \mathbf{n}_1 \cdot \mathbf{D}(\mathbf{v}) \cdot \tau_j = -\frac{\alpha\nu}{\sqrt{\tau_j \cdot \kappa \cdot \tau_j}} \mathbf{v} \cdot \tau_j, \\ \qquad\qquad\qquad\qquad j = 1, 2 \text{ on } \Gamma \end{array}\right. \qquad \left\{\begin{array}{l} \mathcal{S}(\mathbf{u}_1^*, p^*) = \mathbf{f}_1 \text{ in } \Omega_1 \\ \mathbf{B}_{\mathcal{S}}(\mathbf{u}_1^*) = \mathbf{g}_1 \text{ on } \partial\Omega_1 \backslash \Gamma \\ \mathbf{u}_1^* = 0 \text{ on } \Gamma \\ -2\nu \mathbf{n}_1 \cdot \mathbf{D}(\mathbf{u}_1^*) \cdot \tau_j = 0, \\ \qquad\qquad\qquad\qquad j = 1, 2 \text{ on } \Gamma. \end{array}\right. \tag{2.27}$$

On Ω_2 , with $K_{\mathcal{D}} : \Lambda \to H_2$

$$\left\{\begin{array}{l} \mathcal{D}(K_{\mathcal{D}} \lambda) = 0 \text{ in } \Omega_2 \\ \mathbf{B}_{\mathcal{D}}(K_{\mathcal{D}} \lambda) = 0 \text{ on } \partial\Omega_2 \backslash \Gamma \\ -\frac{1}{\epsilon} \mathbf{n}_2 \cdot \mathbf{K} \cdot \text{grad } (K_{\mathcal{D}} \lambda) = \lambda \\ \qquad\qquad\qquad\qquad \text{on } \Gamma \end{array}\right. \qquad \left\{\begin{array}{l} \mathcal{D}(\phi^*) = \mathbf{f}_2 \text{ in } \Omega_2 \\ \mathbf{B}_{\mathcal{D}}(\phi^*) = \mathbf{g}_2 \text{ on } \partial\Omega_2 \backslash \Gamma \\ -\frac{1}{\epsilon} \mathbf{n}_2 \cdot \mathbf{K} \cdot \text{grad } (K_{\mathcal{D}} \phi^*) = 0 \\ \qquad\qquad\qquad\qquad \text{on } \Gamma \end{array}\right. \tag{2.28}$$

We note that in the previous formulation we have split the velocity by means of

$$\mathbf{v} = K^{\mathbf{u}}_{\mathcal{S}} \lambda + \mathbf{u}_1^0 \cdot \tau_1 + \mathbf{u}_1^0 \cdot \tau_2 \ , \tag{2.29}$$

separating explicitly the normal and the tangential components of the velocity and using the fact that the normal component is given by the extension of λ to Ω_1.

Lemma 4 *Let λ be the solution of the Poincaré–Steklov problem*

$$-K^p_{\mathcal{S}} p + 2\nu \mathbf{n}_1 \cdot \mathbf{D}(K^{\mathbf{u}}_{\mathcal{S}} \lambda) \cdot \mathbf{n}_1 + g K_{\mathcal{D}} \lambda = p^* - 2\nu \mathbf{n}_1 \cdot \mathbf{D}(\mathbf{u}_1^*) \cdot \mathbf{n}_1 - g\phi^* \ \ \textit{on } \Gamma \ . \tag{2.30}$$

Then, the solution of Problem 3 is given by

$$\left[\begin{array}{c} \mathbf{u}_1 \\ p \end{array}\right] = \left[\begin{array}{c} \mathbf{v} + \mathbf{u}_1^* \\ K^p_{\mathcal{S}} p + p^* \end{array}\right] \quad , \quad \phi = K_{\mathcal{D}} \ \lambda + \phi^* \ .$$

Remark
The Poincaré–Steklov problem is nothing but an expression of the continuity of the normal stress across the interface. Indeed, observing

$$\mathbf{n}_1 \cdot \mathbf{D}(K^{\mathbf{u}}_{\mathcal{S}} \lambda) \cdot \mathbf{n}_1 = \mathbf{n}_1 \cdot \mathbf{D}(\mathbf{v}) \cdot \mathbf{n}_1 \ ,$$

we can write

$$(K_{\mathcal{S}}^p p + p^*) - 2\nu \mathbf{n}_1 \cdot \mathbf{D}(\mathbf{v} + \mathbf{u}_1^*) \cdot \mathbf{n}_1 = g(K_{\mathcal{D}}\lambda + \phi^*) \text{ on } \Gamma \ ,$$

which coincides with (2.6).

Proof:
By direct inspection, it can be seen that the functions $(\mathbf{v} + \mathbf{u}_1^*, K_{\mathcal{S}}^p p + p^*)$ and $K_{\mathcal{D}}\lambda + \phi^*$ satisfy $\mathcal{S}(\mathbf{v} + \mathbf{u}_1^*, K_{\mathcal{S}}^p p + p^*) = \mathbf{f}_1$ and $\mathcal{D}(K_{\mathcal{D}}\lambda + \phi^*) = f_2$, i.e., (2.12.a), (2.12.b), and (2.13.a), (2.13.b). Moreover, they satisfy the boundary conditions $\mathbf{B}_{\mathcal{S}}$ on $\partial\Omega_1\backslash\Gamma$ (see (2.12.c) and (2.12.d)) and $\mathbf{B}_{\mathcal{D}}$ on $\partial\Omega_2\backslash\Gamma$ (see (2.13.c) and (2.13.d)). With regard to the transmission conditions, these functions satisfy the Beavers/Joseph/Saffman condition (2.11) as well as the continuity of the normal component of the velocity (2.7). The continuity of the normal stress is guaranteed, since λ is the solution of the Poincaré–Steklov problem (2.30). ■

In order to analyze the properties of the Poincaré–Steklov operator, we write the dual pairing between Λ and Λ', $\langle S\eta, \mu\rangle$ as follows

$$\langle S\eta, \mu\rangle = -\int_\Gamma \mu K_{\mathcal{S}}^p \eta + \int_\Gamma 2\nu \mathbf{n}_1 \cdot \left[\mathbf{D}\left(K_{\mathcal{S}}^{\mathbf{u}}\eta\right)\right]_\Gamma \cdot \mathbf{n}_1 \mu + \int_\Gamma \mu g(K_{\mathcal{D}}\eta)_{|\Gamma} \ .$$

We consider the first integral and an arbitrary extension $H\mu$ of μ vanishing on $\partial\Omega_1\backslash\Gamma$ such that $H\mu \cdot \mathbf{n}_1 = \mu$ on Γ:

$$\begin{aligned}\int_\Gamma \mu K_{\mathcal{S}}^p \eta &= \int_{\partial\Omega_1\backslash\Gamma} (H\mu \cdot \mathbf{n}_1) K_{\mathcal{S}}^p \eta + \int_\Gamma (H\mu \cdot \mathbf{n}_1) K_{\mathcal{S}}^p \eta = \\ &= \int_{\partial\Omega_1} (H\mu \cdot \mathbf{n}_1) K_{\mathcal{S}}^p \eta = \int_{\Omega_1} \operatorname{div}\left[(H\mu) K_{\mathcal{S}}^p \eta\right] \ ,\end{aligned}$$

where we have used the Gauss theorem. Moreover,

$$\int_{\Omega_1} \operatorname{div}\left[(H\mu) K_{\mathcal{S}}^p \eta\right] = \int_{\Omega_1} \operatorname{div}(H\mu) K_{\mathcal{S}}^p \eta + \int_{\Omega_1} (H\mu) \cdot \operatorname{grad}\left[K_{\mathcal{S}}^p \eta\right] \ . \tag{2.31}$$

Next, we consider the second integral and an arbitrary extension $H\mu$ of μ

$$\begin{aligned}&\int_\Gamma 2\nu\mu \mathbf{n}_1 \cdot \mathbf{D}(K_{\mathcal{S}}^{\mathbf{u}}\eta) \cdot \mathbf{n}_1 = \\ &= \int_{\partial\Omega_1\backslash\Gamma} 2\nu \left[(H\mu) \cdot \mathbf{n}_1\right] \mathbf{n}_1 \cdot \mathbf{D}(K_{\mathcal{S}}^{\mathbf{u}}\eta) \cdot \mathbf{n}_1 + \int_\Gamma 2\nu \left[(H\mu) \cdot \mathbf{n}_1\right] \mathbf{n}_1 \cdot \mathbf{D}(K_{\mathcal{S}}^{\mathbf{u}}\eta) \cdot \mathbf{n}_1 = \\ &= \int_{\partial\Omega_1} 2\nu \left[(H\mu) \cdot \mathbf{n}_1\right] \mathbf{n}_1 \cdot \mathbf{D}(K_{\mathcal{S}}^{\mathbf{u}}\eta) \cdot \mathbf{n}_1 = \int_{\Omega_1} \operatorname{div}\left[2\nu \left[(H\mu) \cdot \mathbf{n}_1\right] \mathbf{n}_1 \cdot \mathbf{D}(K_{\mathcal{S}}^{\mathbf{u}}\eta)\right] \ .\end{aligned}$$

We have

$$\int_{\Omega_1} \operatorname{div}\left[2\nu\left[(H\mu)\cdot\mathbf{n}_1\right]\mathbf{n}_1\cdot\mathbf{D}(K_{\mathcal{S}}^{\mathbf{u}}\eta)\right] =$$
$$= \int_{\Omega_1} 2\nu\mathbf{D}(K_{\mathcal{S}}^{\mathbf{u}}\eta) : \operatorname{grad}(H\mu) + \int_{\Omega_1}\left[(H\mu)\cdot\mathbf{n}\right]\operatorname{div}\left[2\nu\mathbf{n}_1\cdot\mathbf{D}(K_{\mathcal{S}}^{\mathbf{u}}\eta)\right] \ .$$

Due to the symmetry of $\mathbf{D}(\cdot)$, this can be written as

$$\int_{\Omega_1} \operatorname{div}\left[2\nu(H\mu)\mathbf{n}_1\cdot\mathbf{D}(K_{\mathcal{S}}^{\mathbf{u}}\eta)\right] =$$
$$= \int_{\Omega_1} 2\nu\mathbf{D}(K_{\mathcal{S}}^{\mathbf{u}}\eta) : \mathbf{D}(H\mu) + \int_{\Omega_1}(H\mu)\cdot\operatorname{div}\left[2\nu\mathbf{n}_1\cdot\mathbf{D}(K_{\mathcal{S}}^{\mathbf{u}}\eta)\right] \ . \tag{2.32}$$

Subtracting the last integral in (2.32) from the last integral in (2.31), we obtain

$$\int_{\Omega_1}(H\mu)\cdot\operatorname{grad}\left[K_{\mathcal{S}}^{p}\eta\right] - \int_{\Omega_1}(H\mu)\cdot\operatorname{div}\left[2\nu\mathbf{n}_1\cdot\mathbf{D}(K_{\mathcal{S}}^{\mathbf{u}}\eta)\right] =$$
$$= \int_{\Omega_1}(H\mu)\cdot\left\{\operatorname{grad}\left[K_{\mathcal{S}}^{p}\eta\right] - \operatorname{div}\left[2\nu\mathbf{n}_1\cdot\mathbf{D}(K_{\mathcal{S}}^{\mathbf{u}}\eta)\right]\right\} = 0.$$

In fact, the terms between brackets vanish due to $\mathcal{S}(K_{\mathcal{S}}^{\mathbf{u}}\eta, K_{\mathcal{S}}^{p}\eta) = 0$ in Ω_1. The resulting expression for $\langle S\eta, \mu\rangle$ is

$$\langle S\eta,\mu\rangle = -\int_{\Omega_1}\operatorname{div}(H\mu)K_{\mathcal{S}}^{p}\eta + \int_{\Omega_1} 2\nu\mathbf{D}(K_{\mathcal{S}}^{\mathbf{u}}\eta) : \mathbf{D}(H\mu) + \int_{\Gamma}\mu g(K_{\mathcal{D}}\eta)_{|\Gamma} \ . \tag{2.33}$$

The following properties will be used later to derive convergence results.

Lemma 5 *Properties of the Poincaré–Steklov operator*

1. *The Poincaré–Steklov operator can be split according to* $S = S_{\mathcal{S}} + S_{\mathcal{D}}$.
2. $S_{\mathcal{S}}$ *is symmetric, continuous, and coercive.*
3. $S_{\mathcal{D}}$ *is symmetric, continuous, and coercive.*

Proof:

1. In view of (2.33), we define

$$\langle S_{\mathcal{S}}\eta, \mu\rangle := -\int_{\Omega_1} \operatorname{div}(H\mu) K^p_{\mathcal{S}}\eta + \int_{\Omega_1} 2\nu \mathbf{D}(K^{\mathbf{u}}_{\mathcal{S}}\eta) : \mathbf{D}(H\mu) \ , \tag{2.34}$$

   and

$$\langle S_{\mathcal{D}}\eta, \mu\rangle := \int_{\Gamma} \mu g (K_{\mathcal{D}}\eta)_{|\Gamma} \ . \tag{2.35}$$

2. We choose $H\mu = K^{\mathbf{u}}_{\mathcal{S}}\mu$ in (2.36) and obtain

$$\langle S_{\mathcal{S}}\eta, \mu\rangle = -\int_{\Omega_1} \operatorname{div}(K^{\mathbf{u}}_{\mathcal{S}}\mu) K^p_{\mathcal{S}}\eta + \int_{\Omega_1} 2\nu \mathbf{D}(K^{\mathbf{u}}_{\mathcal{S}}\eta) : \mathbf{D}(K^{\mathbf{u}}_{\mathcal{S}}\mu) \ .$$

   Furthermore, observing $\int_{\Omega_1} q \ \operatorname{div}(K^{\mathbf{u}}_{\mathcal{S}}\eta) = 0$ for all $q \in Q$, it follows that

$$\langle S_{\mathcal{S}}\eta, \mu\rangle = \int_{\Omega_1} 2\nu \mathbf{D}(K^{\mathbf{u}}_{\mathcal{S}}\eta) : \mathbf{D}(K^{\mathbf{u}}_{\mathcal{S}}\mu) \ . \tag{2.36}$$

   We have

$$\begin{aligned} \left| \int_{\Omega_1} 2\nu \mathbf{D}(K^{\mathbf{u}}_{\mathcal{S}}\eta) : \mathbf{D}(K^{\mathbf{u}}_{\mathcal{S}}\mu) \right| &= 2\nu | \left((K^{\mathbf{u}}_{\mathcal{S}}\eta)', (K^{\mathbf{u}}_{\mathcal{S}}\mu)' \right)_{L^2} | \\ &\leq 2\nu \|(K^{\mathbf{u}}_{\mathcal{S}}\eta)'\|_{L^2} \ \|(K^{\mathbf{u}}_{\mathcal{S}}\mu)'\|_{L^2} \\ &\leq 2\nu \|(K^{\mathbf{u}}_{\mathcal{S}}\eta)\|_{1,\Omega_1} \ \|(K^{\mathbf{u}}_{\mathcal{S}}\mu)\|_{1,\Omega_1} \\ &\leq 2\nu \hat{C}_1^2 \|\eta\|_{\Lambda} \ \|\mu\|_{\Lambda} \ , \end{aligned}$$

   which proves continuity.
   To prove coercivity, we use the Korn's inequality (cf., e.g., [QV99]):

$$\int_{\Omega_1} \mathbf{D}(\mathbf{v}) : \mathbf{D}(\mathbf{v}) \geq \frac{\kappa_{\mathcal{S}}}{4} \|\mathbf{v}\|^2_{1,\Omega_1} \ \ \forall \ \mathbf{v} \in H_1 \ .$$

We get

$$\langle S_{\mathcal{S}}\eta,\eta\rangle = 2\nu\int_{\Omega_1}\mathbf{D}(K^{\mathbf{u}}_{\mathcal{S}}\eta):\mathbf{D}(K^{\mathbf{u}}_{\mathcal{S}}\eta) \geq \frac{\nu\kappa_{\mathcal{S}}}{2}\|K^{\mathbf{u}}_{\mathcal{S}}\eta\|^2_{1,\Omega_1}\ ,$$

and in view of the trace inequality

$$\langle S_{\mathcal{S}}\eta,\eta\rangle \geq \frac{\nu\kappa_{\mathcal{S}}}{2\tilde{C}}\|\eta\|^2_{\Lambda}\ ,$$

which proves coercivity.

3. By definition

$$\frac{1}{\epsilon}\mathbf{n}_2\cdot\mathbf{K}\cdot\mathrm{grad}(K_{\mathcal{D}}\lambda) = \lambda \quad \text{on } \Gamma\ ,$$

and hence,

$$\begin{aligned}
\int_\Gamma \frac{\mu}{\epsilon}\mathbf{n}_2\cdot[\mathbf{K}\cdot\mathrm{grad}(K_{\mathcal{D}}\lambda)]_\Gamma &= \int_\Gamma \mu\lambda \\
\int_{\partial\Omega_2}\frac{K_{\mathcal{D}}\mu}{\epsilon}\mathbf{n}_2\cdot\mathbf{K}\cdot\mathrm{grad}(K_{\mathcal{D}}\lambda) &= \int_\Gamma\mu\lambda \\
\int_{\Omega_2} g\mathrm{grad}(K_{\mathcal{D}}\mu)\mathbf{n}_2\cdot\frac{\mathbf{K}}{\epsilon}\cdot\mathrm{grad}(K_{\mathcal{D}}\lambda) = \int_\Gamma g\mu(K_{\mathcal{D}}\lambda)_{|\Gamma} &= \langle S_{\mathcal{D}}\lambda,\mu\rangle\ .
\end{aligned}$$

This gives us the symmetry.
Moreover, we can write

$$\begin{aligned}
|\langle S_{\mathcal{D}}\eta,\mu\rangle| &= \left|\int_\Gamma g(K_{\mathcal{D}}\eta)_{|\Gamma}\mu\right| \leq g\|K_{\mathcal{D}}\eta\|_{L^2(\Gamma)}\|\mu\|_{L^2(\Gamma)} \\
&\leq g\hat{C}_2\|K_{\mathcal{D}}\eta\|_{1,\Omega_2}\|\mu\|_\Lambda\ , \qquad (2.37)
\end{aligned}$$

where the trace inequality has been used. To evaluate $\|K_{\mathcal{D}}\eta\|_{1,\Omega_2}$, by a Poincaré inequality

$$\frac{1}{1+C_P^2}\|K_{\mathcal{D}}\eta\|^2_{1,\Omega_2} \leq |K_{\mathcal{D}}\eta|^2_{1,\Omega_2} = \int_{\Omega_2}\mathrm{grad}(K_{\mathcal{D}}\eta)\cdot\mathrm{grad}(K_{\mathcal{D}}\eta)\ .$$

Consequently, setting $m_{\mathbf{K}} = \inf_{\|\alpha\|=1}\frac{\alpha\cdot\mathbf{K}\cdot\alpha}{\epsilon}$, we obtain

$$\|K_{\mathcal{D}}\eta\|^2_{1,\Omega_2} \leq \frac{1+C_P^2}{m_{\mathbf{K}}}\int_{\Omega_2}\mathrm{grad}(K_{\mathcal{D}}\eta)\cdot\mathrm{grad}(K_{\mathcal{D}}\eta)\ .$$

Taking advantage of trace inequalities, we get

$$\begin{aligned}\int_{\Omega_2} \mathrm{grad}(K_{\mathcal{D}}\eta)\cdot\mathrm{grad}(K_{\mathcal{D}}\eta) &\leq \left\{\int_{\Omega_2}\mathrm{grad}^2(K_{\mathcal{D}}\eta)\right\}^{1/2}\left\{\int_{\Omega_2}\mathrm{grad}^2(K_{\mathcal{D}}\eta)\right\}^{1/2}\\ &\leq \hat{C}_2\|K_{\mathcal{D}}\eta\|_{1,\Omega_2}\|\eta\|_{\Lambda}\,.\end{aligned}$$

and hence,

$$|\langle S_{\mathcal{D}}\eta,\mu\rangle| \leq g\left[\frac{1+C_P^2}{m_{\mathbf{K}}}\right]\hat{C}_2^2\|\eta\|_{\Lambda}\|\mu\|_{\Lambda}\ ,$$

which proves continuity. The coercivity follows from

$$\begin{aligned}\langle S_{\mathcal{D}}\eta,\eta\rangle &= \int_{\Gamma} g(K_{\mathcal{D}}\eta)_{|\Gamma}\eta = \int_{\Omega_2} g\mathrm{grad}(K_{\mathcal{D}}\eta)\cdot\frac{\mathbf{K}}{\epsilon}\cdot\mathrm{grad}(K_{\mathcal{D}}\eta)\\ &\geq gm_{\mathbf{K}}|K_{\mathcal{D}}\eta|^2_{1,\Omega_1}\ .\end{aligned}$$

Using Poincaré's inequality

$$\langle S_{\mathcal{D}}\eta,\eta\rangle \geq \frac{gm_{\mathbf{K}}}{C_P}\|K_{\mathcal{D}}\eta\|^2_{1,\Omega_1}\ ,$$

and a trace inequality, we deduce $\|K_{\mathcal{D}}\eta\|_{1,\Omega_1}\geq\check{C}_2\|\eta\|_{\Lambda}$. Hence,

$$\langle S_{\mathcal{D}}\eta,\eta\rangle \geq \frac{gm_{\mathbf{K}}}{C_P}\check{C}_2^2\|\eta\|_{\Lambda}\ ,$$

which proves coercivity.

■

2.6 Finite element approximation

The finite element approximation comes up in a straightforward manner: Assume that $\Omega_{1,h}$ and $\Omega_{2,h}$ are conforming triangulations of the subdomains Ω_1,Ω_2, which match at the interface Γ. The finite element spaces are based on the following discrete spaces

$$\begin{aligned} H_{\Gamma_1,h} &:= \{v_h \in C(\overline{\Omega}_1) : v_h = 0 \text{ on } \Gamma_1^D, v_{h|E} \in \mathrm{isoP}_2(E), \forall E \in \Omega_{1,h}\} , \\ H_{1,h} &:= \{H_{\Gamma_1,h}\}^d, \\ Q_h &:= \{q_h \in C(\overline{\Omega_1}) : q_{h|E} \in P_1(E), \forall E \in \Omega_{1,h}\} , \\ H_{2,h} &:= \{\psi_h \in C(\overline{\Omega}_2) : \psi_h = 0 \text{ on } \Gamma_2^D, \psi_{h|E} \in P_1(E), \forall E \in \Omega_{2,h}\} . \end{aligned}$$

Let ϕ_h^D and $\mathbf{u}_h^D$ be the FEM analogs of ϕ_e and $\mathbf{u}_e$, respectively. Then, the following splitting is performed

$$\mathbf{u}_{1h} = \mathbf{u}_{1h}^0 + \mathbf{u}_h^D,\ \mathbf{u}_{1h}^0 \in H_{1,h} \quad , \quad \phi_h = \phi_{0h} + \phi_h^D,\ \phi_{0h} \in H_{2,h} . \tag{2.38}$$

Introducing the bilinear forms

$$a_{\mathcal{D}}^h(\lambda_h, \mu_h) := \int_{\Omega_2} \text{grad } \mu_h \cdot \mathbf{K} \cdot \text{grad } \lambda_h \ , \tag{2.39}$$

$$a_{\mathcal{S}}^h(\mathbf{v}_{1_h}, \mathbf{v}_{2_h}) := \int_{\Omega_1} 2\nu \mathbf{D}(\mathbf{v}_{1_h}) : \mathbf{D}(\mathbf{v}_{2_h}) - \sum_{i=1}^{d-1} \int_\Gamma \left[\frac{\alpha\nu}{\sqrt{\tau_j \cdot \kappa \cdot \tau_j}} \mathbf{v}_{1_h} \cdot \tau_j \right] , \tag{2.40}$$

the coupled FEM problem can be stated as follows:

Problem 6 *Find $\mathbf{u}_{1h}^0 \in H_{1,h}$, $\phi_{0h} \in H_{2,h}$ and $p_h \in Q_h$ such that:*

$$\begin{aligned} a_{\mathcal{D}}(\phi_{0h}, \psi_h) - \int_\Gamma \epsilon \psi_h (\mathbf{u}_{1h}^0 + \mathbf{u}_e) \cdot \mathbf{n}_1 = \\ = \int_{\Omega_2} f_{2h}\ \psi_h - a_{\mathcal{D}}(\phi_h^D, \psi_h) - \int_{\Gamma_2^N} \phi_h^N \psi_h, \forall \psi_h \in H_{2,h} \\ a_{\mathcal{S}}(\mathbf{u}_{1h}^0, \mathbf{w}_h) - \int_{\Omega_1} p_h\ div\, \mathbf{w}_h + \int_\Gamma g(\phi_{0h} + \phi_h^D)\mathbf{n}_1 \cdot \mathbf{w}_h = \\ = \int_{\Gamma_1^N} m_h \mathbf{n}_1 \cdot \mathbf{w}_h + \int_{\Omega_1} \left[\mathbf{f}_{1h} + 2\nu\, div\, \mathbf{D}(\mathbf{u}_h^D) \right] \cdot \mathbf{w}_h, \forall \mathbf{w}_h \in H_{1,h} \\ \int_{\Omega_1} q_h\, div\, \mathbf{u}_{1h}^0 = - \int_{\Omega_1} q_h\, div\, \mathbf{u}_h^D, \forall q_h \in Q_h \end{aligned}$$

■

The discrete counterparts of the Poincaré–Steklov problems and operators can be obtained by introducing

$$\Lambda_h := \{w_{h_{|\Gamma}} = \mathbf{w}_h \cdot \mathbf{n}_1 | \mathbf{w}_h \in H_{1,h}\} \ .$$

Discrete operators for the case of balance of normal stress

For $\eta_h, \mu_h \in \Lambda_h$, we define

$$\langle S^h_{\mathcal{S}} \eta_h, \mu_h \rangle := \int_\Gamma \mu_h (\mathbf{n}_1 \cdot K^{\mathbf{u}}_{\mathcal{S}} \eta_h)_{|\Gamma} \ , \tag{2.41}$$

$$\langle S^h_{\mathcal{D}} \eta_h, \mu_h \rangle := \int_\Gamma \frac{\mu_h}{\epsilon} \mathbf{n}_2 \cdot \mathbf{K} \cdot \mathrm{grad}(K_{\mathcal{D}} \eta_h) \ . \tag{2.42}$$

Discrete operators for the case of continuity of flux

For $\eta_h, \mu_h \in \Lambda_h$, we define

$$\langle S^h_{\mathcal{S}} \eta_h, \mu_h \rangle := -\int_{\Omega_1} \mathrm{div}(H\mu_h) K^p_{\mathcal{S}} \eta_h + \int_{\Omega_1} 2\nu \mathbf{D}(K^{\mathbf{u}}_{\mathcal{S}} \eta_h) : \mathbf{D}(H\mu_h) \ , \tag{2.43}$$

$$\langle S^h_{\mathcal{D}} \eta_h, \mu_h \rangle := \int_\Gamma \mu_h g(K_{\mathcal{D}} \eta_h)_{|\Gamma} \ . \tag{2.44}$$

Chapter 3

An iterative substructuring method

In this chapter, we discuss an iterative substructuring approach to the coupled Problem 4. As suggested in Section 1.3, the Neumann–Dirichlet iteration is constructed and analyzed on the simplified version of the problem assuming that the constant α in the Beavers/Joseph/Saffman condition is zero. This transforms the transmission condition 2.11 into a natural boundary condition. With this hypothesis and recalling the spaces defined in Section 2.4, we rewrite the coupled problem as follows:

Problem 7 *Find* $\mathbf{u}_1^0 \in H_1$, $\phi_0 \in H_2$ *and* $p \in Q$ *such that:*

$$\int_{\Omega_2} grad\ \psi \cdot \mathbf{K} \cdot grad\ \phi_0 - \int_{\Gamma} \epsilon\psi(\mathbf{u}_1^0 + \mathbf{u}_e) \cdot \mathbf{n}_1 =$$

$$= \int_{\Omega_2} f_2\ \psi - \int_{\Omega_2} grad\ \psi \cdot \mathbf{K} \cdot grad\ \phi_e - \int_{\Gamma_2^N} \phi^N \psi \qquad \forall \psi \in H_2\ ,$$

$$\int_{\Omega_1} \nu grad\ (\mathbf{u}_1^0) : grad\ \mathbf{w} - \int_{\Omega_1} p\ div\, \mathbf{w} + \int_{\Gamma} g(\phi_0 + \phi_e)\mathbf{n}_1 \cdot \mathbf{w} =$$

$$= \int_{\Gamma_1^N} m\mathbf{n}_1 \cdot \mathbf{w} + \int_{\Omega_1} [\mathbf{f}_1\ + 2\nu div\, \mathbf{D}(\mathbf{u}_e)] \cdot \mathbf{w} \qquad \forall \mathbf{w} \in H_1\ ,$$

$$\int_{\Omega_1} q div\, \mathbf{u}_1^0 = -\int_{\Omega_1} q div\, \mathbf{u}_e \qquad \forall q \in Q\ .$$

■

3.1 The Neumann–Dirichlet (N-D) iteration

In order to derive the Neumann–Dirichlet (N-D) iteration, we start from the differential form of the coupled problem. We use an approach which iteratively matches the fluxes across Γ while imposing the continuity of the normal stress across it. This is implemented by incorporating the values of the normal stress as boundary conditions on the interface to ensure continuity, and then iterating on the function λ as defined in (2.26). Recalling the notation used in Section 2.5, we consider the following subproblems:

Find $(\mathbf{u}^*, p^*) : \Omega_1 \to \Re^d \times \Re$ and $\phi^* : \Omega_2 \to \Re$, such that:

$$\begin{cases} \mathcal{S}(\mathbf{u}^*, p^*) = \mathbf{f}_1 & \text{in } \Omega_1 \\ \mathbf{B}_{\mathcal{S}}(\mathbf{u}^*) = \mathbf{g}_1 & \text{on } \partial\Omega_1 \backslash \Gamma \\ p^* - 2\nu \mathbf{n}_1 \cdot \mathbf{D}(\mathbf{u}^*) \cdot \mathbf{n}_1 = 0 & \text{on } \Gamma \\ -2\nu \mathbf{n}_1 \cdot \mathbf{D}(\mathbf{u}^*) \cdot \tau_j = 0, & j = 1, 2 \text{ on } \Gamma. \end{cases} \qquad \begin{cases} \mathcal{D}(\phi^*) = \mathbf{f}_2 & \text{in } \Omega_2 \\ \mathbf{B}_{\mathcal{D}}(\phi^*) = \mathbf{g}_2 & \text{on } \partial\Omega_2 \backslash \Gamma \\ \phi^* = 0 & \text{on } \Gamma \end{cases}$$

We define the following scheme:

Procedure 2 Differential form of the N-D iteration
Let $(\mathbf{u}^*, p^*)$ *and* ϕ^* *be given as solutions of the previous problems. For* $k \geq 0$*:*

1. *Find* ϕ_0^{k+1}*, such that*

$$\begin{cases} \mathcal{D}(\phi_0^{k+1}) = 0 & \text{in } \Omega_2 \\ \mathbf{B}_{\mathcal{D}}(\phi_0) = 0 & \text{on } \partial\Omega_2 \backslash \Gamma \\ \phi_0^{k+1} = \lambda^k & \text{on } \Gamma \end{cases}$$

   and compute $\phi^{k+1} = \phi_0^{k+1} + \phi^*$.

2. *Find* $((\mathbf{u_1^0})^{k+1}, p_0^{k+1})$*, such that*

$$\begin{cases} \mathcal{S}((\mathbf{u}_1^0)^{k+1}, p_0^{k+1}) = 0 & \text{in } \Omega_1 \\ \mathbf{B}_{\mathcal{S}}((\mathbf{u}_1^0)^{k+1}) = 0 & \text{on } \partial\Omega_1 \backslash \Gamma \\ p_0 - 2\nu \mathbf{n}_1 \cdot \mathbf{D}[(\mathbf{u}_1^0)^{k+1}] \cdot \mathbf{n}_1 = g\phi^{k+1} & \text{on } \Gamma \\ -2\nu \mathbf{n}_1 \cdot \mathbf{D}((\mathbf{u}_1^0)^{k+1}) \cdot \tau_j = 0, & j = 1, 2 \text{ on } \Gamma. \end{cases}$$

   and compute $(\mathbf{u}_1^{k+1}, p^{k+1}) = ((\mathbf{u}_1^0)^{k+1} + \mathbf{u}^*, p^{k+1} + p^*)$.

3. *Update*

$$\lambda^{k+1} = \theta \mathbf{n}_1 \cdot (\mathbf{u}_1^0)_{|\Gamma}^{k+1} + (1 - \theta)\lambda^k.$$

■

The corresponding variational form is given by:

Procedure 3 VARIATIONAL FORM OF N-D ITERATIONS
Let the initial guess $\lambda^0 \in \Lambda_h$ and the relaxation parameter θ be given. For $k \geq 0$:

1. *Find $\phi_0^{k+1} \in H_2$ such that*

$$\int_{\Omega_2} grad\ \psi \cdot \mathbf{K} \cdot grad\ \phi_0^{k+1} - \int_{\Gamma} \epsilon\psi\ \lambda^k = \\ = -\int_{\Omega_2} grad\ \psi \cdot \mathbf{K} \cdot grad\ \phi^D + \int_{\Gamma_2^N} \phi^N\ \psi + \\ + \int_{\Omega_2} f_2\ \psi\ + \int_{\Gamma} \epsilon\psi\ \lambda^D\ \forall \psi \in H_2$$

   and set $\phi^{k+1} = \phi_0^{k+1} + \phi^D$.

2. *Find $(\mathbf{u}_1^0)^{k+1} \in H_1$ and $p^{k+1} \in Q$ such that*

$$\int_{\Omega_1} \nu grad\ (\mathbf{u}_1^0)^{k+1} : grad\ \mathbf{w} - \int_{\Omega_1} p^{k+1} div\ \mathbf{w} + \\ + \int_{\Gamma} g\phi^{k+1}\mathbf{w} \cdot \mathbf{n}_1 = \int_{\Gamma_1^N} \mathbf{m} \cdot \mathbf{w} + \\ - \int_{\Omega_1} \nu grad\ \mathbf{u}^D : grad\ \mathbf{w}\ + \int_{\Omega_1} \mathbf{f}_1\ \cdot \mathbf{w}\ \ \forall \mathbf{w} \in H_1 \\ \int_{\Omega_1} q div (\mathbf{u}_1^0)^{k+1} = -\int_{\Omega_1} q div\ \mathbf{u}^D\ \ \forall q \in Q$$

   and set $\mathbf{u}_1^{k+1} = (\mathbf{u}_1^0)^{k+1} + \mathbf{u}^D$.

3. *Update*

$$\lambda^{k+1} = \theta\ (\mathbf{u}_1^0)^{k+1} \cdot \mathbf{n}_{1|\Gamma} + (1-\theta)\lambda^k\ .$$

■

3.2 Analysis of the N-D iteration

In this section, we provide an analysis of the iterative procedure. First, we derive a result that plays a central role in the convergence analysis of the N-D iteration.

Lemma 6 *The Neumann–Dirichlet iteration –Procedure 2 or equivalently Procedure 3– is equivalent to a preconditioned Richardson iteration.*

Proof:
Consider the differential form of the N-D iteration and observe the following equivalence:

$$2\nu \mathbf{n}_1 \cdot \mathbf{D}[(\mathbf{u}_1^0)^{k+1}] \cdot \mathbf{n}_1 = 2\nu \mathbf{n}_1 \cdot \mathbf{D}[(\mathbf{n}_1 \cdot \mathbf{u}_1^0)^{k+1}] \cdot \mathbf{n}_1 \ .$$

Hence, on Γ

$$p_0 + p^* - 2\nu \mathbf{n}_1 \cdot \mathbf{D}[(\mathbf{n}_1 \cdot \mathbf{u}_1^0)^{k+1} + \mathbf{u}^*] \cdot \mathbf{n}_1 = g\phi^{k+1} \quad \text{on } \Gamma \ .$$

Moreover, in view of Step 1 of Procedure 2, $\phi^{k+1} = K_{\mathcal{D}}\lambda^k + \phi^*$, whence

$$p_0 + p^* - 2\nu \mathbf{n}_1 \cdot \mathbf{D}[(\mathbf{n}_1 \cdot \mathbf{u}_1^0)^{k+1} + \mathbf{u}^*] \cdot \mathbf{n}_1 = gK_{\mathcal{D}}\lambda^k + \phi^* \quad \text{on } \Gamma \ .$$

In terms of the Poincaré–Steklov operators, we obtain

$$\begin{aligned} S_{\mathcal{S}}\tilde{\lambda} &:= -K_{\mathcal{S}}^p\tilde{\lambda} + 2\nu \mathbf{n}_1 \cdot \mathbf{D}(K_{\mathcal{S}}^{\mathbf{u}}\tilde{\lambda}) \cdot \mathbf{n}_1, \\ S_{\mathcal{D}}\tilde{\lambda} &:= gK_{\mathcal{D}}\tilde{\lambda}, \\ \chi &:= p^* - 2\nu \mathbf{n}_1 \cdot \mathbf{D}(\mathbf{u}^*) \cdot \mathbf{n}_1 - \phi^* \ , \end{aligned}$$

where $\tilde{\lambda} \in \Lambda$ is an appropriately chosen. Consequently,

$$\mathbf{n}_1 \cdot (\mathbf{u}_1^0)^{k+1} = S_{\mathcal{S}}^{-1}[\chi - S_{\mathcal{D}}\lambda^k] \ .$$

Replacing this expression in Step 3 of Procedure 2, we get

$$\begin{aligned} \lambda^{k+1} &= \theta S_{\mathcal{S}}^{-1}[\chi - S_{\mathcal{D}}\lambda^k] + (1-\theta)\lambda^k \\ \lambda^{k+1} &= \lambda^k + \theta S_{\mathcal{S}}^{-1}[\chi - S\lambda^k] \ , \end{aligned} \tag{3.1}$$

a preconditioned Richardson iteration with $S_{\mathcal{S}}$ as the preconditioner. ■

Now, we are in a position to analyze the iteration. The main result for the preconditioned Richardson iteration is the following theorem from [QV99] (cf. Theorem 4.2.2):

Theorem 2 *Consider the solution of the problem $\mathcal{Q}\lambda = \mathcal{G}$, with $\lambda \in X$, X is a Hilbert space and $\mathcal{G} \in X^*$, its dual space, and where $\mathcal{Q} = \mathcal{Q}_1 + \mathcal{Q}_2$. Suppose that $\mathcal{Q}_1$ is continuous and coercive, i.e., there exist $\beta_1 > 0$, $\alpha_1 > 0$ such that*

$$\langle \mathcal{Q}_1\eta, \mu\rangle \le \beta_1\|\eta\|_X\|\mu\|_X, \quad \langle \mathcal{Q}_1\eta, \eta\rangle \ge \alpha_1\|\eta\|_X^2 \quad \forall \eta, \mu \in X \ .$$

Also assume that $\mathcal{Q}_2$ is continuous, i.e., there exists $\beta_2 > 0$ such that

$$\langle \mathcal{Q}_2\eta, \mu\rangle \le \beta_2\|\eta\|_X\|\mu\|_X \quad \forall \eta, \mu \in X \ ,$$

and that there is some $\kappa^* > 0$ such that

$$\langle \mathcal{Q}_1\eta, \mathcal{Q}_1^{-1}\mathcal{Q}\eta\rangle + \langle \mathcal{Q}\eta, \eta\rangle \ge \kappa^*\|\eta\|^2 \ \ \forall \eta \in X \ .$$

Then, for any given λ^0 in X and for any θ satisfying $0 < \theta < \theta_{MAX}$, with

$$\theta_{MAX} := \frac{\kappa^*\alpha_1^2}{\beta_1(\beta_1 + \beta_2)^2},$$

the sequence

$$\lambda^{k+1} = \lambda^k + \theta\mathcal{Q}_1^{-1}(\mathcal{G} - \mathcal{Q}\lambda^k)$$

converges in X to the solution of the problem.

Proof:
The operator $\mathcal{Q}_1$ is invertible due to the Lax–Milgram lemma.
Let us introduce the $\mathcal{Q}_1$-inner product

$$(\eta, \mu)_{\mathcal{Q}_1} := \frac{1}{2}(\langle \mathcal{Q}_1\eta, \mu\rangle + \langle \mathcal{Q}_1\mu, \eta\rangle).$$

The corresponding $\mathcal{Q}_1$-norm $\|\eta\|_{\mathcal{Q}_1} := (\eta, \eta)_{\mathcal{Q}_1}^{1/2} = \langle \mathcal{Q}_1\eta, \eta\rangle^{1/2}$ is equivalent to the norm $\|\eta\|_X$:

$$\alpha_1\|\eta\|_X^2 \le \|\eta\|_{\mathcal{Q}_1}^2 \le \beta_1\|\eta\|_X^2 \qquad \forall\, \eta \in X \ .$$

To prove convergence of the sequence $\{\lambda^k\}$, it is sufficient to show that the mapping

$$T_\theta : X \to X, \ \ T_\theta\eta := \eta - \theta\mathcal{Q}_1^{-1}\mathcal{Q}\eta$$

is a contraction with respect to the $\mathcal{Q}_1$-norm. For $\theta \geq 0$, we have

$$\begin{aligned} \|T_\theta \eta\|^2_{\mathcal{Q}_1} &= \|\eta\|^2_{\mathcal{Q}_1} + \theta^2 \langle \mathcal{Q}\eta, \mathcal{Q}_1^{-1}\mathcal{Q}\eta\rangle - \theta\left(\langle \mathcal{Q}_2\eta, \mathcal{Q}_1^{-1}\mathcal{Q}\eta\rangle + \langle \mathcal{Q}\eta, \eta\rangle\right) \\ &\leq \|\eta\|^2_{\mathcal{Q}_1} + \theta^2 \frac{(\beta_1+\beta_2)^2}{\alpha_1^2}\|\eta\|^2_X - \theta\kappa^*\|\eta\|^2_X \ . \end{aligned}$$

Setting

$$K_\theta = 1 + \theta^2 \frac{(\beta_1+\beta_2)^2}{\alpha_1^2} - \theta\frac{\kappa^*}{\beta_1} \ ,$$

we obtain

$$\|T_\theta \eta\|^2_{\mathcal{Q}_1} \leq K_\theta \|\eta\|^2_{\mathcal{Q}_1} \ .$$

The bound $K_\theta < 1$ is guaranteed by $0 < \theta < \theta_{MAX}$. ■

Lemma 7 *The Neumann–Dirichlet iteration –Procedure 2 or equivalently Procedure 3– converges.*

Proof:
Associate the Poincaré–Steklov operator $S = S_{\mathcal{S}} + S_{\mathcal{D}}$ with the operator $\mathcal{Q} = \mathcal{Q}_1 + \mathcal{Q}_2$ in the previous theorem. Then, in view of Lemma 5 and by direct application of Theorem 2, we conclude that the preconditioned Richardson iteration converges and that this ensures the convergence of the Neumann–Dirichlet scheme. ■

Remark:
In the theorem, the contraction constant K_θ and the upper bound θ_{MAX} only depend on the constants α_1, β_1, β_2 and κ^*. Consequently, the rate of convergence of the preconditioned Richardson iteration in the $\mathcal{Q}_2$ only depends on these parameters.

In order to estimate the rate of convergence of the Richardson iteration, we proceed from the results in Section 2.5.2. As indicated before, the rate of convergence only depends on the continuity and coercivity constants of $S_{\mathcal{S}}$ and $S_{\mathcal{D}}$. With the notation used in Theorem 2 and in accordance with Lemma 5, these three constants are:

$$\alpha_1 = \frac{\nu\kappa_{\mathcal{S}}}{2\check{C}_1} \quad , \quad \beta_1 = 2\nu\hat{C}_1^2 \quad , \quad \beta_2 = g\left[\frac{1+C_P^2}{m_{\mathbf{K}}}\right]\hat{C}_2^2 \ . \tag{3.2}$$

In [DQ04], it is shown that $\kappa^* = \alpha$. Then, if we are interested in the dependence of the convergence rate on the parameters, the maximum damping factor θ_{MAX} will be an indicator of this behavior. We see that

$$\beta_1 \sim \mathcal{O}(\nu) \quad , \quad \beta_2 \sim \mathcal{O}(g/m_{\mathbf{K}}) \quad , \quad \kappa \sim \alpha_1 \sim \mathcal{O}(\nu) \ , \tag{3.3}$$

and hence,

$$\theta_{MAX} \sim \mathcal{O}\left(\frac{\nu^2}{[\nu + g/(m_{\mathbf{K}})]^2}\right) .$$

Table 3.1 shows several values of θ_{MAX} for water flow and for different isotropic materials.

Material	K in [m/seg]	ϵ	$\mathcal{O}(\theta_{MAX})$
coarse sand	10^{-6} to 10^{-2}	10^{-1} to $3\ 10^{-1}$	10^{-12} to $3\ 10^{-4}$
clay	10^{-11} to 10^{-8}	$3.5\ 10^{-1}$ to $5\ 10^{-1}$	10^{-22} to $3\ 10^{-16}$
fractured bedrock	10^{-8} to 10^{-3}	$\leq 10^{-1}$	10^{-16} to 10^{-6}
basalt	10^{-11} to 10^{-6}	$\leq 2.5\ 10^{-1}$	10^{-21} to 10^{-11}
limestone	10^{-9} to 10^{-5}	$\leq 2\ 10^{-1}$	10^{-18} to 10^{-10}

Table 3.1: Values of θ_{MAX} for different isotropic materials (values from [DS90])

3.3 Implementation at the finite element level

Consider the spaces $H_{1,h}$, $H_{2,h}$, Q_h y Λ_h, introduced in Section 2.6. Define $\lambda_h^D := \mathbf{u}_h^D \cdot \mathbf{n}_1$ on $\Gamma \cap \Gamma_1^D$ and $\lambda_h := \mathbf{u}_{1h}^0 \cdot \mathbf{n}_1 \in \Lambda_h$.

Consider the discrete counterpart of Equation 2.26:

$$\int_\Gamma (\lambda_h + \lambda_h^D)\psi_h = -\int_\Gamma \frac{1}{\epsilon}\mathbf{n}_1 \cdot \mathbf{K} \cdot \mathrm{grad}(\phi_{0h} + \phi_0^D)\ \psi_h, \quad \forall \psi_h \in \Lambda_h. \tag{3.4}$$

In these expressions, ϕ_h^D and $\mathbf{u}_h^D$ are, as in Section 2.6, the FEM analogs of ϕ_e and $\mathbf{u}_e$, $\phi_{0h} \in H_{2,h}$ and $\mathbf{u}_{1h}^0 \in H_{1,h}$.

Using this expression as an auxiliary equation, it is possible to propose the following iterative process to solve coupled problem:

Procedure 4 N-D ITERATIONS AT THE FINITE ELEMENT LEVEL
Let the initial guess $\lambda_h^0 \in \Lambda_h$ and the relaxation parameter θ be given; for $k \geq 0$

1. *find $\phi_{0h}^{k+1} \in H_{2,h}$ such that*

$$\int_{\Omega_2} grad\psi_h \cdot \mathbf{K} \cdot grad\phi_{0h}^{k+1} - \int_{\Gamma} \epsilon\psi_h \, \lambda_h^k =$$
$$= -\int_{\Omega_2} grad\psi_h \cdot \mathbf{K} \cdot grad\phi_h^D + \int_{\Gamma_2^N} \phi^N \, \psi_h +$$
$$+ \int_{\Omega_2} f_2\psi_h \, + \int_{\Gamma} \epsilon \, \psi_h \, \lambda_h^D \quad \forall\psi_h \in H_{2h}$$

   and set $\phi_h^{k+1} = \phi_{0h}^{k+1} + \phi_h^D$;

2. *find $(\mathbf{u}_{1h}^0)^{k+1} \in H_{1,h}$ and $p_h^{k+1} \in Q_h$ such that*

$$\int_{\Omega_1} \nu grad\,(\mathbf{u}_{1h}^0)^{k+1} \cdot grad\,\mathbf{w}_h - \int_{\Omega_1} p_h^{k+1} div\mathbf{w}_h +$$
$$+ \int_{\Gamma} g\phi_h^{k+1}\mathbf{w}_h \cdot \mathbf{n}_1 = \int_{\Gamma_1^N} \mathbf{m} \cdot \mathbf{w}_h +$$
$$- \int_{\Omega_1} \nu grad\mathbf{u}_h^D \cdot grad\mathbf{w}_h \, + \int_{\Omega_1} \mathbf{f}_1 \cdot \mathbf{w}_h \quad \forall\mathbf{w}_h \in H_{1,h}$$
$$\int_{\Omega_1} q_h div(\mathbf{u}_{1h}^0)^{k+1} = -\int_{\Omega_1} q_h div\mathbf{u}_h^D \quad \forall q_h \in Q_h$$

   and set $\mathbf{u}_{1h}^{k+1} = (\mathbf{u}_{1h}^0)^{k+1} + \mathbf{u}_h^D$;

3. *find new iterative guess*

$$\lambda_h^{k+1} = \theta \, (\mathbf{u}_{1h}^0)^{k+1} \cdot \mathbf{n}_{1|\Gamma} + (1-\theta)\lambda_h^k.$$

■

As it was mentioned in Section 2.6, it is possible to define the discrete Poincaré–Steklov operators, and thus, it is also possible to write a discrete Poincaré–Steklov problem $S^h\lambda_h = \chi_h$. Analysis of the properties of this problem can be found e.g. in [Ste03]. In particular, for the discrete Poincaré–Steklov operator defined from (2.43) and (2.44), the following theorem holds (see [DMQ02]):

Theorem 3 *The operator $S^h_{\mathcal{S}}$ is continuous and coercive on Λ_h, while $S^h_{\mathcal{D}}$ is continuous and positive definite on Λ_h. Therefore, as $S^h = S^h_{\mathcal{S}} + S^h_{\mathcal{D}}$, S^h and $S^h_{\mathcal{S}}$ are spectrally equivalent, i.e. there exist two constants ρ_1 y ρ_2 independent of h such that*

$$\rho_1 \leq \frac{\nu_{MAX}}{\nu_{MIN}} \leq \rho_2$$

ν_{MAX}, ν_{MIN} are the maximum and minimum eigenvalues of $(S^h_{\mathcal{S}})^{-1}S^h$. ■

Remark:
As a consequence of Theorem 3, $S^h_{\mathcal{S}}$ is an optimal preconditioner to S^h for the solution of the discrete Pincaré–Steklov problem.

3.4 Algebraic form of the iterative procedure

Let $\Omega_{1,h/2}$ indicate the triangulation obtained by splitting each tetrahedron from $\Omega_{1,h}$ into eight subtetrahedra. Let the vector U_0 denote the values of $\mathbf{u}^0_{1h}$ at the nodes of $\Omega_{1,h/2}\backslash(\Gamma \cup \bar{\Gamma}^D_1)$ and U_Γ denote the vector of the values of $\mathbf{u}^0_{1h}$ at the interface nodes of $\Omega_{1,h/2}\backslash\bar{\Gamma}^D_1$, and P denote the vector of the values of the fluid pressure at the nodes of $\Omega_{1,h}$. In addition, let Φ_0 indicate the value of the piezometric head ϕ_{0h} at nodes of $\Omega_{1,h}\backslash(\Gamma\cup\bar{\Gamma}^D_2)$, and Φ_Γ those at the nodes on $\Gamma\backslash\bar{\Gamma}^D_2$. The algebraic representation of the Problem 6 is

$$\begin{bmatrix} A_0 & A_{0\Gamma} & B_0^T & 0 & 0 \\ A_{0\Gamma}^T & A_\Gamma & B_\Gamma^T & P_{\mathbf{n}_\Gamma}^T M_{\Phi_\Gamma} & 0 \\ B_0 & B_\Gamma & 0 & 0 & 0 \\ 0 & -M_\lambda P_{\mathbf{n}_\Gamma} & 0 & D_\Gamma & D_{0\Gamma}^T \\ 0 & 0 & 0 & D_{0\Gamma} & D_0 \end{bmatrix} \begin{bmatrix} U_0 \\ U_\Gamma \\ P \\ \Phi_\Gamma \\ \Phi_0 \end{bmatrix} = \begin{bmatrix} F_0 \\ F_\Gamma \\ F_p \\ G_\Gamma \\ G_0 \end{bmatrix}.$$

In order to write Procedure 4 in algebraic terms, we denote by $\lambda^k = P_{\mathbf{n}_\Gamma} U_\Gamma$ the vector of the values of λ^k_h at the nodes of $(\Omega_{1,h}\backslash\bar{\Gamma}^D_1)\cap\Gamma$. Then the iteration results

Procedure 5 Algebraic N-D iteration

1. *find* $\begin{bmatrix} \Phi_\Gamma^{k+1} \\ \Phi_0^{k+1} \end{bmatrix}$ *such that*

$$\begin{bmatrix} D_\Gamma & D_{0\Gamma}^T \\ D_{0\Gamma} & D_0 \end{bmatrix} \begin{bmatrix} \Phi_\Gamma^{k+1} \\ \Phi_0^{k+1} \end{bmatrix} = \begin{bmatrix} G_\Gamma + M_\lambda \lambda^k \\ G_0 \end{bmatrix}$$

2. find $\begin{bmatrix} U_0^{k+1} \\ U_\Gamma^{k+1} \\ P^{k+1} \end{bmatrix}$ *such that*

$$\begin{bmatrix} A_0 & A_{0\Gamma} & B_0^T \\ A_{0\Gamma}^T & A_\Gamma & B_\Gamma^T \\ B_0 & B_\Gamma & 0 \end{bmatrix} \begin{bmatrix} U_0^{k+1} \\ U_\Gamma^{k+1} \\ P^{k+1} \end{bmatrix} = \begin{bmatrix} F_0 \\ F_\Gamma - P_{\mathbf{n}_\Gamma}^T M_{\Phi_\Gamma} \Phi_\Gamma^{k+1} \\ F_p \end{bmatrix}$$

3. update λ^k $\qquad \lambda^{k+1} = \theta P_{\mathbf{n}_\Gamma} U_\Gamma^{k+1} + (1-\theta)\lambda^k.$

■

Realization of steps in the procedure, implies the iterative solution of the symmetric positive definite and saddle point systems. Preconditioned conjugate gradient method and generalized minimum residual method are the appropriate iterative techniques for each of the subproblems.

3.5 Numerical experiments

3.5.1 Approximation of an analytical solution

Let $\Omega_1 = (0,1)^2 \times (1,2)$, $\Omega_2 = (0,1)^3$, $\Gamma = \{z = 1\} \cap \bar{\Omega}_1$, $\Gamma_1^N = \emptyset$, $\Gamma_2^N = \{y = 0 \text{ or } y = 1\} \cap \bar{\Omega}_2$. Consider the homogeneous case $\mathbf{K} = k\mathbf{I}$, with unit coefficients, $k = \epsilon = \nu = g = 1$. The functions [DQ04]

$$\begin{aligned} \mathbf{u}_1 &= \begin{pmatrix} -\cos(\pi x/2)\sin(\pi z/2) + 1 \\ 0 \\ \sin(\pi x/2)\cos(\pi z/2) - 3 \end{pmatrix} \\ p &= -(2/\pi + \pi/2)\sin(\pi x/2)\sin(\pi z/2) + 3z \\ \phi &= -2/\pi \sin(\pi x/2)\sin(\pi z/2) + 3z \end{aligned}$$

are the solution to the Problem 4 with

$$\begin{aligned} \mathbf{f}_1 &= \begin{pmatrix} -(0.75\pi^2 + 1)\cos(\pi x/2)\sin(\pi z/2) \\ 0 \\ (0.25\pi^2 - 1)\sin(\pi x/2)\cos(\pi z/2) + 3 \end{pmatrix} \\ f_2 &= -\pi \sin(\pi x/2)\sin(\pi z/2) \end{aligned}$$

A coarse tetrahedral mesh is generated from partitioning of a unit cube $(0,1)^3$ into 8 sub cubes, and splitting each sub cube into 6 tetrahedra and mapping

the mesh into $(0,1)^2 \times (0,2)$. A sequence of uniform meshes is generated by subsequent refinement of each tetrahedron of this coarse tetrahedral mesh. The following parameters are employed:

- residual tolerance for step 1 of Procedure 5 is 10^{-7},
- residual tolerance for step 2 of Procedure 5 is 10^{-6},
- ND iteration is terminated when $\|\lambda^{k+1} - \lambda^k\| \leq 10^{-4}\|\lambda^k\|$.

The performance of Process 5, as well as subproblem arithmetic complexity are reported in Table 3.2. Here,

Mesh size	$\#ND$	$\#G_1$	$\#P_1$	$\#G_{15}$	$\#P_{15}$	CPU_{itS}	CPU_{itD}	CPU_{tot}
$h = 1/8$	15	55	5	2	4	0.04	<0.01	12.7
$h = 1/16$	15	60	9	3	3	0.65	0.015	204
$h = 1/32$	15	62	12	3	3	6.5	0.17	2108

Table 3.2: Performance of iterative solvers for a sequence of refined meshes.

$\#ND$: number of N-D iterations,
$\#G_k$: number of GMRES iterations at step 1 of k-th N-D iteration.
$\#P_k$: number of PCG iterations at step 2 of k-th N-D iteration.
CPU_{itS} (CPU_{itD}): execution time of one GMRES (PCG) iteration
CPU_{tot} total execution time.

In Table 3.3 we show the error of the discrete solution measured on meshes with different mesh size. The data indicate that the L_∞-error for $\mathbf{u}$ and ϕ decreases almost quadratically as $h \to 0$, whereas L_2-error for p is almost proportional to h.
As it follows from Table 3.2, the number of coupling iterations does not depend on the mesh size, whereas the numbers of GMRES and PCG iterations decrease in the course of coupling iterations, due to better initial guesses. We notice that the convergence rate of GMRES iterations saturates as $h \to 0$ and the boundness of the number of PCG iterations is not observed clearly. We explain the latter phenomenon by the extremely high convergence rate of the PCG for small Darcy problems. On the other hand, the cost per iteration (for both GMRES and PCG) and the total CPU time are linear with respect to the number of unknowns (each refinement results in 8-fold increase of the number of unknowns).

Mesh size	$\|\mathbf{u}_{\mathbf{x},\mathbf{y},\mathbf{z}_h} - \mathbf{u}_{\mathbf{x},\mathbf{y},\mathbf{z}}\|_{L_\infty}$	$\|p_h - p\|_{L_2}$	$\|\phi_h - \phi\|_{L_\infty}$
$h = 1/8$	0.00349 0.000607 0.00388	0.0101	0.010
$h = 1/16$	0.00121 0.000219 0.00141	0.0033	0.00317
$h = 1/32$	0.00033 0.000075 0.00051	0.00143	0.00096

Table 3.3: Errors of finite element solutions on a sequence of refined meshes.

3.5.2 Effects of boundary conditions

The main objective of the experiments of this Section is to show the importance of the boundary conditions as well as to present the performance of the coupling iterations.
All the coefficients of the numerical modelare set to unity: $\epsilon = \nu = g = 1$ whereas $\mathbf{K} = I$.
Let $\Omega_2 = (0,1)^2 \times (0,0.5)$ and $\Omega_1 = (0,1)^2 \times (0.5,1)$. We define $\Omega_{1,h}$ and $\Omega_{2,h}$ as the tetrahedral partitionings of the cubic mesh with the mesh step $h = 1/16$. In the absence of the interaction between the flows in Ω_1 and Ω_2, the boundary conditions on $\partial\Omega_1$ would be the trace of the Poiseuille flow:

$$\mathbf{u}_{1|\partial\Omega_1} = (24(1-y)y(1.5-z)(z-0.5), 0, 0).$$

Due to the Beavers/Joseph/Saffman condition, the Stokes velocity does not vanish at Γ, and the flow may not satisfy the Poiseuille boundary conditions (Figure 3.1).
To find the appropriate boundary conditions, a preliminary simulation is performed. The following boundary conditions are employed:

- On the inlet ($x = 0$), the top ($z = 1$) and lateral faces ($y = 0, y = 1$) of Ω_1, apply the Poiseuille flow traces as Dirichlet boundary conditions, whereas on the outlet ($x = 1$) set "do nothing" condition with $\mathbf{m} = 0$.

- On the four lateral faces of $\partial\Omega_2$, apply homogeneous Neumann boundary condition, and on the bottom face, apply homogeneous Dirichlet condition.

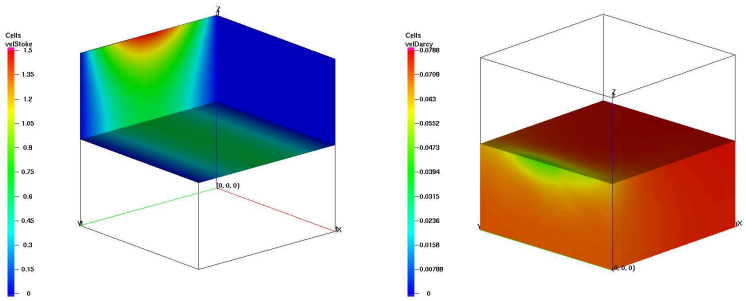

Figure 3.1: Typical velocity distributions in Ω_1 (left) and Ω_2 (right) subdomains.

After the solution of the coupled problem, we take the traces at the outlet of all three components of the Stokes velocity. These traces will be assign to the inlet instead of the Poiseuille flow trace. This boundary condition at the inlet and Poiseuille at the top and the lateral faces together with the "do nothing" condition at the outlet define the Stokes flow.
We consider four case studies for the boundary conditions for the Darcy flow. The objective is to evaluate the impact of boundary condition at the inlet and outlet of the Darcy region. We cover the possible combinations employed in practical applications, the appropriate choice of which depends on the hydrological configuration. We fix the boundary conditions at the bottom ($z = 0$) and lateral faces ($y = 0, y = 1$) of Ω_2, impossing homogeneous Neumann boundary conditions on them, and we consider the following cases:

Case study I : homogeneous Dirichlet conditions on inlet and outlet.
Assigning to both inlet and outlet traces of the piezometric head zero values implies uniform x-directional flows on inlet and outlet and an that the gradient of piezometric head will be driven by the Stokes flow. In effect, as ilustrated in Figure 3.2, the fluid flows from Ω_1 through the interface and leaves Ω_2 through the inlet and outlet.

Case study II : homogeneous Neumann conditions on inlet and outlet.
Assigning to both inlet and outlet zero normal velocity (homogeneous Neumann) implies that there is no flow across the inlet and outlet and total flux of fluid through the interface should be equal to zero. As a consequence, the fluid flows across the interface in different directions (Figure 3.3).

Case study III : homogeneous Neumann conditions on inlet and homogeneous Neumann condition on the outlet.
Setting zero normal velocity at the inlet and zero piezometric head at the outlet implies the impermeability of the inlet (e.g. rock wall) and an uniform x-directional flow at the outlet (Figure 3.4).

Case study IV : prescription of a piezometric head difference between inlet and outlet.
Assigning to the traces of the piezometric head two different values at the inlet and outlet implies, in the ansence of interaction, a uniform x-directional flows. The difference of the values defines the mean direction of the Darcy flow (Figure 3.5).
Note: In this case study, the outlet value may be set to zero whereas the inlet value should be determined somehow. For instance, assuming that the Stokes flow at the outlet is slightly affected by the inlet condition for Darcy flow, one could extrapolate the piezometric head at the inlet on the basis of x-component of the Stokes pressure gradient at the outlet.

Figures 3.2, 3.3, 3.4 and 3.5 display the cross-sections by XZ plane $y = 0.5$ of the solution for the four case studies. On top the isolines of moduli of Stokes and Darcy velocity are displayed, followed by the piezometric head (middle), and by the vector field of the Darcy velocity at bottom.

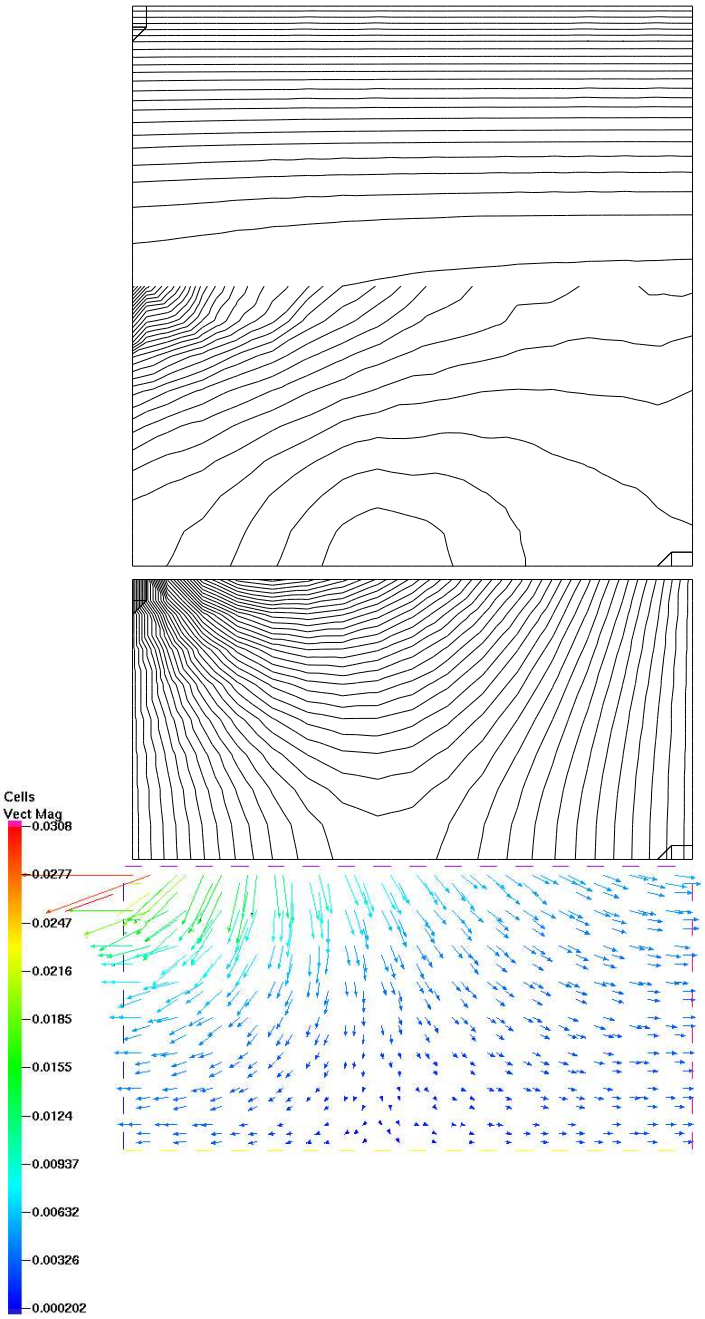

Figure 3.2: Cross section of the solution for Case study I: Darcy velocity (top), the piezometric head (middle), and for the vector field of the Darcy velocity (bottom).

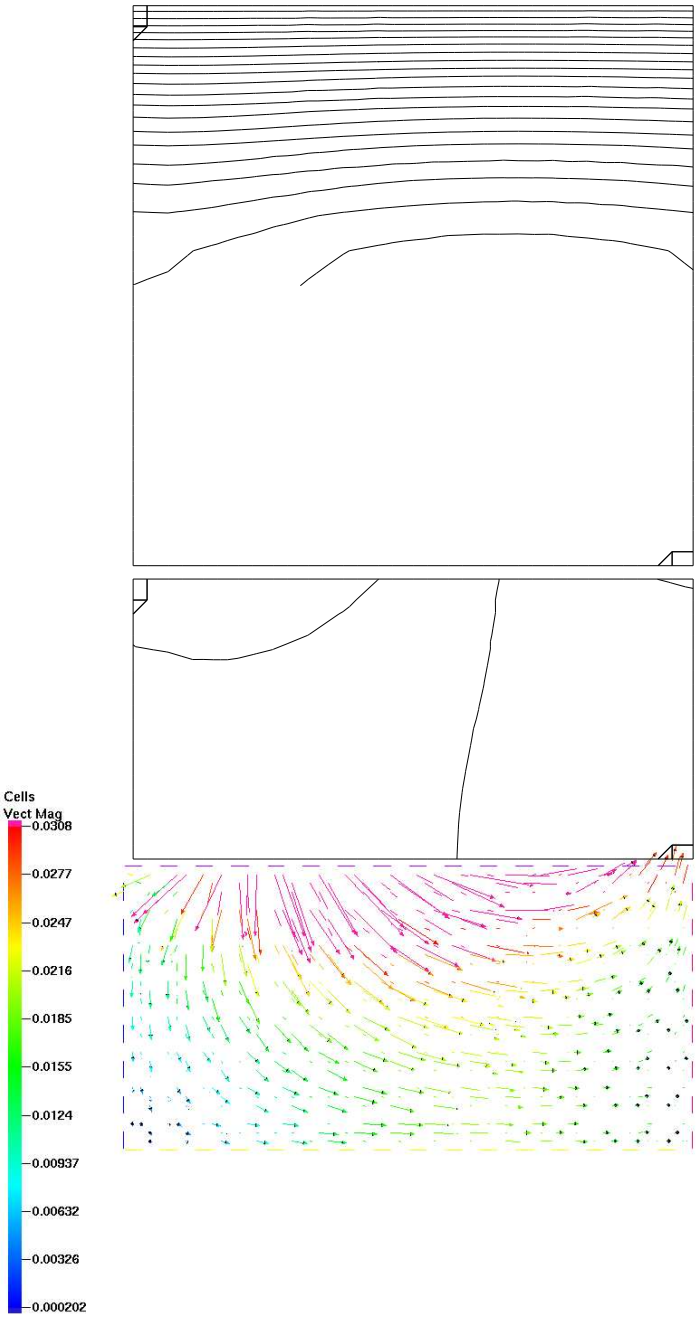

Figure 3.3: Cross section of the solution for Case study II: Darcy velocity (top), the piezometric head (middle), and for the vector field of the Darcy velocity (bottom).

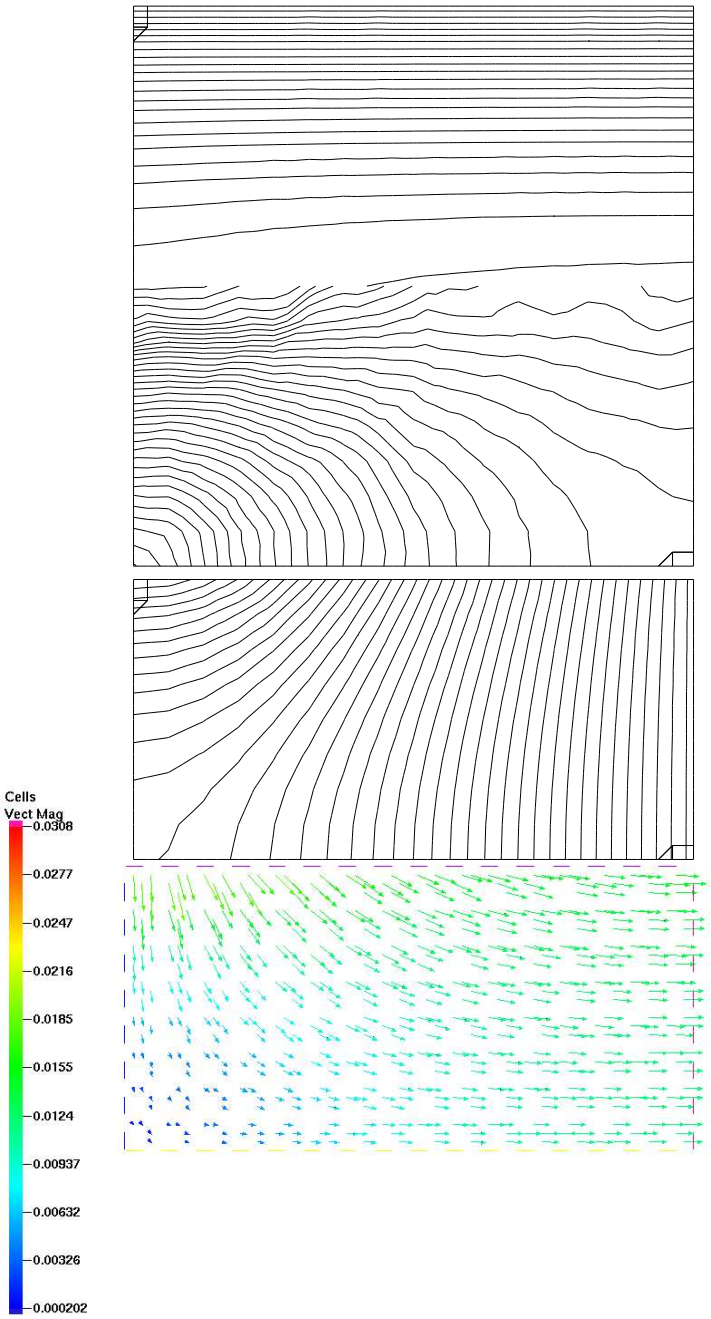

Figure 3.4: Cross section of the solution for Case study III: Darcy velocity (top), the piezometric head (middle), and for the vector field of the Darcy velocity (bottom).

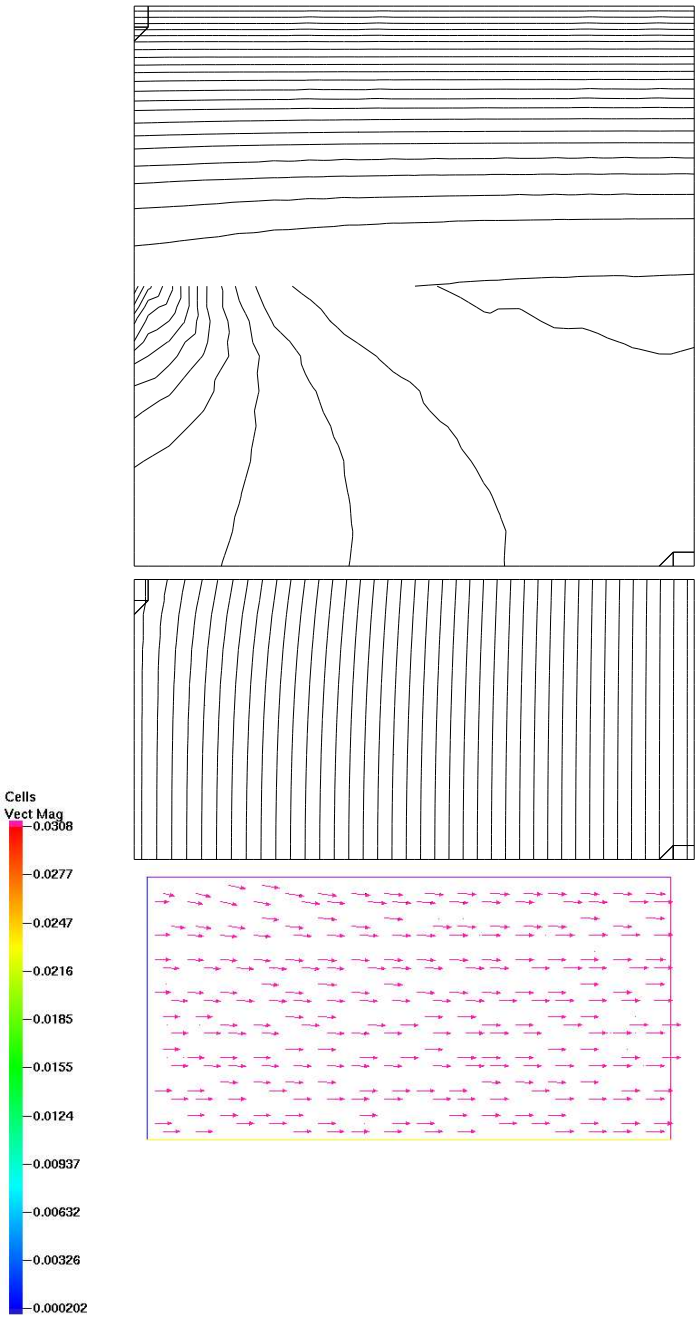

Figure 3.5: Cross section of the solution for Case study IV: Darcy velocity (top), the piezometric head (middle), and for the vector field of the Darcy velocity (bottom).

Comparing the four cases of boundary conditions for the piezometric head, we notice that given appropriate boundary conditions, the Stokes flow is slightly affected by the variations of Darcy flow.

The technical details of the solution procedure are as follows:

- number of tetrahedra in each subdomain: 12288,
- number of degrees of freedom for Stokes problem: $3 \times 18513 + 2601 = 58140$,
- number of degrees of freedom for Darcy problem: 2601,

The relaxation parameter θ was chosen to be 0.5. For the numerical solvers, the following stopping criteria were adopted:

- stopping criteria for PCG: residual norm tolerance fixed in 10^{-6},
- stopping criteria for GMRES: residual norm tolerance fixed in 10^{-6},
- stopping criteria for Neumann-Dirichlet iteration: $\left\| \frac{\lambda_h^{k+1} - \lambda_h^k}{\lambda_h^k} \right\| \leq 10^{-4}$

The number of Neumann-Dirichlet iterations required was 14, and it resulted independent of the choice of boundary condition, and of mesh size. With the stopping criteria for the GMRES and PCG iterations fixed as above, the number of iterations needed vary with k, the count of Neumann-Dirichlet iterations, as showed in Table 3.4. One GMRES iteration and one PCG iteration took 0.5 sec and 0.01 sec, respectively, at Pentium4 2.5 GHz processor. The overall simulation (including the preliminary stage) took approximately one minute and 26 Neumann-Dirichlet iterations.

ND iteration	1	3	5	7	9	11
#PCG	4	4	3	3	2	1
#GMRES	48	15	10	5	2	1

Table 3.4: Performance of PCG and GMRES iteration counts for different Neumann-Dirichlet steps.

3.5.3 Channel/subsurface flow: Influence of model coefficients

We consider the interaction of water from a 3D channel with a solid top lid into a porous media: in the sequel, this problem will be refer as the channel/subsurface flow problem. To investigate the impact of coefficient values, two case studies for two porous material are considered:
case study I, with high conductivity (coarse sand, gravel or carstic limestone or permeable basalt), and **case study II**, with low conductivity (e.g. limestone, sandstone or dolomite). Table 3.5 shows the coefficent values employed in both simulations:

Case study	$\mathbf{K}$ $[\frac{m}{seg}]$	ϵ	ν $[\frac{m^2}{seg}]$	g $[\frac{m}{seg^2}]$
I	$10^{-2}\mathbf{I}$	0.1	1	10
II	$10^{-5}\mathbf{I}$	0.1	1	10

Table 3.5: Coefficent employed in channel/subsurface flow simulations.

Let $\Omega_1 = (0, 40) \times (8.175, 11.825) \times (8.175, 10)$ and let Γ_1^D consists of the inlet ($x = 0$), the outlet ($x = 40$) and the top ($z = 10$) of Ω_1. At the inlet of the channel $\Gamma_{IN} = 0 \times (8.175, 11.825) \times (8.175, 10)$, Dirichlet conditions are imposed:

$$\mathbf{u}_{1|\Gamma_{IN}} = ((11.825 - y)(y - 8.175)(10 - z)(z - 8.175)4/1.825^4, 0, 0),$$

while on the outlet and the top of Γ_1^D, homogeneous Dirichlet boundary conditions are imposed. This implies that all the water entering the channel will enter the porous medium through Γ.
Let $\Omega_2 = (0, 40) \times (0, 20) \times (0, 10) \setminus \Omega_1$ and let Γ_2^D be the bottom face of the domain Ω_2 on which an homogeneous condition is imposed. Homogeneous Neumann boundary conditions are applied on Γ_2^N. This implies that all the fluid entering the channel through the inlet, leaves the porous media through the bottom face.
The mesh is a tetrahedral partitioning of the rectangular grid with 32 steps in x and y directions, and 16 steps in z direction, see Figure 3.6.
In case study I (high conductivity), it is possible to perform the simulation using the Procedure 5 with $\theta = 0.01$. The stopping criteria for the Neumann-

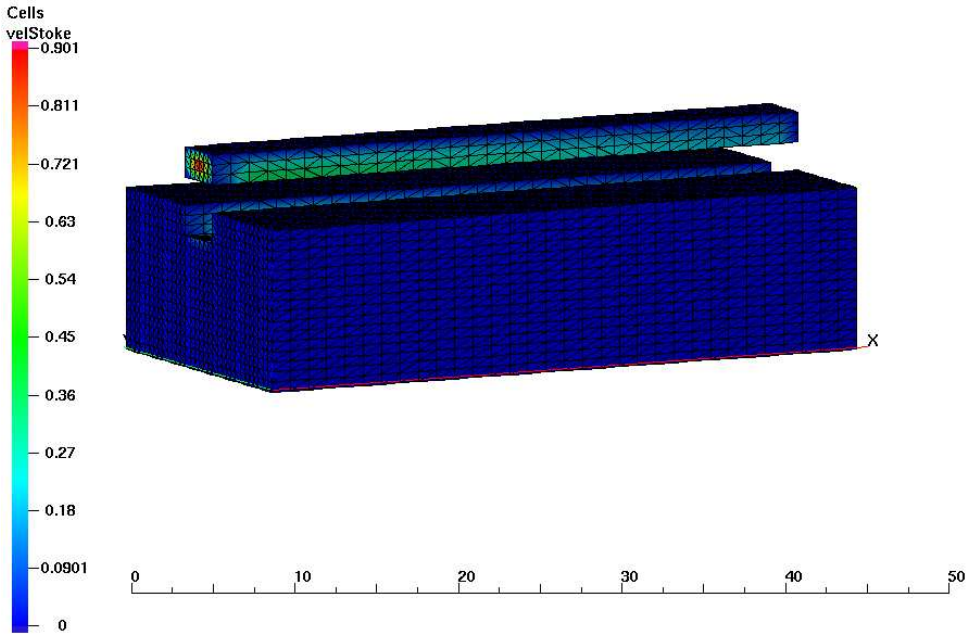

Figure 3.6: Channel and porous media subdomains and meshes, with the distribution of the inlet velocity.

Dirichlet iteration requieres that

$$\left\| \frac{\lambda_h^{k+1} - \lambda_h^k}{\lambda_h^k} \right\| \leq 10^{-4},$$

while for steps 1 and 2 of Procedure 5, the residual tolerances are fixed in 10^{-7} and 10^{-6}, respectively. The number of nodes in $\Omega_{1,h}$ and $\Omega_{2,h}$ were 924 and 18018. Both Stokes and Darcy systems had 20000 unknowns approximately. This requiered 683 iterations and 4144 seconds on a Pentium 4.
In case study II (low conductivity) it was not possible to use this approach: the requirements for θ exclude the Procedure 5 from the set of solution techniques.

The computed Darcy velocity vectors are neither normal to the interface (as may be seen in Figure 3.7), nor constant along x-axis. Figures 3.8, 3.9 show cross sections by planes $z = 9$ and $y = 10$, respectively. The absolute value of the Darcy velocity at the bottom face of Ω_2 ranges from 0 to $6 \cdot 10^{-3}$. The Stokes velocity demonstrates a linear decrease of the magnitude along x-axis, up to vanishing at the plane $x = 40$ as well as a singularity at the plane $x = 0$ (see Figures 3.10).

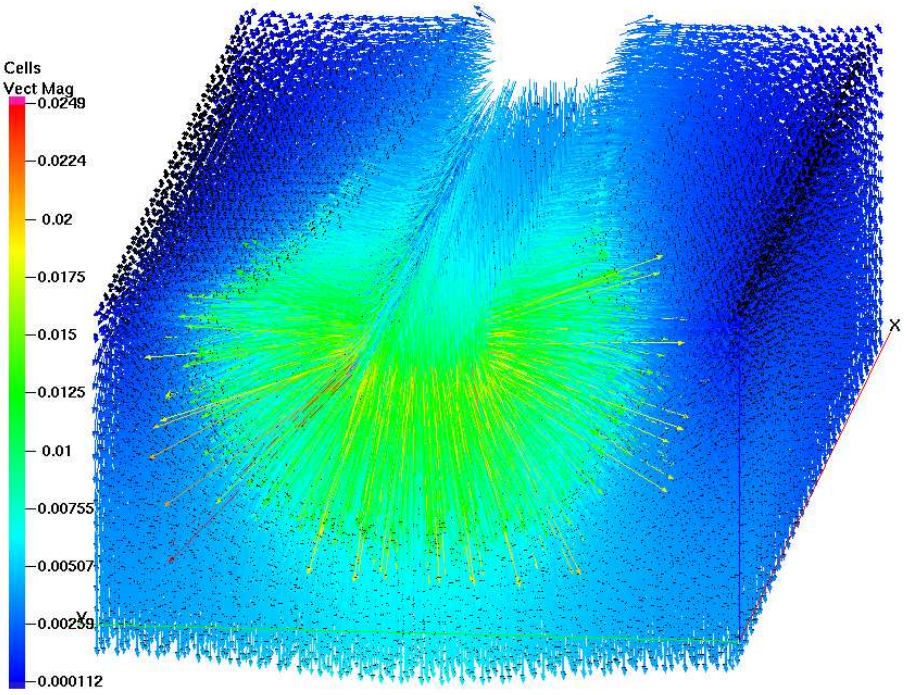

Figure 3.7: Darcy velocities in the case study I: sand.

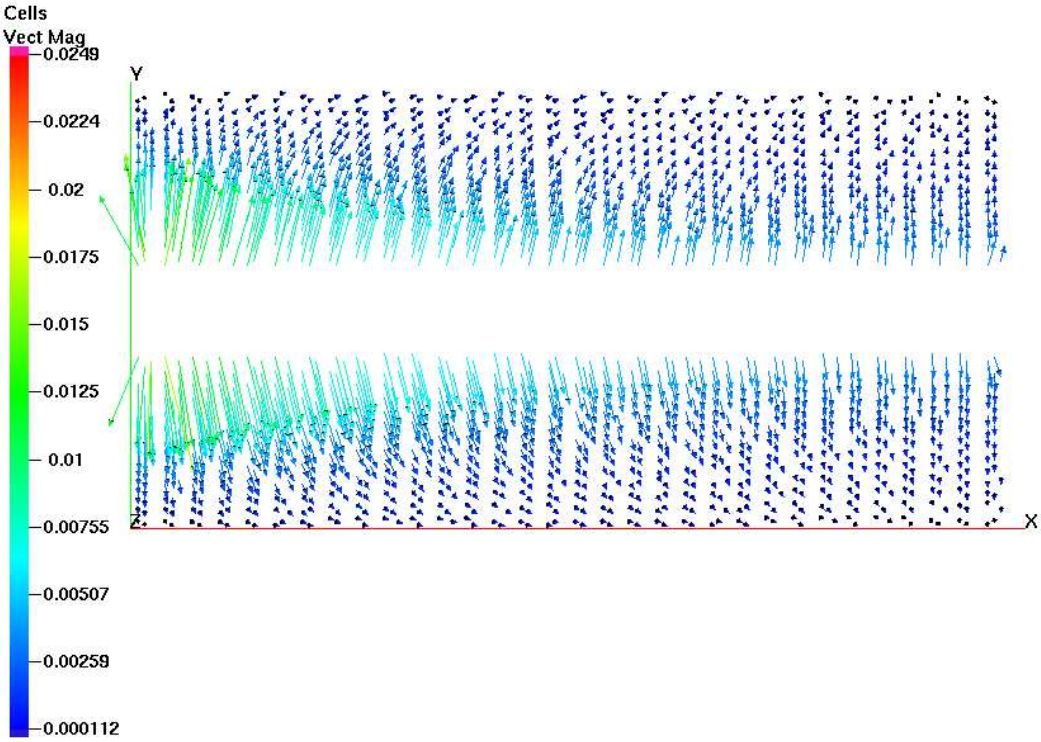

Figure 3.8: XY cross section of the Darcy velocity field in the case study I: sand.

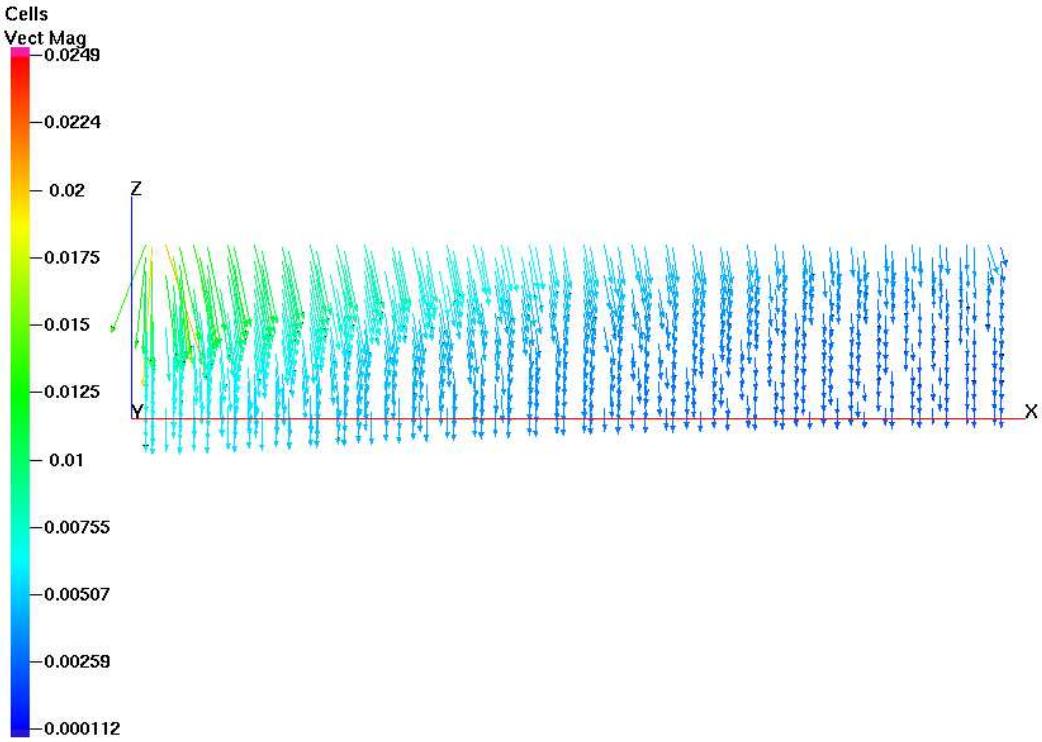

Figure 3.9: XZ cross section of the Darcy velocity field in the case study I: sand.

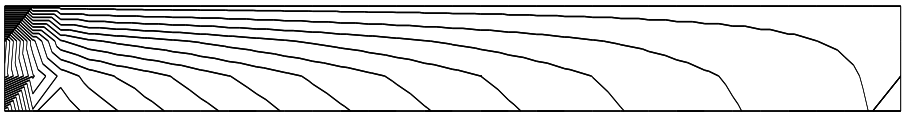

Figure 3.10: Isolines of Stokes velocity modulo in the case study I: sand. Cross section $y = 10$.

Chapter 4

An alternative direct method

4.1 Direct recovery of the iteration operator for the error

As indicated in Section 3.2, the convergence rate for Procedure 5 depends on an appropriate choice of the relaxation parameter θ. Its value depends on the coefficients ϵ, ν, $\mathbf{K}$, g, as well as on the shape of Ω_1 and Ω_2. As shown in Table 3.1, for several relevant applications, the iterations in Procedure 5 become impractical due to a very small value of θ. In order to solve Problem 6 in such cases, we propose an alternative technique based on the recovery of the iteration operator for the error. The underlying idea is simple: assume that λ_h^0, λ_h^1 and λ_h^2 are three predictions of the interface solution λ_h. Then, due to the linearity of the iteration operator T_Λ

$$\lambda_h - \lambda_h^1 = T_\Lambda(\lambda_h - \lambda_h^0) \quad , \quad \lambda_h - \lambda_h^2 = T_\Lambda(\lambda_h - \lambda_h^1) \ , \tag{4.1}$$

and

$$\lambda_h^2 - \lambda_h^1 = T_\Lambda(\lambda_h^1 - \lambda_h^0). \tag{4.2}$$

Eliminating λ_h^2 in (4.1), we obtain an equation for λ_h

$$(I - T_\Lambda)\lambda_h = \lambda_h^1 - T_\Lambda \lambda_h^0 \ . \tag{4.3}$$

This equation suggests the following procedure:

Procedure 6 RECOVERY OF THE ERROR OPERATOR

1. *For every node on the interface* $\Gamma \setminus \Gamma_1^D$*, indexed by* $k = 1, \ldots, N$*, choose* $\lambda_{h,k}^0 = e_k$ *as the* k*-th unit vector, and find* $\lambda_{h,k}^1$ *and* $\lambda_{h,k}^2$ *by performing two steps of Procedure 5.*

2. *Form the matrices* T_{01} *and* T_{12} *with columns* $\lambda_{h,k}^0 - \lambda_{h,k}^1$ *and* $\lambda_{h,k}^1 - \lambda_{h,k}^2$*, respectively.*

3. *Recover the iteration operator* $T_\Lambda = T_{12} T_{01}^{-1}$*.*

4. *For an arbitrary* k*, recover the solution* $\lambda_h = (I - T_\Lambda)^{-1}(\lambda_{h,k}^1 - T_\Lambda \lambda_{h,k}^0)$*.*

■

The cost of this procedure is dominated by the construction of the matrices T_{01} and T_{12}. In effect, the construction of a pair of columns corresponding to a node at the interface implies solving the coupled problem two times, to obtain λ_h^1 and λ_h^2. Each of the coupled iterations consists of solving Stokes problem and Darcy problem: if M_S and M_D are the number of nodes used respectively in Ω_1 and Ω_2 discretizations, then the cost for the Stokes solver is $\log\varepsilon^{-1}\mathcal{O}(3{\times}8{\times}M_S{+}M_S)$ and the cost for the Darcy solver is $\log\varepsilon^{-1}\mathcal{O}(M_D)$, thanks to the preconditioners, which are based on the AMG method [Stu83] which provides the linear arithmetic complexity and the convergence rate independent of the mesh size. The relation between M_S, M_D and the order N of matrix T_Λ, depends on the geometry. In the case of an uniform grid in the unit cube partitioned into two equal subdomains by a plane, $N = h^{-2}$, $M_S = M_D = \frac{1}{2}h^{-3}$, from where the cost of forming T_{01}, T_{12} is $2N\log\varepsilon^{-1}\mathcal{O}(26 \times N^{1.5})$.

4.2 Recovery of the iteration operator for the error on a lower dimensional space

As a "direct" method for the solution of Problem 4, the above procedure can be rather expensive, if the number N of nodes on the interface is more than a few hundreds. In certain cases, the cost of the recovery of T_Λ can be considerably reduced. Assume that the solution $(\mathbf{u}_1, \phi)$ of Problem 4 is a smooth function in the vicinity of Γ. Then, the finite element spaces $H_{1,h}, Q_h, H_{2,h}$ can be replaced by their counterparts on grids $\tilde{\Omega}_{1,h}$, $\tilde{\Omega}_{2,h}$ which are coarser than $\Omega_{1,h}$, $\Omega_{2,h}$ in the neighborhood of Γ. Possessing less degrees

of freedom, the coarse grid counterpart of Λ_h yields a smaller sized iteration matrix.

Let the interface be decomposed into L nonoverlapping patches

$$\Gamma = \bigcup_{i=1}^{L} \delta_i \ .$$

Correspondingly, let the set of interface nodes of $(\Omega_{1,h} \cap \Omega_{2,h}) \backslash \partial\Gamma$ be partitioned into L disjoint subsets γ_i, $i = 1, \ldots, L$. Each subset γ_i is associated with aggregated finite element basis functions

$$\Psi_i = \sum_{j \in \gamma_i} \psi_{h,j} \quad , \quad Q_i = \sum_{j \in \gamma_i} q_{h,j} \ ,$$

where $\psi_{h,j}$ and $q_{h,j}$ are the nodal basis functions of $H_{2,h}$ and Q_h. The aggregated finite element basis functions for the velocity space $H_{1,h}$ are built on the basis of partitioning the fine grid interface nodes into L subsets $\gamma_i^{(2)}$: the nodes of γ_i contribute to $\gamma_i^{(2)}$, the nodes located between two nodes of γ_i contribute to $\gamma_i^{(2)}$, the nodes located between a node of γ_i and a node of γ_j contribute to $\gamma_{\min(i,j)}^{(2)}$. The aggregated FE spaces are denoted by $\tilde{H}_{1,h}$, $\tilde{Q}_h$, $\tilde{H}_{2,h}$, respectively. The aggregated problem differs from Problem 6 only in finite element spaces. Correspondingly, we replace the space Λ_h by its aggregated subspace $\tilde{\Lambda}_h$. The Procedure 6 is applied to the aggregated counterpart of Problem 6 as well. Being less accurate approximation of the Problem 3, the aggregated finite element discretization provides less degrees of freedom for $\tilde{\Lambda}_h$. Hence, the recovery of the iteration operator requires less arithmetical work equivalent to the cost of $2L$ coupling iterations.

4.3 Numerical experiments

4.3.1 Interaction of channel and subsurface flows

We consider again the interaction of water from a 3D channel with a solid top lid into a porous media. We address the same two cases of porous material, coarse sand and limestone, with the same boundary conditions as in Section 3.5.3.

We perform the solution of the channel and subsurface flows interaction for

the case of sand using the recovery technique. The solution does not differ from the one obtained in Section 3.5.3 by the N-D iteration –Procedure 5, but performance is very different, as expected. A comparison is presented in Table 4.1, in Section 4.3.2.

We also apply the direct recovery technique to the case of limestone. In regard to performance, with the stopping criteria described in the preceding section, one needed 683 iterations and 4144 seconds. The numbers of nodes in Ω_1 and Ω_2 were 924 and 18018. Both Stokes and Darcy systems had 20000 unknowns approximately.

The computed Darcy velocity vectors are almost normal to the interface (see Figure 4.1), and are constant along x-axis (Figures 4.2, 4.3 show cross sections by planes $z = 9$ and $y = 10$, respectively). The absolute value of the Darcy velocity at the bottom face of Ω_2 is $4 \cdot 10^{-5}$. Regarding the Stokes flow, the velocity field exhibits a small decrease of the magnitude along the x-axis and a boundary layer at the plane $x = 40$ as well as a singularity at the plane $x = 0$ due to inconsistency of boundary conditions (Figure 4.4).

As pointed before, in the case of sand, the flow pattern is different. The basic reason for such a different behaviour of the solution for the coupled problem is the conductivity of the porous material. Indeed, in the case of sand, the fluid easily penetrates the interface, and almost all the amount of injected water is capable to infiltrate in the vicinity of the inlet; as a counterpart, the flow in the Stokes region accommodates to fit the conservation of mass. The other part of the domain is occupied by almost stagnated fluid. In the case of limestone, the infiltration is not that strong near the inlet and is more uniformly distributed along the interface (compare the Figures 4.2, 4.3 and 3.8, 3.9). The uniformity of the infiltration into Darcy region and the symmetry of boundary conditions result in the orthogonality of Darcy velocities to the interface. The non-uniformity of the infiltration produces regions (in the inlet neighbourhood) with an excess of inflow. In the presence of impervious boundary condition, the conservation of mass promotes a flushing flow along the interface, additional to the one normal to the interface. The module of velocity of the Stokes flow is dominated by the longitudinal component. In accordance to the conservation of mass, the above mentioned excess of injection into the sand results in a stronger decrease of longitudinal velocity along the channel, when compared with that in the case of limestone. In both cases, the solution vanishes at the end of the channel, in accordance to the boundary condition. This, together with the higher longitudinal velocity,

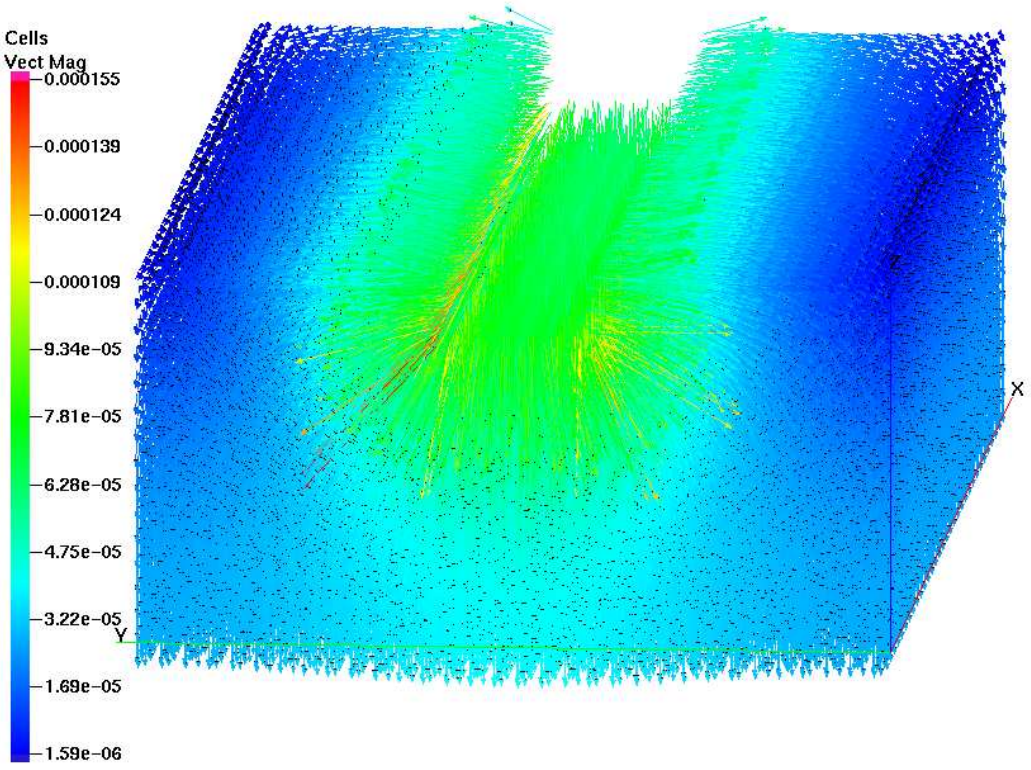

Figure 4.1: Darcy velocities in the case of limestone.

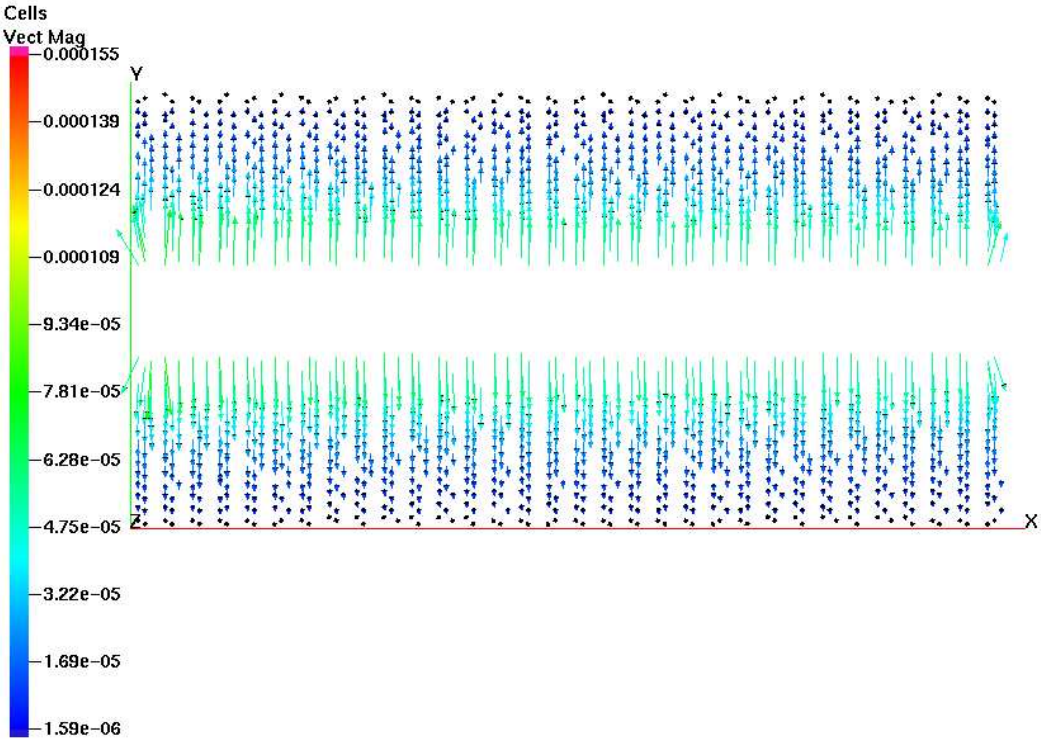

Figure 4.2: XY cross section of the Darcy velocity field in the case of limestone.

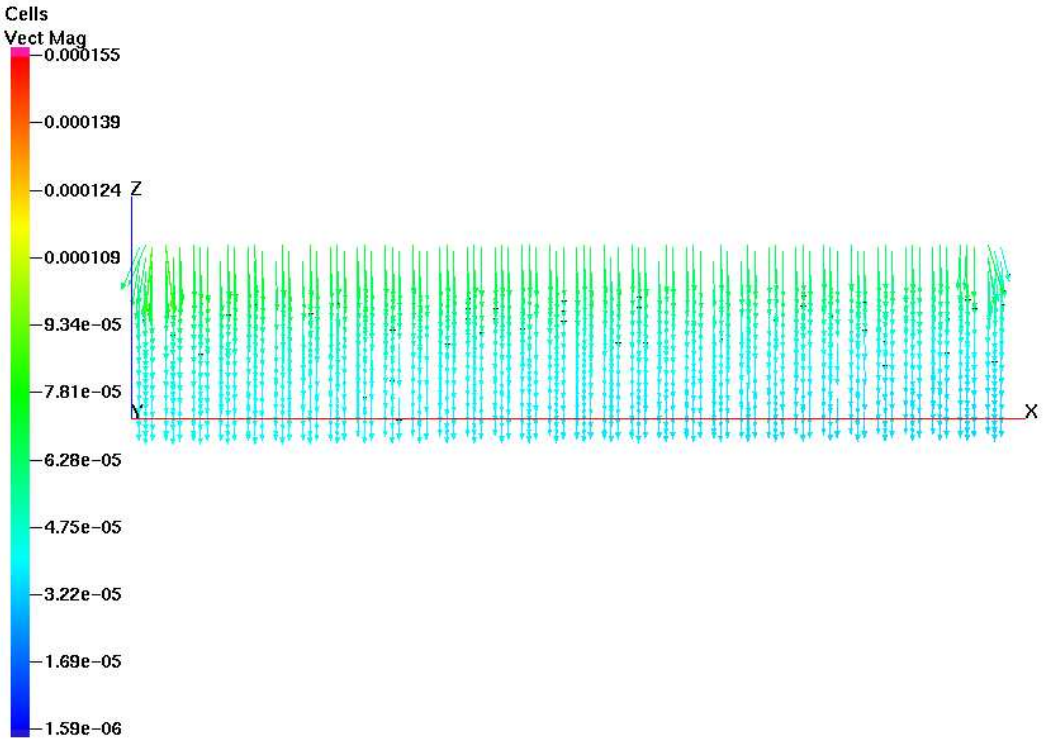

Figure 4.3: XZ cross section of the Darcy velocity field in the case of limestone.

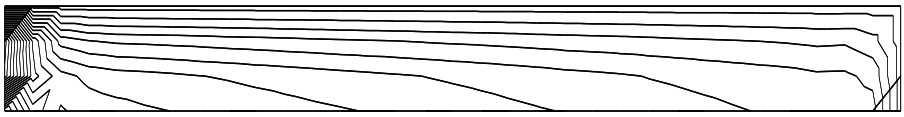

Figure 4.4: Isolines of Stokes velocity modulo in the case of limestone, cross section $y = 10$.

explains the formation of a stronger boundary layer in the case of limestone.

We want to stress that, although the direct method is applicable to the sand case, its performance is not satisfactory as comes clear from Table 4.1.

4.3.2 Approximate recovery for channel problem

We consider now the approximate recovery counterpart for Problem 6 which may be described via the definition of L disjoint subsets γ_i of interface nodes. Let us define γ_i as follows: the interface nodes with x-coordinates satisfying $x \leq 2h$ or $x \geq 40-h$, $h = 40/32$, generate individual sets γ_i, all the remaining interface nodes are partitioned into 27 subsets forming 9 equal patches per each of 3 plane faces of Γ. The total number of interface degrees of freedom is 63, and the recovery of the iteration operator requires 63 pairs of iterations steps in Procedure 5. We do not aggregate the interface degrees of freedom in regions where the singularity or boundary layer is observed, in order to avoid the impact of a large approximation error caused by the aggregation in those regions.

The total number of coupled iterations reduced to 128, and the solution procedure took 2304 seconds for the case of limestone. Similarly to the recovery of the iteration operator on the fine grid, the number of GMRES iterations needed for the Stokes residual norm reduction to 10^{-12} was 160-180. The Darcy velocity obtained from the aggregated problem is very close to that from the fine grid problem. The insignificant difference may be seen at the boundaries of the aggregation patches (see Figures 4.2, 4.5, and Figures 4.3, 4.6).
However, the Stokes flow exhibits considerable differences (see Figures 4.4 and 4.7). Albeit the infiltration velocity is recovered correctly, it is small $O(10^{-4})$ in comparison to $O(1)$ values of slipping velocity. The latter is not in accordance to that obtained without aggregation. We suspect, that it is unstable with respect to errors induced by the aggregation process.
We performed the same experiments for the case of sand (see Figures 4.8, 4.9) and 4.10). We found that the deterioration of the Stokes solution remains, confirming our hypothesis that the effect is due to the aggregation process:
We conclude that the use of the aggregation procedure is limited to the cases in which there is interest only in the Darcy flow.

As a final remark, the following Table resumes the performance of N-D iter-

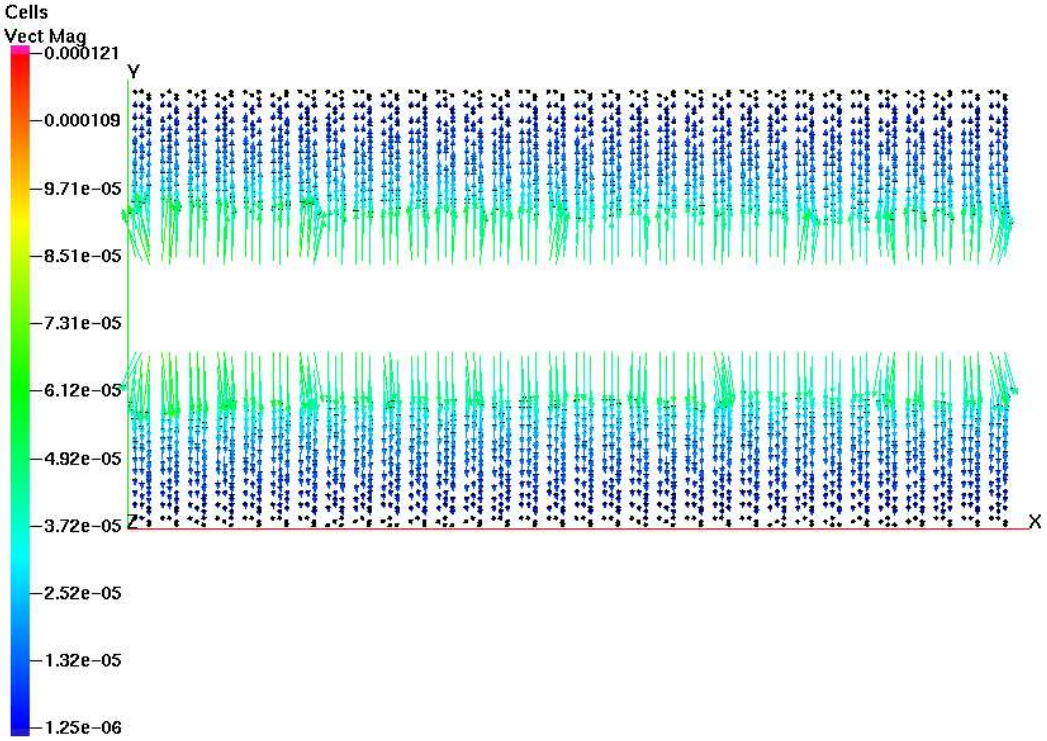

Figure 4.5: XY cross section of the Darcy velocity field of the aggregated problem in the case of limestone.

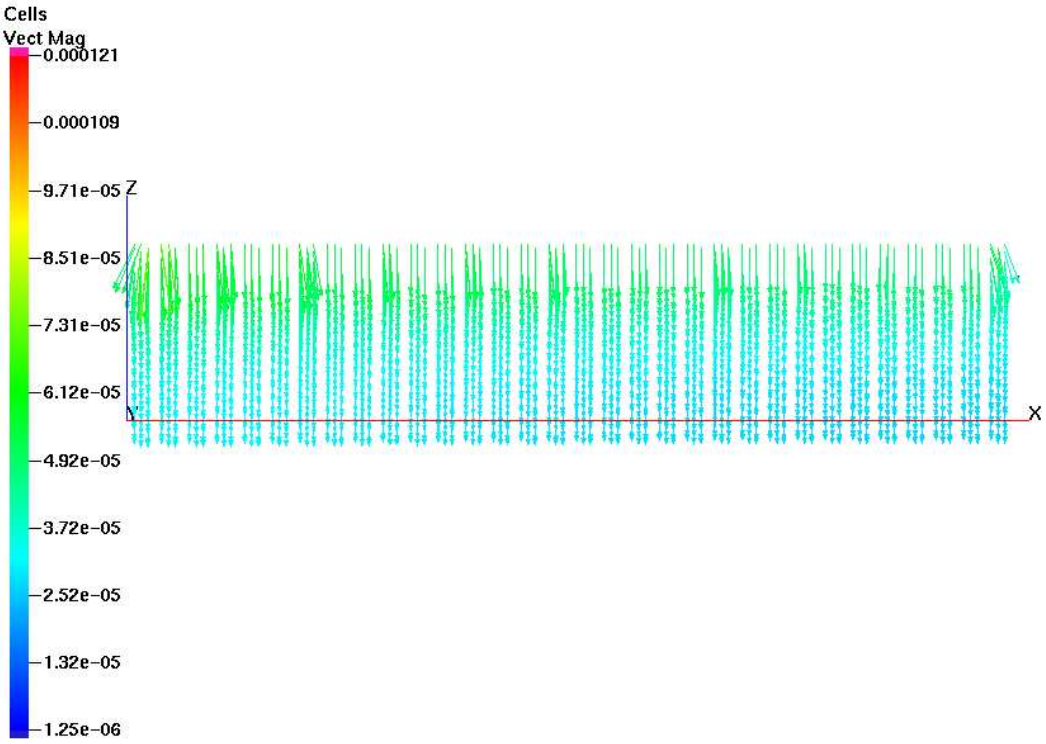

Figure 4.6: XZ cross section of the Darcy velocity field of the aggregated problem in the case of limestone.

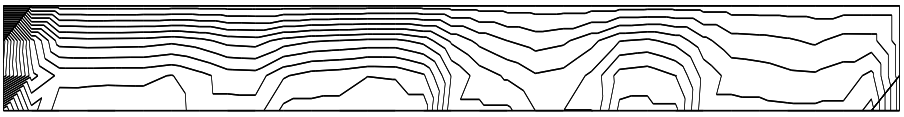

Figure 4.7: Isolines of Stokes velocity modulo of the aggregated problem in the case of limestone, cross section $y = 10$.

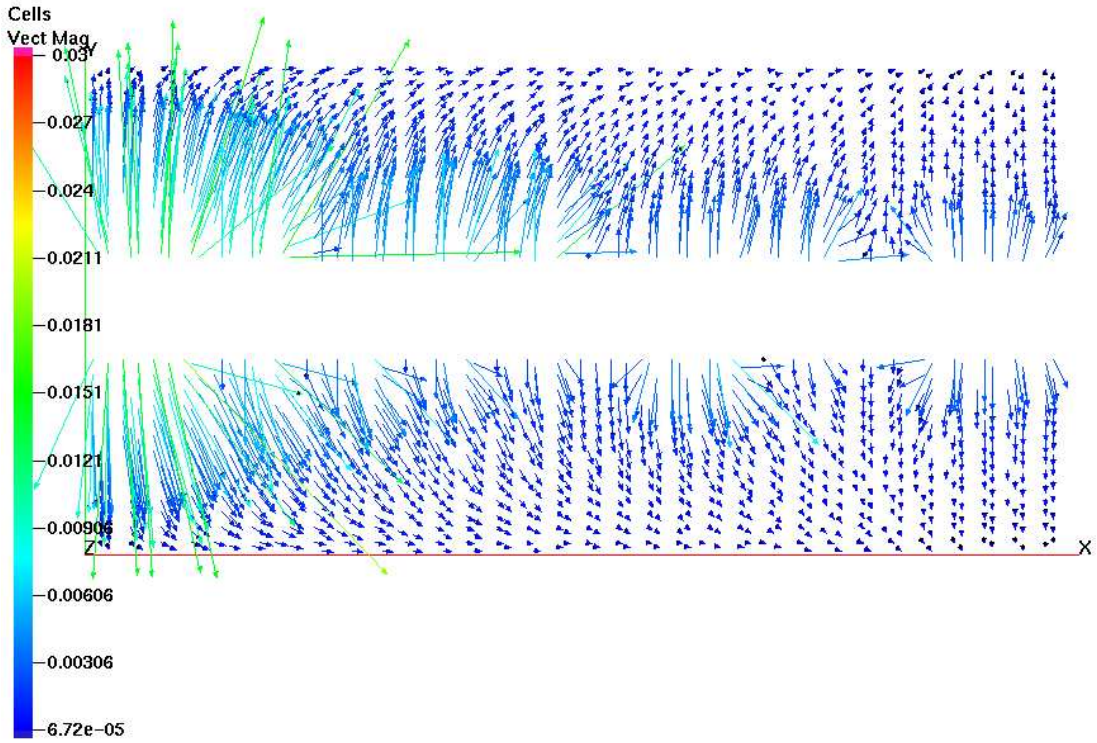

Figure 4.8: XY cross section of the Darcy velocity field of the aggregated problem in the case of sand.

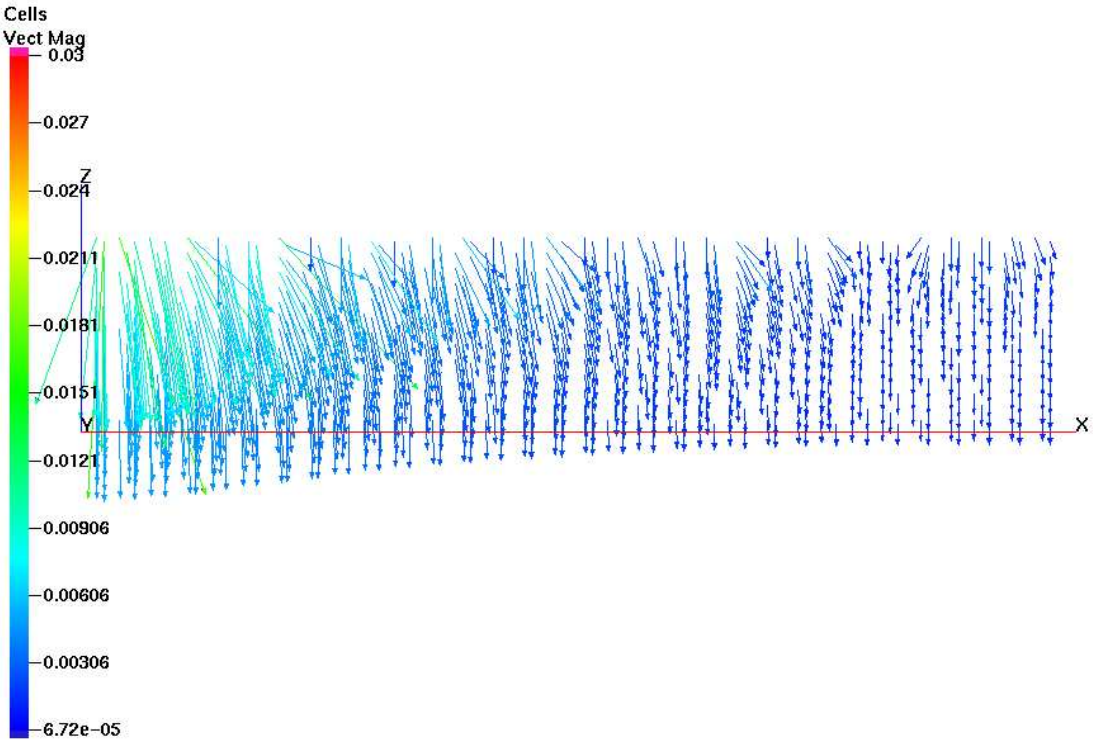

Figure 4.9: XZ cross section of the Darcy velocity field of the aggregated problem in the case of sand.

Figure 4.10: Isolines of Stokes velocity modulo of the aggregated problem in the case of sand, cross section $y = 10$.

ation, direct recovery and approximate recovery, for the case of coarse sand.

Method	Total number of iterations	Mean iteration count for both subproblems	CPU_{tot} in $[seg]$
N-D iteration	15	35	204
Direct recovery	683	136	5390.29
Approximate recovery	128	129	772.09

Table 4.1: Comparative performance of N-D iteration and Procedure 6.

Chapter 5

Reduction of the problem to an interface equation

One possible approach for solving the coupled Stokes-Darcy flow is the reduction of the problem to the interface. To this end, it is necessary to write the *interface equation*. In this Chapter, we address the analysis of the possible interface equations for Problem 3 with transmission conditions given by (2.6), (2.7), (2.11), and its associated Poincaré–Steklov operators.
As indicated in Section 2.5, the coupling between both flows is represented by the continuity of flux across the interface (2.7) and the balance of normal stress on the interface (2.6). Any of these relations may be used as interface equation.

We will make our analysis for the discrete problem, keeping in mind the computational implementation. So, for completeness, we write again the algebraic form of the finite element formulation: let again $\Omega_{1,h/2}$ indicate the triangulation obtained by splitting each tetrahedron from $\Omega_{1,h}$ into eight subtetrahedra. Let the vector U_0 denote the values of $\mathbf{u}_{1h}^0$ at the nodes of $\Omega_{1,h/2}\backslash(\Gamma \cup \bar{\Gamma}_1^D)$ and U_Γ denote the vector of the values of $\mathbf{u}_{1h}^0$ at the interface nodes of $\Omega_{1,h/2}\backslash\bar{\Gamma}_1^D$, and P denote the vector of the values of the fluid pressure at the nodes of $\Omega_{1,h}$. In addition, let Φ_0 indicate the value of the piezometric head ϕ_{0h} at nodes of $\Omega_{1,h}\backslash(\Gamma \cup \bar{\Gamma}_2^D)$, and Φ_Γ those at the nodes

on $\Gamma\backslash\bar{\Gamma}_2^D$. The algebraic representation of Problem 6 is

$$\begin{bmatrix} A_0 & A_{0\Gamma} & B_0^T & 0 & 0 \\ A_{0\Gamma}^T & A_\Gamma & B_\Gamma^T & P_{\mathbf{n}_\Gamma}^T M_{\Phi_\Gamma} & 0 \\ B_0 & B_\Gamma & 0 & 0 & 0 \\ 0 & -M_\lambda P_{\mathbf{n}_\Gamma} & 0 & D_\Gamma & D_{0\Gamma}^T \\ 0 & 0 & 0 & D_{0\Gamma} & D_0 \end{bmatrix} \begin{bmatrix} U_0 \\ U_\Gamma \\ P \\ \Phi_\Gamma \\ \Phi_0 \end{bmatrix} = \begin{bmatrix} F_0 \\ F_\Gamma \\ F_p \\ G_\Gamma \\ G_0 \end{bmatrix}. \tag{5.1}$$

5.1 The case of flux continuity across the interface

The case of flux continuity across the interface has been analyzed in several papers (cf., e.g, [DMQ02, DQ03, DQ04]). In those papers, the construction of the algebraic system hinges on the assumption that the vector U_Γ only contains normal velocities. In our setting, U_Γ contains the whole velocity vector on the interface, i.e., we have three velocity components (the normal and two tangential ones) at each interface node. This allows us to treat arbitrary interfaces rather than interfaces whose normal is orthogonal to a coordinate plane. As will be shown below, this can be done at the expense of a limitation arising in some specific cases. The interface equation is obtained by the elimination of the unknowns U_0, P, Φ_0:

$$\begin{bmatrix} A_{0\Gamma}^T & B_\Gamma^T \end{bmatrix} \begin{bmatrix} A_0 & B_0^T \\ B_0 & 0 \end{bmatrix}^{-1} \left\{ \begin{bmatrix} F_0 \\ F_p \end{bmatrix} - \begin{bmatrix} A_{0\Gamma} \\ B_\Gamma \end{bmatrix} U_\Gamma \right\} + A_\Gamma U_\Gamma + P_{\mathbf{n}_\Gamma}^T M_{\Phi_\Gamma} \Phi_\Gamma = F_\Gamma$$

$$-M_\lambda P_{\mathbf{n}_\Gamma} U_\Gamma + (D_\Gamma - D_{0\Gamma}^T D_0^{-1} D_{0\Gamma}) \Phi_\Gamma = G_\Gamma - D_{0\Gamma}^T D_0^{-1} G_0$$

and elimination of $\Phi_\Gamma = S_D^{-1}(G_S + M_\lambda P_{\mathbf{n}_\Gamma} U_\Gamma)$:

$$(S_S + P_{\mathbf{n}_\Gamma}^T M_{\Phi_\Gamma} S_D^{-1} M_\lambda P_{\mathbf{n}_\Gamma}) U_\Gamma = F_S - P_{\mathbf{n}_\Gamma}^T M_{\Phi_\Gamma} S_D^{-1} G_S \tag{5.2}$$

where

$$S_D = D_\Gamma - D_{0\Gamma}^T D_0^{-1} D_{0\Gamma}, \quad G_S = G_\Gamma - D_{0\Gamma}^T D_0^{-1} G_0$$

$$S_S = A_\Gamma - \begin{bmatrix} A_{0\Gamma}^T & B_\Gamma^T \end{bmatrix} \begin{bmatrix} A_0 & B_0^T \\ B_0 & 0 \end{bmatrix}^{-1} \begin{bmatrix} A_{0\Gamma} \\ B_\Gamma \end{bmatrix}$$

$$F_S = F_\Gamma - \begin{bmatrix} A_{0\Gamma}^T & B_\Gamma^T \end{bmatrix} \begin{bmatrix} A_0 & B_0^T \\ B_0 & 0 \end{bmatrix}^{-1} \begin{bmatrix} F_0 \\ F_p \end{bmatrix}.$$

Equation (5.2) is the interface equation. Two remarks are in order. First, in the case that U_Γ represents normal component only, the equation (5.2) may be transformed to the equivalent formulation of (5.2)

$$\lambda + P_{\mathbf{n}_\Gamma} S_S^{-1} P_{\mathbf{n}_\Gamma}^T M_{\Phi_\Gamma} S_D^{-1} M_\lambda \lambda = P_{\mathbf{n}_\Gamma} S_S^{-1} (F_S - P_{\mathbf{n}_\Gamma}^T M_{\Phi_\Gamma} S_D^{-1} G_S). \tag{5.3}$$

Second, the equation (5.2) implies that the right hand side may be computed. However, the computation of F_S infers the solvability of the Stokes problem

$$\begin{bmatrix} A_0 & B_0^T \\ B_0 & 0 \end{bmatrix} \begin{bmatrix} \tilde{U}_0 \\ \tilde{P} \end{bmatrix} = \begin{bmatrix} F_0 \\ F_p \end{bmatrix}. \tag{5.4}$$

In our setting, the system matrix is FE discretization of the Stokes operator with homogeneous Dirichlet boundary condition on Γ. Hence, the condition $F_p \in ImB_0$ has to be verified. Recall that from (5.1) it follows that there exists U_0 such that $F_p - B_\Gamma U_\Gamma = B_0 U_0$, i.e., $F_p - B_\Gamma U_\Gamma \in ImB_0$. Therefore, $F_p \in ImB_0$ if and only if $B_\Gamma U_\Gamma \in ImB_0$, i.e. there exists W_0 such that $B_\Gamma U_\Gamma = B_0 W_0$. By the definition of B_0 and B_Γ

$$(B_0 W_0, q) = \int\limits_{\Omega_1} q_h div \mathbf{W}_0^h = \int\limits_{\Gamma_1^N} q_h (\mathbf{n}_\Gamma \cdot \mathbf{W}_0^h)$$

$$(B_\Gamma W_\Gamma, q) = \int\limits_{\Omega_1} q_h div \mathbf{U}_\Gamma^h = \int\limits_{\Gamma} q_h (\mathbf{n}_\Gamma \cdot \mathbf{U}_\Gamma^h)$$

for any q_h from Q_h. Here, $\mathbf{W}_0^h$ and $\mathbf{U}_\Gamma^h$ denote the FE extensions of the vectors W_0 and U_Γ, respectively. Therefore,

$$(B_0 W_0 - B_\Gamma W_\Gamma, q) = \int\limits_{\Gamma_1^N} q_h (\mathbf{n}_\Gamma \cdot \mathbf{W}_0^h) - \int\limits_{\Gamma} q_h (\mathbf{n}_\Gamma \cdot \mathbf{U}_\Gamma^h) \quad \forall q_h \in Q_h. \tag{5.5}$$

Since $\mathbf{W}_0^h = 0$ on Γ, $\mathbf{U}_\Gamma^h = 0$ on Γ_1^N, the left hand side of (5.5) can not vanish for any q except the case $(\mathbf{n}_\Gamma \cdot \mathbf{U}_\Gamma^h) = 0$. Therefore, the compatibility of (5.4) is conditioned by $(\mathbf{n}_\Gamma \cdot \mathbf{U}_\Gamma^h) = 0$, that implies the decoupled problem.

We conclude that in the case of U_Γ representing all velocity components, the system (5.1) can not be reduced to an equation for the interface velocities. We recall that the assignment of normal components to U_Γ confines the set of possible interfaces to patches on a coordinate plane, which, e.g. is not adequate for the channel problem. We remind also that in the case of U_Γ representing the normal components, the interface equation (5.3) may be solved iteratively [DQ03, DQ04]. In particular, the proposed Richardson iteration was shown to be equivalent with the N-D iteration –Procedure 5. The alternative choice may be on of the Krylov subspace iterations (CG,GMRES).

5.2 Normal stress continuity on the interface

Let C denote the matrix block given by:

$$C = \begin{bmatrix} A_0 & A_{0\Gamma} & B_0^T \\ A_{0\Gamma}^T & A_\Gamma & B_\Gamma^T \\ B_0 & B_\Gamma & 0 \end{bmatrix} . \tag{5.6}$$

For the derivation of the interface equation, we consider the first three equations of (5.1):

$$C \begin{bmatrix} U_0 \\ U_\Gamma \\ P \end{bmatrix} + \begin{bmatrix} 0 \\ P_{\mathbf{n}_\Gamma}^T M_{\Phi_\Gamma} \Phi_\Gamma \\ 0 \end{bmatrix} = \begin{bmatrix} F_0 \\ F_\Gamma \\ F_p \end{bmatrix} , \tag{5.7}$$

so that

$$\begin{bmatrix} U_0 \\ U_\Gamma \\ P \end{bmatrix} = C^{-1} \begin{bmatrix} F_0 \\ F_\Gamma \\ F_p \end{bmatrix} - C^{-1} \begin{bmatrix} 0 \\ P_{\mathbf{n}_\Gamma}^T M_{\Phi_\Gamma} \Phi_\Gamma \\ 0 \end{bmatrix} . \tag{5.8}$$

Eliminating Φ_0 in the last equation of (5.1), we obtain:

$$\Phi_0 = D_0^{-1}(G_0 - D_{0\Gamma}\Phi_\Gamma) .$$

Hence, the fourth equation implies

$$\begin{bmatrix} 0 & -M_\lambda P_{\mathbf{n}_\Gamma} & 0 \end{bmatrix} \left(C^{-1} \begin{bmatrix} F_0 \\ F_\Gamma \\ F_p \end{bmatrix} - C^{-1} \begin{bmatrix} 0 \\ P_{\mathbf{n}_\Gamma}^T M_{\Phi_\Gamma} \Phi_\Gamma \\ 0 \end{bmatrix} \right) + \tag{5.9}$$

$$+D_\Gamma\Phi_\Gamma + D_{0_\Gamma}^T D_0^{-1}(G_0 - D_{0_\Gamma}\Phi_\Gamma) = G_\Gamma \ .$$

Defining $S_D = D_\Gamma - D_{0_\Gamma}^T D_0^{-1} D_{0_\Gamma}$, we obtain

$$\begin{bmatrix} 0 & M_\lambda P_{\mathbf{n}_\Gamma} & 0 \end{bmatrix} C^{-1} \begin{bmatrix} 0 \\ P_{\mathbf{n}_\Gamma} M_\lambda \Phi_\Gamma \\ 0 \end{bmatrix} + S_D\Phi_\Gamma =$$

$$= G_\Gamma - D_{0\Gamma}^T D_0^{-1} G_0 + \begin{bmatrix} 0 & M_\lambda P_{\mathbf{n}_\Gamma} & 0 \end{bmatrix} C^{-1} \begin{bmatrix} F_0 \\ F_\Gamma \\ F_p \end{bmatrix} \tag{5.10}$$

Denoting

$$F_D = G_\Gamma - D_{0\Gamma}^T D_0^{-1} G_0 + \begin{bmatrix} 0 & M_\lambda P_{\mathbf{n}_\Gamma} & 0 \end{bmatrix} C^{-1} \begin{bmatrix} F_0 & F_\Gamma & F_p \end{bmatrix}^T$$

and

$$\mathcal{C}^{-1} = \begin{bmatrix} 0 & I & 0 \end{bmatrix} C^{-1} \begin{bmatrix} 0 & I & 0 \end{bmatrix}^T$$

we can write

$$(S_D + M_\lambda P_{\mathbf{n}_\Gamma} \mathcal{C}^{-1} P_{\mathbf{n}_\Gamma}^T M_{\Phi_\Gamma})\Phi_\Gamma = F_D, \tag{5.11}$$

or equivalently,

$$(I + S_D^{-1} M_\lambda P_{\mathbf{n}_\Gamma} \mathcal{C}^{-1} P_{\mathbf{n}_\Gamma}^T M_{\Phi_\Gamma})\Phi_\Gamma = S_D^{-1} F_D \ . \tag{5.12}$$

Equation 5.11 induces the following iteration:

$$\Phi_\Gamma^{k+1} = \Phi_\Gamma^k + \theta S_D^{-1} \left(F_D - (S_D + M_\lambda P_{\mathbf{n}_\Gamma} \mathcal{C}^{-1} P_{\mathbf{n}_\Gamma}^T M_{\Phi_\Gamma})\Phi^k \right), \tag{5.13}$$

which is a preconditioned Richardson iteration, where $S_{\mathcal{D}}$ plays the role of the preconditioner.
Finally we underline that, according to Theorem 3, the matrix S_D provides an optimal preconditioner for the discrete Poincaré–Steklov problem on Γ. This means that the same preconditioner can be used with other iterative methods for the interface problem, as GMRES.

5.3 Numerical experiments

In this Section we consider basic features of the iterative solution of the interface equation (5.12) for two different applications. The first application is the case study, of the interaction of water from a straight rectangular channel with a solid lid into surrounding porous media. The second application is the simulation of Darcy flow induced by the interaction between flows in a system of channels and porous media. The simple geometry of the first case allows us to examine the iterative performance on a sequence of refined grids as well as to verify the feasibility of the solution, whereas the second case is presented to demonstrate interesting effects of the interaction between flows in non-trivial geometries. In both cases, algebraic multigrid [Stu83] preconditioner is used in the iterative solution of subdomain problems, with GMRES and PCG acceleration for Stokes and Darcy subproblems, respectively.

5.3.1 Infiltration from a straight channel

We consider again the 3D channel problem of Section 3.5.3, with same boundary conditions and for materials with different conductivity coefficients, ranking from coarse sand with $\mathbf{K} = 10^{-2}\mathbf{I}$ to limestone with $\mathbf{K} = 10^{-5}\mathbf{I}$ (in the international system of units). The other problem coefficients are $\epsilon = 0.1$, $\nu = 1$, $g = 10$. We observe again the same general pattern for the coupled flow in the two cases: the computed Darcy velocity vectors are normal to the interface and are constant along x-axis in the case of limestone, while they are not normal to the interface and not constant along x-axis in the case of coarse sand. The Stokes velocity field exhibits a small decrease of the magnitude along the x-axis and a boundary layer at the plane $x = 40$ in the case of limestone, whereas in the case of coarse sand it demonstrates a linear decrease of the magnitude along x-axis, up to vanishing at the plane $x = 40$. In both cases, singularity of the flow fields due to inconsistency of boundary conditions is observed at the plane $x = 0$. Reasons for such a different behaviour of the coupled flows were discussed in Section 4.3.1. Figures 5.1 and 5.2 show cross sections of Darcy and Stokes velocity fields by the plane $y = 10$.

The grid sequence is formed from tetrahedral partitions of the rectangular grids with 2^k steps in x and y directions, and 2^{k-1} steps in z direction, $k = 4, 5, 6$. In Table 5.1 we present the number of GMRES iterations, N_{GMRES}, needed to reduce the initial residual of (5.12) (due to zero ini-

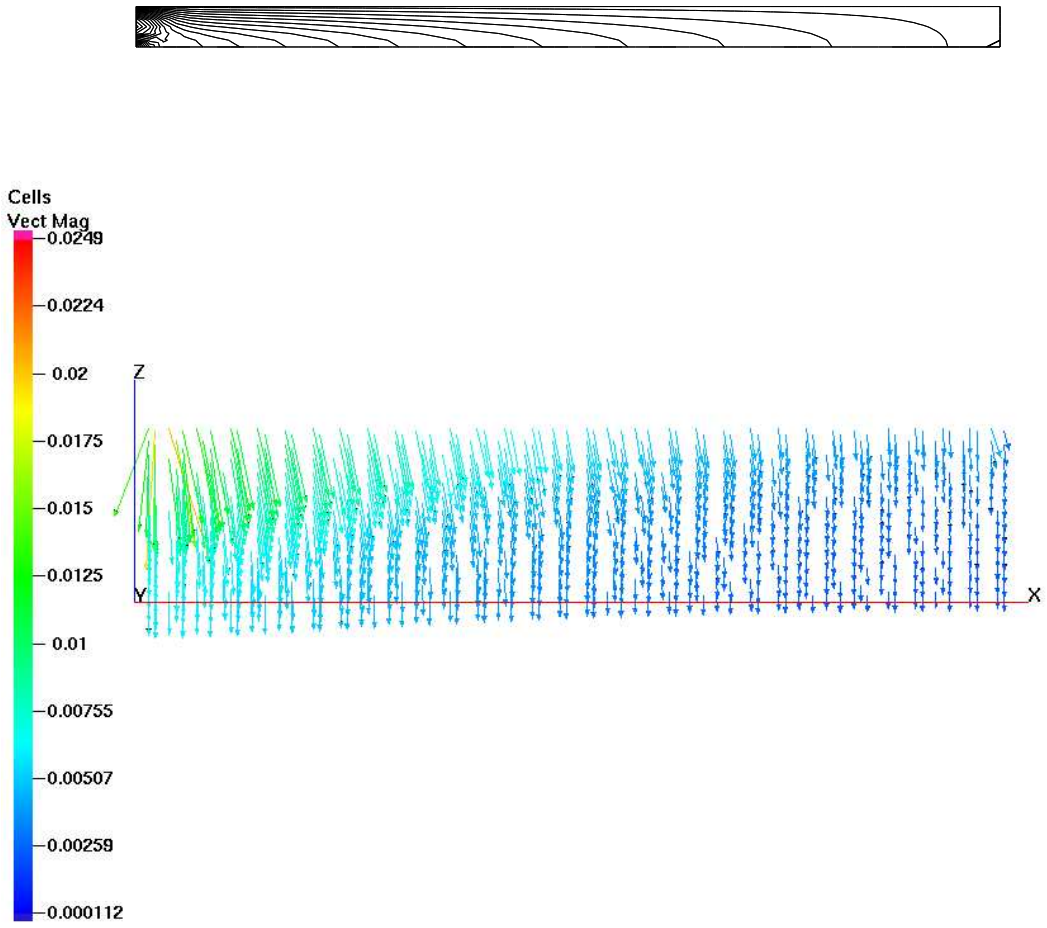

Figure 5.1: XZ cross section of iso-surfaces of Stokes velocity modulo (top) and the Darcy velocity field (bottom) in the case of sand.

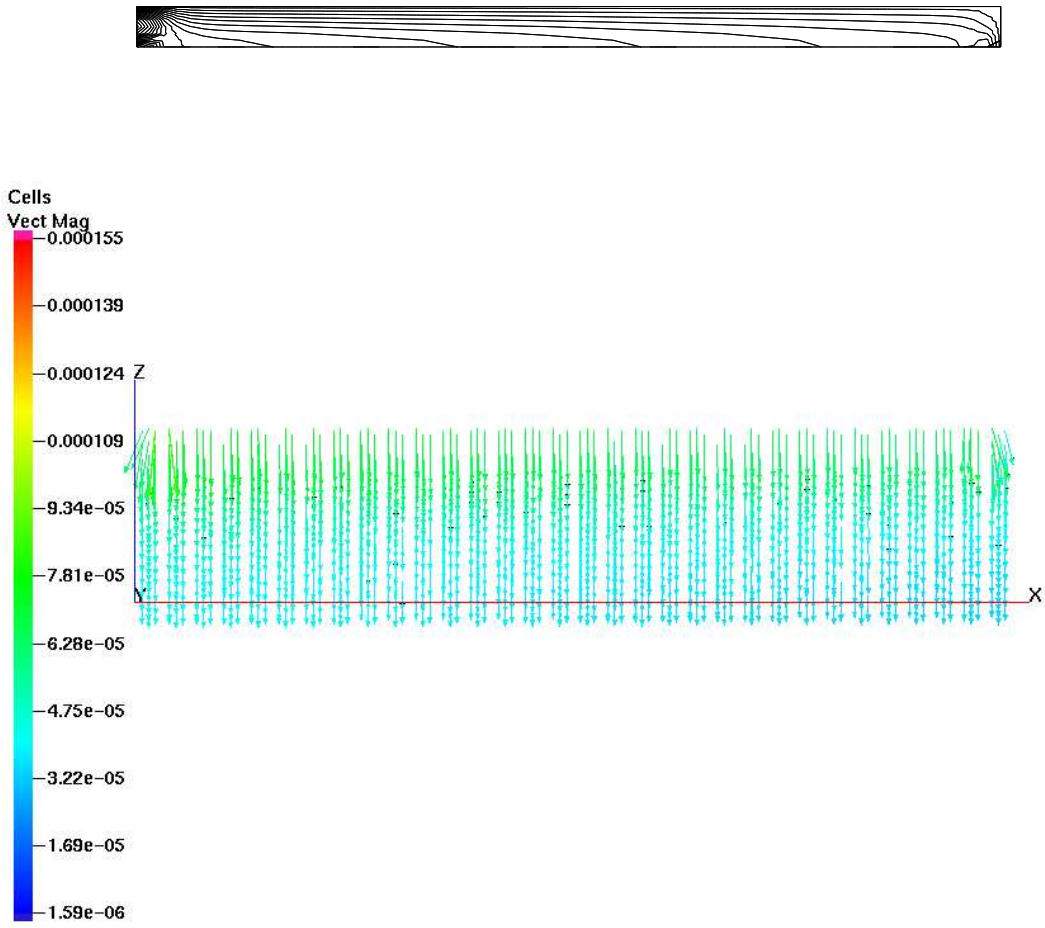

Figure 5.2: XZ cross section of iso-surfaces of Stokes velocity modulo (top) and the Darcy velocity field (bottom) in the case of limestone.

tial guess) by a factor of 10^{-6}, in the case of a material with $\mathbf{K} = \mathbf{I}$. The stopping criteria for subdomain iterative solvers are residual reductions till 10^{-10} and 10^{-6} in Ω_2 and Ω_1, respectively. The number of degrees of freedom for (5.12) is denoted by #DOF, the mean number of iterations applied to Stokes and Darcy subproblems are N_{St} and N_{Dr}, respectively. The last column is the total computational time in seconds measured at Pentium 4, (2.5GH). Iteration counts for solving (5.12) and Stokes subproblem are practically independent of grid size, and N_{Dr} grows slowly with grid refinement. The numbers of unknowns in Ω_2 and Ω_1 are approximately equal to 130 thousands for $k = 6$. Total computational time per coupling iteration exhibits approximate proportionality to the total number of unknowns, since each refinement multiplies the total number of unknowns by a factor of 8.

Mesh	#DOF	N_{GMRES}	N_{St}	N_{Dr}	CPU
$k = 4$	153	10	58	15	8.8
$k = 5$	429	8	55	20	74
$k = 6$	1625	9	62	24	1098

Table 5.1: Iteration counts for the case of coarse sand.

In Table 5.2 the dependence on conductivity coefficient $\mathbf{K}$ is shown. Two interesting effects may be observed in this table: saturation of N_{GMRES} as $\mathbf{K} \to 0$ and dependence of N_{GMRES} on the mesh size for small conductivities. From the first glance, both observations contradict our estimates from the previous section. However, the mismatching is explained easily by the optimality property of GMRES iterations in the case of matrices with real spectrum. Indeed, let us assume that bad (i.e. sensitive to problem coefficients and θ_{MAX}) spectral properties of the operator $I + (S^h_{\mathcal{D}})^{-1} M_\lambda P_{\mathbf{n}_\Gamma} \mathcal{C}^{-1} P^T_{\mathbf{n}_\Gamma} M_{\Phi_\Gamma}$ are conditioned by a few eigenvectors whose number n_{bad} depends on the mesh size reciprocally. Then the number of GMRES iterations required for reduction of the residual by a factor of ϵ may be estimated (for CG applied to SPD matrices, see [Axe96, IJ99]) by a sum of n_{bad}, $C_1(h) \log \epsilon^{-1}$, and possibly, $n_{bad} C_2(h) \log \theta^{-1}_{MAX}$, where $C_1(h), C_2(h)$ are functions independent of θ_{MAX}.

For large conductivity coefficients, the effect of "bad" eigenvalues is very small since their absolute values are not separated from those of the remaining part of the spectrum. According to the data, the increase of iteration count when passing from $\mathbf{K} = \mathbf{I}$ to $\mathbf{K} = 10^{-5}\mathbf{I}$ is $\sim$60 and $\sim$120 on the

coarse and fine grids, that is indicative of the reciprocal dependence of n_{bad} on the mesh size. The presence of these eigenfunctions may be caused by, for example, an inconsistency in boundary conditions at the inlet boundary between the Stokes and Darcy flows.

Mesh $\setminus$ $\mathbf{K} = \mathbf{I}\times$	1	10^{-1}	10^{-2}	10^{-3}	10^{-4}	10^{-5}
$k = 5$	8	20	42	64	72	73
$k = 6$	9	22	47	88	120	127

Table 5.2: Iteration count N_{GMRES} for different porous materials.

5.3.2 Impact of channel configuration

In this example we are going to examine the impact of a non-trivial geometry of a channel system to the Darcy flow coupled with incompressible flow in the channel. The system of channels is formed by the confluence of rivers Wertach and Lech, nearby Augsburg in Baviera, as shown in Figure 1.1. For simplicity, the cross section of the rivers is assumed to be rectangular, and the depth of the rivers is set to 1 m, whereas the sizes of the computational domain are 1080, 700 and 10 m. We exclude the global average drop of the piezometric head over Ω_2 assigning homogeneous Dirichlet boundary conditions on vertical side faces of Ω_2. Setting homogeneous Neumann condition on the top and bottom faces of $\partial\Omega_2 \setminus \Gamma$ makes them impervious, so the fluid (water) can flow through the lateral sides of Ω_2 only. Concerning the Stokes flow, we impose parabolic profiles of velocity (with maximum velocity 1 m/s) at the inlets and outlet, respectively, and a 2D divergence free field (Figure 5.3) at the top surface of the rivers. The mass discharge at the outlet is 99% of that for the inflows. This implies that 1% of the water entering the river system through the inlet, leaves the porous media through the vertical side faces of Ω_2. The problem coefficients are $\nu = 1$ (fluid is water), $g = 10$ (Earth gravity), $\epsilon = 0.1$, $\mathbf{K} = 10^{-5}\mathbf{I}$ (porous material is limestone).
The numbers of mesh nodes in the Stokes and Darcy regions are 11044 and 61076, respectively, that results in ∼240 thousands unknowns for the Stokes subproblem and ∼60 thousands unknowns for the Darcy subproblem (Figure 5.4). The iterative solution of (5.12) required 224 GMRES iterations to reduce the initial residual by a factor of 10^{-6}, starting from zero initial guess. The stopping criteria for subdomain iterative solvers are residual reductions

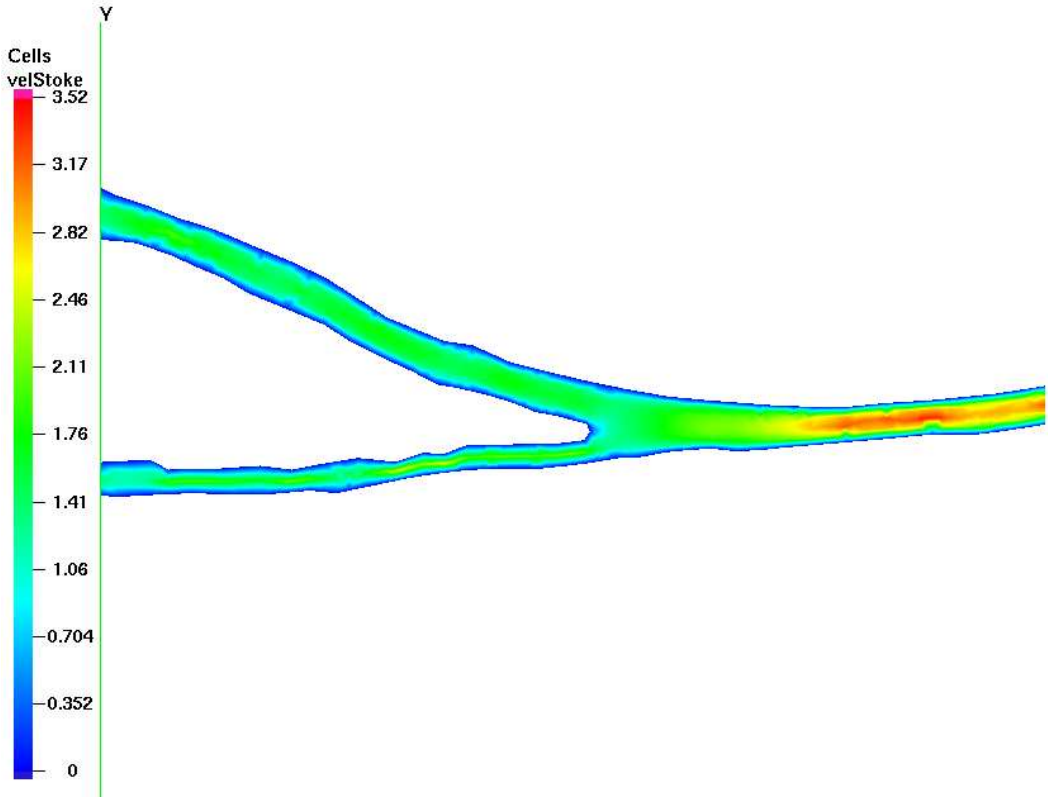

Figure 5.3: Stokes velocity modulo at the top of the rivers, calculated from boundary condition.

till 10^{-8} and 10^{-4} in Ω_2 and Ω_1, respectively. The overall simulation took 14556 seconds at Pentium 4 (2.5 GH).
We emphasize that the application of the Richardson iteration to the solution (5.12) is of no practical application due to necessity of choosing very small parameter θ. Perhaps, the limit of acceptable performance of the Richardson iterations is given for values of $\mathbf{K}$ not less than 10^{-3} (medium sand), which requires 20-30 hours of computation with relaxed stopping criteria in subdomains.

The results of the simulation are presented in Figures 5.5 and 5.6 where cross sections of Darcy velocity field and the piezometric head are shown. It

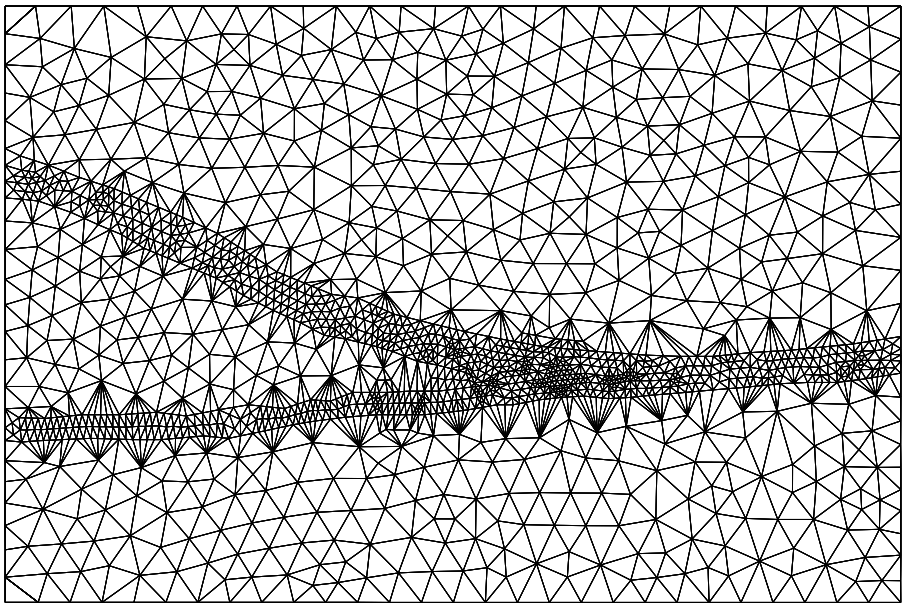

Figure 5.4: Horizontal cross section of the mesh.

is interesting to observe circulation zones for $\mathbf{u_2}$ and singularities of ϕ caused by the inconsistency of boundary conditions of the subproblems. The Darcy velocity at depth 1 m ranks from 10^{-6} to 10^{-5} m/s, with maximum values in the vicinity of the interface.

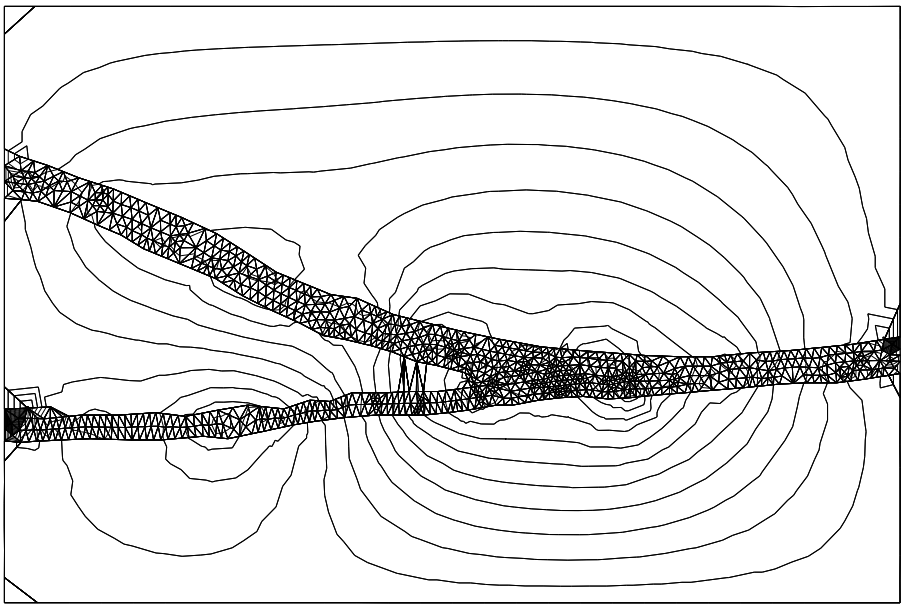

Figure 5.5: Isolines of the piezometric head in the plane $z = 9$.

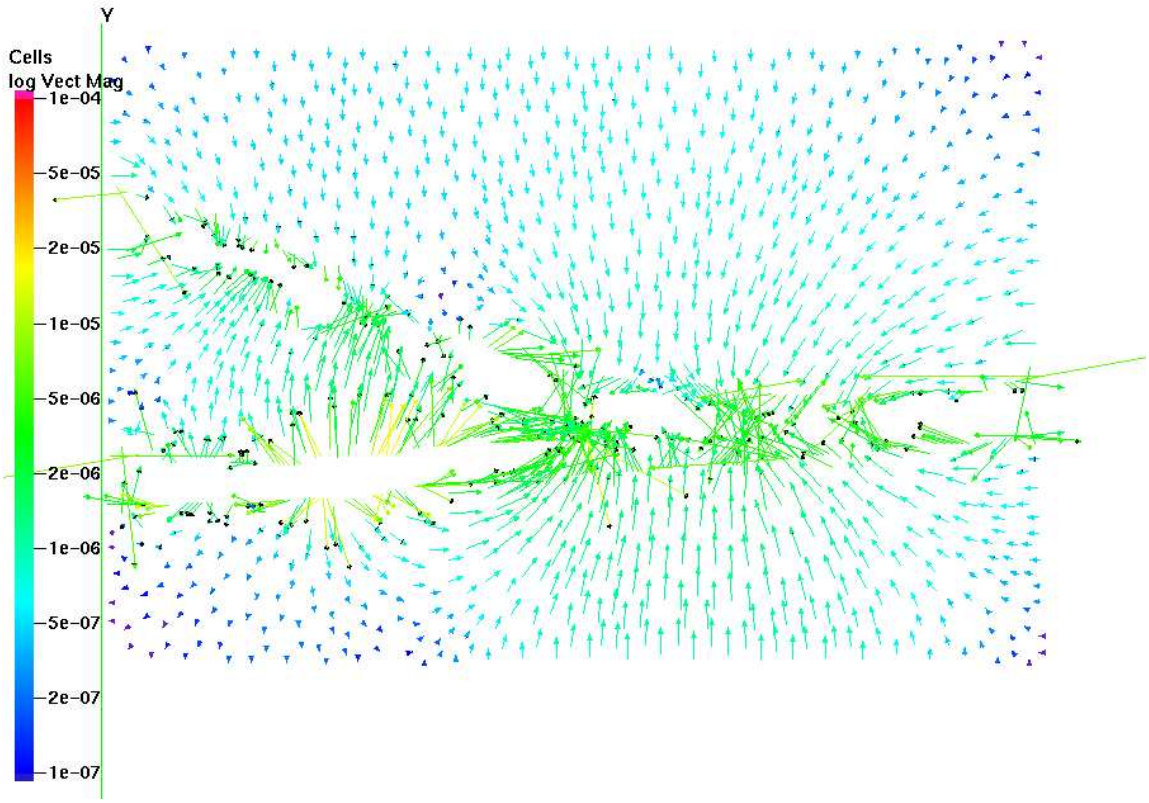

Figure 5.6: Darcy velocity field in the plane $z = 9$.

Conclusions

The main aim of this work has been the evaluation of coupled surface and subsurface flow to compute the velocity field to be used in the calculation of contaminant transport.

We have formulated a mathematical model for the coupled Stokes/Darcy flow and discussed the transmission conditions at the common interface. Using an appropriate weak formulation, our numerical approach has been based on a heterogeneous domain decomposition for which we have suggested three solution strategies:

- an iterative substructuring method resulting in a Neumann-Dirichlet iteration (N-D iteration),
- a direct method relying on the recovery of the iteration operator for the error,
- and 'reduction to the interface' strategies featuring the solution of interface problems.

With regard to the N-D iteration, we have provided a theoretical analysis and performed several numerical experiments. The convergence of the iteration has been proved by means of the equivalence with a preconditioned Richardson iteration. Our findings led us to the conclusion that the N-D iteration is restricted to porous media with a high conductivity. For relevant practical applications, the limit for an acceptable performance of the N-D iterations are values of $\mathbf{K}$ not less than 10^{-3} (medium sand) requiring 20-30 hours of computation with relaxed stopping criteria in the subdomains.

Therefore, we have suggested a direct method which shows good accuracy, but is of high computational complexity. A computationally less expensive

algorithm, based on a low dimensional approximation of the recovery procedure, has been implemented which, however, suffers from a loss in accuracy, especially in the solution of the Stokes flow.

Finally, we have investigated 'reduction to the interface' strategies. We have studied two possible implementations, one based on the continuity of the flux across the interface and the other relying on the continuity of the normal stress. We have reported on some difficulties with the first approach in case of complicated interface geometries, whereas we have observed good flexibility and robustness of the second approach.

Bibliography

[Axe96] O. Axelsson. *Iterative solution methods*. Campbridge University Press, New York, 1996.

[BB90] J. Bear and Y. Bachmat. *Introduction to modelling of transport phenomena in porous media*. Theory and Applications of Transport in Porous Medium. Riedel, Dordrecht, 1990.

[Bea79] J. Bear. *Hydraulics of groundwater*. McGraw-Hill, New York, 1979.

[BF91] F. Brezzi and M. Fortin. *Mixed and hybrid finite element methods*, volume 15 of *Springer Series in Computational Mechanics*. Springer, New York, 1991.

[BJ67] G. S. Beavers and D. D. Joseph. Boundary conditions at a naturally permeable wall. *J. Fluid Mech.*, 30:197–207, 1967.

[Bre74] F. Brezzi. On the existence, uniqueness and approximation of saddle-point problems arising from Lagrange multipliers. *Rev. Francaise Automat.Informat. Recherche Opérationelle*, 8:129–151, 1974.

[Bri47] H. C. Brinkman. A calculation of the viscous force exerted by a flowing fluid on a dense swarm of particles. *App. Sci. Res.*, 1:27–34, 1947.

[BSM74] G. S. Beavers, E. M. Sparrow, and B. A. Masha. Boundary condition at a porous surface which bounds a fluid flow. *AIChE Journal*, 20:596–597, 1974.

[BV87] J. Bear and A. Verruijt. *Modelling groundwater flow and pollution*. Theory and Applications of Transport in Porous Medium. Riedel, Dordrecht, 1987.

[Dag79] G. Dagan. Models for groundwater flow in statistically homogeneous porous formation. *Water Resources Research*, 13:17–63, 1979.

[DMQ02] M. Discacciati, E. Miglio, and A. Quarteroni. Mathematical and numerical models for coupling surface and groundwater flows. *Appl. Num. Math.*, 43:57–74, 2002.

[DQ03] M. Discacciati and A. Quarteroni. Analysis of a domain decomposition method for the coupling of stokes and darcy equations. In F. Brezzi, A. Buffa, S. Corsaro, and A. Murili, editors, *Numerical mathematics and advance applications, ENUMATH 2001*, pages 3–20, Milano, 2003. Springer.

[DQ04] M. Discacciati and A. Quarteroni. Convergence analysis of a subdomain iterative method for the finite element approximation of the coupling of stokes and darcy equtions. *Computing and Visualization in Science*, VI, 2004.

[DS90] P. Domenico and F. Schwartz. *Physical and chemical hydrology.* John Willey and Sons, New York, 1990.

[ESP75] H. Ene and E. Sánchez-Palencia. Equations et phènomenés de surface pour l'écoulement dans un modelle de lieux poreux. *J. Méchanique*, 14(1):73–108, 1975.

[GO76] W. G. Gray and K. O'Neill. On the general equations for flow in porous media and their reduction to Darcy's law. *Water Resources Research*, 12:148–154, 1976.

[GR79] V. Girault and P. A. Raviart. *Finite element approximation of the Navier-Stokes equations*, volume 749 of *Lecture Notes in Mathematics*. Springer, Berlin, 1979.

[Hor92] U. Hornung. Applications of the homogenization method to flow and transport in porous media. In Xiao Shutie, editor, *Flow and transport in porous media*. Singapore: World Scientific, 1992.

[IJ99] Graham I. and Hagger J. Unstructured additive schwarz-conjugate gradient method for elliptic problems with highly discontinuous coefficients. *SIAM J. Sci. Comput.*, 20:2041–2066, 1999.

[JM00] W. Jäger and A. Mikelić. On the interface boundary condition of Beavers, Joseph and Saffman. *SIAM J. Appl. Math.*, 60(4):1111–1127, 2000.

[Jon73] I. P. Jones. Low reynolds number flow past a porous spherical shell. *Proc. Camb. Phil. Soc.*, 73:231–238, 1973.

[Lio96] P. L. Lions. *Mathematical topics in fluid mechanics*, volume 1 of *Oxford Science Publications*. Oxford University Press, Oxford, 1996.

[LM68] J. L. Lions and E. Magenes. *Non homogeneous boundary value problems and applications*, volume 1 of *Die Grundlehren der mathematischen Wissenschaften in Einzeldarstellungen*. Spinger, Berlin, 1968.

[LSY03] W. Layton, F. Schieweck, and I. Yotov. Coupling fluid flow with porous media flow. *SIAM J. Numer. Anal.*, 40(6):2195–2218, 2003.

[NB92] D. A. Nield and A. Bejan. *Convection in porous media*. Springer, New York, 1992.

[Pir89] O. Pironneau. *The finite element methods for fluids*. John Wiley and Sons, New York, 1989.

[PS98] L. E. Payne and B. Straughan. Analysis of the boundary condition at the interface between a viscous fluid and a porous medium and related modeling questions. *J. Math. Pures Appl.*, 77:317–354, 1998.

[QV91a] A. Quarteroni and A. Valli. Theory and application of the Steklov-Poincaré operators for boundary problems. In R. Spiegler, editor, *Applied and industrial mathematics*, Proceedings of a Symopsium conducted by the Mathematics Research Center, pages 179–203, Dordrecht, 1991. Kluwer Academic Publishers.

[QV91b] A. Quarteroni and A. Valli. Theory and application of the Steklov-Poincaré operators for boundary problems: the heterogeneous operators case. In R. et al. Glowinski, editor, *Domain decomposition methods for partial differential equations, IV*, pages 58–81,

Philadelphia, 1991. Society for Industrial and Applied Mathematics.

[QV94] A. Quarteroni and A. Valli. *Numerical approximation of partial differential equations*. Springer, Berlin, 1994.

[QV99] A. Quarteroni and A. Valli. *Domain decomposition methods for partial differential equations*. Oxford University Press, Oxford, 1999.

[Saf71] P. Saffman. On the boundary condition at the interface of a porous medium. *Stud. Appl. Math.*, 1:93–101, 1971.

[SK92] M. Sahraoui and M. Kaviany. Slip and no-slip velocity boundary conditions at interface of porous, plain media. *Int. J. Heat Mass Transfer*, 1:927–943, 1992.

[Ste03] O. Steinbach. *Stability estimates for hybrid coupled domain decomposition methods*, volume 1809 of *Lecture notes in Mathematics*. Springer, Berlin, 2003.

[Stu83] K. Stuben. Algebraic multigrid (amg): experiences and comparisons. *Appl.Math.Comput.*, 13:419–452, 1983.

[Tay71] G. I. Taylor. A model for the boundary condition of a porous material. I. *J. fluid Mech.*, 49:319–326, 1971.

[Tem84] R. Temam. *Navier-Stokes equations*. Studies in Mathematics and its Applications. North-Holland, Amsterdam, 1984.

[Whi99] S. Whitaker. *The method of volume averaging*. Kluwer Academic Publishers, Dordrecht, 1999.

Curriculum Vitae

Paulo Porta

November 2004

Paulo Porta,	two children, borned in Rosario, Pcia. de Santa Fe, Argentina on January the 16^{th}, 1968.
Degrees	Aronautical Engineer Facultad Regional Haedo, Universidad Tecnológica Nacional August 1992.

Present and past appoinments

Since May 2002, Resercher in the Unweltsimulation Zentrum, University of Augsburg, Germany, working on numerical simulation of reactive transport processes in grounwater and on the interaction and coupling of surface and subsurface flow.

From April 1996 to March 2001, Lecturer of Continuum Mechanics and of Numerical Analysis at the Facultad Regional Haedo, Universidad Tecnológica Nacional, Argentina. From April 2001 to April 2002, Senior Lecturer int he same institution.

Grants for Studies

Scientific Research Comittee, Provincia de Buenos Aires, (CIC-BA). Poder Ejecutivo de la Pcia. de Buenos Aires, Argentina. To workin collaboration with the Theoretical Physico Chemical Group, at the Institute for Theoretical and Applied Physicochemical Research (INIFTA). Director: Dr. Eduardo Mola, Principal Researcher, CONICET and DR. José Luis Vicente, Independent Researcher, CIC-BA. (1999).

Grants for Professional Development

National Agency for Scientific Research, Argentina. To work in the Materials Science Department, MechanicalProperties Laboratory, Centro Atómico Constituyentes, CONEA. Director: Dr. Francisco Póvolo, Principal Researcher, CONICET. (1998).